Investigation of exhaust chamber resonance for single-cylinder Formula SAE based engines

A thesis

submitted in fulfilment

of the requirements for the degree

of

Master of Engineering

at

The University of Waikato

by

Jonathan van Harselaar

THE UNIVERSITY OF
WAIKATO
Te Whare Wānanga o Waikato

2019

Abstract

Noise pollution is a factor that affects many people in their day to day lives. One of the more prevalent forms of noise is generated from passenger vehicles. With this in mind, vehicle manufacturers design and stringently test their mufflers that are bound for vehicles to ensure they provide the optimum characteristics needed to lower noise to suitable levels. In addition, these manufacturers continue to be proactive in researching improved methods of the design and build aspects of their vehicles, so it is common to see large production companies sponsoring development and racing events. One such event is the Formula SAE competition.

This competition series is aimed at university students who design, build, and race their vehicle against other universities globally. Formula SAE is designed to provide students with valuable experience in a range of topics as both static and dynamic events occur and are judged. Consequently, the competition has evolved into more than just a racing series, it also includes business presentations, costing reports, and design judging.

With more Formula SAE teams moving to single-cylinder engines, noise suppression is becoming an important issue from the exhaust noise characteristics of the large engines available today. As part of the competition, performance is judged based on set criteria for engine noise emissions at different engine speeds. Many teams struggle with this aspect of the competition, where a fail in this test commonly leads to crude forms of noise suppression being quickly added to the vehicle, which in turn usually results in lowering performance. If a team cannot pass the noise tests, then subsequently they are not allowed to enter any of the dynamic events.

This thesis aims to compare theoretical results with measured values for different configurations of exhaust chambers. Inline exhaust chambers have been selected as the topic of interest due to the low-frequency exhaust characteristics of single-cylinder engines suiting the attenuation characteristics of this style of silencing device. The outcome of this research should provide figures and values for future Formula SAE teams to work with in their initial muffler and chamber design. By having this data available, selection of correct parameters will be a more straight-forward process and should assist in building a muffler that will be more assured of passing noise tests at competition.

Acknowledgements

I would like to acknowledge my supervisor Mark Lay for guiding and supporting me in my studies. Your interest and insight proved invaluable to my progression through this thesis. To my unofficial technical supervisor, Shannon McMurray, thank you for the time, support, and discussions around this project.

A special mention should go to Mr. Higgins as without your technical assistance and enthusiasm while constructing the experimental setups, the project would have taken much longer to build (and had much more time sitting in the workshop).

Additionally, I have appreciated the discussions and backing from my colleagues. The positive atmosphere provided by everyone makes working and studying far more enjoyable.

My sincere thanks goes to Graeme Harris for allowing the use of your exhaust testing equipment. Countless hours of machining was saved due to your generosity.

I would like to thank my friends and family for supporting me through these studies. Your continued encouragement will always be appreciated.

Finally, thank you to Samantha Edlin-Burke, for all of your love and support.

Table of Contents

List of Figures

List of Tables

Nomenclature

c	Acoustic velocity [$\mathrm{m/s}$]
A	Area [m^2]
A_r	Area ratio
BMEP	Brake mean effective pressure [bar]
C_p	Specific heat at constant pressure [J/kg^{o}K]
C_v	Specific heat at constant volume [J/kg^{o}K]
γ	Ratio of specific heats
D	Diameter [m]
D_H	Hydraulic diameter [m^2]
f	Frequency [Hz]
f_d	Darcy friction factor
H	Enthalpy [kJ]
λ	Wavelength [m]
L	Length of pipe [m]
M	Molar mass [g/mole]
n	Harmonic number
P_r	Pressure ratio
p	Pressure [Pa]
p_0	Reference pressure [Pa]
ρ	Density [kg/m^2]
R	Gas Constant [8.314 J/Kmol]
rpm	Rotations per minute
T	Temperature [^{o}C]
T_a	Absolute temperature [^{o}K]
TL	Transmission loss [dB]
v	Velocity [m/s]
v	Velocity [m/s]
V	Volume [m^3]
ω	Angular velocity [rad/s]
W	Work [W]

1 Introduction

Formula SAE is a motorsport competition with both static and dynamic events. This event is aimed at university students who are studying engineering. It encourages the students to immerse themselves in the design and building stages of engineering, while reinforcing costing and other business aspects of engineering as a career. Universities from all over the world compete in a series of Formula SAE events at different locations globally, with events held in America, Australia, and under the title "Formula Student" in the United Kingdom.

Figure 1-1: 2018 WESMO team and WP-18 at competition design judging.

In order to be allowed to race their vehicles, each team must first pass scrutineering. This is done to satisfy the safety aspects of the car while also ensuring that the rulebook has been followed. Once a technical inspection of the vehicle has been completed by event officials, the teams then move across to the dynamic scrutineering events; tilt test, brake test, and noise test. Failure to pass one of these events will require the team to solve the problem using the limited tools at the racecourse. If the vehicle is still unable to pass all of the dynamic scrutineering events, then the team will not be able to compete in any of the dynamic racing events.

One major issue faced by Formula SAE and Formula Student teams running in the Internal Combustion class is how to muffle their engines without sacrificing power or gaining weight. With a greater number of IC teams moving to large capacity single cylinder engines, more time and effort need to be put in to silencing these loud engines. The movement from inline-fours, triples, and twin-cylinder engines has been due to the recent advancement in single-cylinder engine design. The single cylinders of old were usually high-compression, carburetted, shaky, and hard to start engines that ended up vibrating cars to pieces, that is if the starter motors did not die first. The newer engines being produced by manufactures such as KTM and Yamaha have been refined to remedy these issues, usually with auto decompression, twin balance shafts, and fuel injection. This change has prompted a shift for some teams where substantial weight has been dropped from their cars, and driveability has increased from the torquey nature of the single cylinder.

While there are many good points to support competing with a single-cylinder engine, one downfall of this mode comes in the form of its exhaust characteristics – predominantly the noise it produces. Where an inline-four engine with a flat-plane crank produces four exhaust pulses for every 720° of crank rotation, with each pulse being a quarter of the engine's capacity (neglecting pumping losses and VE), a single cylinder engine produces one pulse equivalent to the total capacity of the engine. This sets up a large pulse of exhaust gas that needs to be quietened down in a confined space. The much lower frequencies produced by the single-cylinder engine require a muffler or chamber of significantly longer lengths if attenuation through resonance is going to occur, a factor that results in a notable packaging constraint for the small Formula SAE vehicles.

It is therefore desirable to improve the quantifiable values of both noise and convenience especially in relation to the length of the muffler. This study aims to achieve this by focusing on silencing a single cylinder engine by using resonant chambers in the exhaust system. There are two parts to the silencing characteristics of these chambers.

1.) The resonant harmonic frequency of these chambers has the ability to cause destructive interference at certain frequencies, which can be utilised to quieten the exhaust at target frequencies.
2.) The body of the chamber also attenuates noise with the level of attenuation relying on the ratio of the chamber area to the inlet pipe area, or in other words, a change in pressure of the sound wave.

By adding tapered cones to the inlet and outlet of the exhaust chambers, the effect of the harmonic resonance is expected to increase over a larger range of frequencies and quieten the exhaust more efficiently. One other aspect of the tapered cones to consider is that a lower flow loss is involved with a gradual expansion and contraction of the exhaust pipe, which can result in less backpressure and higher engine outputs.

This thesis will review relevant literature on the Formula SAE competition, engines and exhaust noise, and acoustic waves. Using relevant equations and values, the attenuation of tapered mufflers will be graphed for each of the exhaust test chambers and compared to audio recordings from the test engine. The results from the comparison between measured values vs calculated values will be discussed and conclusions made as to the effect of the chamber and how the taper at the ends attenuates noise differently. Further research will be theorised and the validity of the experiment discussed.

To test the effect of different chambers and tapers, a single-cylinder motorcycle engine has been mounted to a custom-built test rig. Loads are applied to the engine via a water-brake dynamometer to simulate loading conditions within the engine's normal operating parameters to see if the mass flow rate will have an effect on the exhaust noise levels. The sound levels for each of the exhaust chamber configurations are recorded and maximum decibel levels noted. This data then has an audio spectrum plotted, the results exported, and a graph of the noise levels produced. This is then plotted and compared to the theoretical results that were derived from equations presented from different sources in literature.

2 Formula SAE and the Internal Combustion Engine (LIT)

2.1 Formula SAE

Alongside regular studies, students are presented with an opportunity to be part of Waikato University's Formula SAE team, WESMO. The Waikato Engineering Students Motorsport Organisation is one of three university teams in New Zealand who regularly compete in the Australasian round of the Formula SAE competition series, usually held on the outskirts of Melbourne, Australia.

The series is designed to give university students an insight into the world of vehicle racing and design. It aims to educate the students in a wide variety of real-world skills while also encouraging team building and communication skills. The competition regularly sees international universities competing, with some teams travelling from as far afield as Germany.

Figure 2-1: 2018 WESMO car, WP-18, during testing at Meremere drag strip prior to shipping to Australia.

The Formula SAE competition itself lasts for four days. It comprises different static and dynamic events where teams present their Formula SAE car and their work for judging and to race against the other teams. Static events include costing reports, business presentations, and design judging which assess each team's ability in the business, research, and design aspects of building a car. Dynamic events include scrutineering, acceleration test, skid pan, auto-x, and endurance, where the rubber meets the track and

the cars will be put to the test to see how successfully the teams have designed and built them.

For teams, the competition does not always go according to plan, with some teams falling into the trap of scrutineering where a rule has been forgotten or misread, or the car breaks during racing, in these cases on the spot changes have to be made in the supplied workshops. Under these circumstances teams have the opportunity to perform minor repairs to enable the car to compete in the next available event, however any major repairs could set the team back many competition points from missing dynamic events.

At the end of the competition, a prize giving is held to present awards to the teams who scored well in each of static and dynamic events and there is, in addition a farewell ceremony. From here the teams will travel back to their universities and with furthered knowledge and renewed inspiration will begin preparing for the following year's competition.

2.1.1 Competition rules, allowed engines, and noise levels

As part of any competition series, there are stringent rules for all teams involved. The internal combustion (IC) class of the competition limits certain aspects for engines and auxiliary components. Engines themselves need to be 710 cc or less in capacity, of a four-stroke cycle, and must breathe through either a 20mm restrictor for 98 octane petrol or 19 mm for ethanol. While forced induction such as turbocharging and supercharging is allowed, many teams disregard these designs due to the added complexity and weight of the system.

With the recent rule change from a capacity limit of 600 cc to 710 cc, and the introduction of KTM's new single-cylinder 690 cc LC4 engine, a new trend is occurring in the internal combustion class of the competition. Gone are the days of the powerful, large, and heavy four-cylinder 600 cc sport bike engines as many teams are making the switch to light-weight and torquey singe-cylinder engines. Part of this shift in vehicle design is driven by decisions such as how the KTM 690 LC4 makes more torque over a useable power band while weighing up to 35kg less than a Suzuki GSX-R600 engine.

Amongst other requirements that need to be met to pass scrutineering, one that many teams struggle with is the noise tests. This part of scrutineering tests the exhaust noise levels at idle and up to a mean piston speed of 914 m/min measured. At the engine idle speed the exhaust volume needs to be lower than 103 dB and at all other engine speeds,

up to the specified mean piston speed, the volume should be less than 110 dB. These volumes can be difficult to obtain for some teams and last-minute tweaks are commonly required to bring noise levels down.

The issue most teams have when fitting the engines into their chassis' is that the factory exhaust systems are too large or heavy to be used on the vehicles. This leads to the issue of having to design an exhaust system specifically for the car – which is not an easy task. Add to this the issue of silencing a loud single-cylinder engine, and a team can really have their work cut out for them.

2.2 A brief history of the Internal Combustion Engine

Patented in 1861 by Beau de Rochas the 'theoretical' atmospheric four-stroke cycle first came into existence. It was not until 1876 that Nikolaus August Otto and fellow German Engineer Eugen Langen developed the first functioning four-stroke compressed charge or 'Otto cycle' engine, which was promptly put to use in a prototype motorcycle. This engine cycle is still widely used today, and while the geometry and functions may have been further developed, the principle of the Otto cycle still remains.

Three years later in 1879, Karl Benz successfully designed and patented a reliable two-stroke gasoline engine based off the Otto cycle. Benz's work continued from this project, with his later design of four-stroke engines making their way into his automobiles, the first passenger vehicles in production (New World Encyclopedia, 2018).

Following this development, another German engineer, Rudolph Diesel, created the Diesel engine in 1892. This engine utilised heavy oils as fuel and while it was heavier in architecture, it was more powerful than a gasoline engine due to its compression-ignition design (RAŢIU, 2003).

While all this development into internal combustion engines was occurring, at the turn of the 20th century electric motors were still the preferred power plant for private vehicles. Electric vehicles at this time did not suffer from the vibration, the smell, and the noise associated with a gasoline engine, and had quicker start-up procedures and a longer range than a comparable steam-powered vehicle.

This trend however did not last. By the 1920's electric car sales had fallen in a large part due to various factors of progress including improvements in intercity roads that

encouraged longer distance travel, the discovery of oil, and the development of electric starter motors. These factors were instrumental in influencing a shift to internal combustion vehicles. (Khajepour, Fallah, & Goodarzi, 2014). From this time forward, the ongoing development and modification of the Otto cycle engine and its derivatives has seen it become the most widely used engine cycle on the planet.

2.3 How a four-stroke Internal Combustion engine functions

In its basic form, the internal combustion engine is an air pump designed to produce useable power from the combustion of a fuel with air. This combustion event converts chemical potential energy into heat, producing pressure in the combustion chamber of the engine. Due to the pressure differential formed across the piston, it is driven down the bore rapidly. This movement of the piston and connected mechanical linkages induces a torque on the crankshaft, producing a rotational movement. Lubrication of this style of engine is generally a 'wet sump' and oil pump setup. The sump at the bottom of the engine collects the oil to feed the oil pump, which in turn pressurises the oil and feeds it through to the bearings and journals.

This engine's crankshaft drives the camshaft/s which use lobes to control intake and exhaust valve movements – which in turn controls the airflow in and the exhaust gases out of the cylinder. In regard to their design, the camshaft lobes are ground into certain profiles to attain different valve lifts and durations based on the purpose of the engine. While there are different methods to actuate the valves, the most common method is using rocker arms that ride on the camshaft lobes and pivot to contact the valves. Other methods of valve actuation can be achieved via buckets and shims – this method is most commonly found on high-revving engines, and pushrods such as those in many older engines.

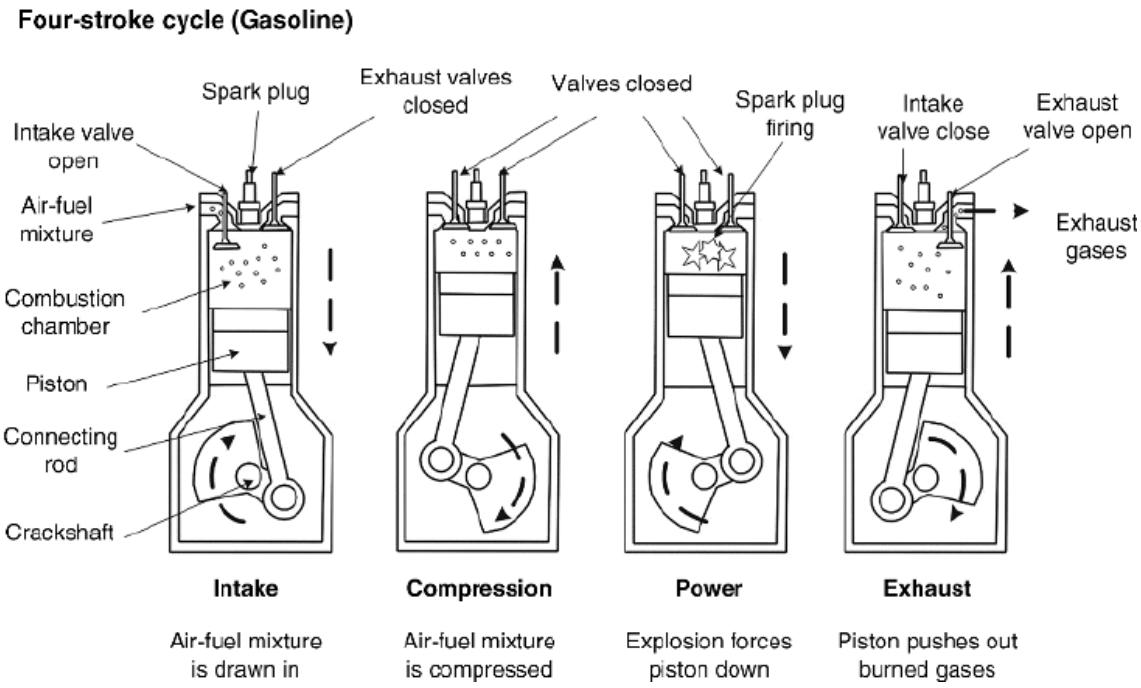

Figure 2-2: Gasoline four-stroke cycle (Fallah, 2014)

While there are now many modified versions of the Otto cycle, the typical four-stroke engine functions in the four main parts shown above - the Intake stroke, Compression stroke, Power stroke, and the Exhaust stroke. This adds up to 720º of crank rotation with each stroke taking up approximately 180º.

On the intake stroke at 0º of crank rotation the piston descends down the bore from top dead centre (TDC) and draws a fresh mixture of air and fuel into the combustion chamber through the open intake valve. This process is possible due to the piston drawing a partial vacuum in the cylinder from the volume increase thus, allowing atmospheric pressure in the intake runner to fill the cylinder. Near bottom dead centre (BDC), or around 180º of crank rotation, the intake valve closes to prevent any of the mixture in the combustion chamber exiting back up the intake runner.

The compression stroke follows where the piston now travels back up to TDC and compresses the mixture. Both the intake and exhaust valve are closed. At this stage the crank has rotated a full 360º without any assistance, relying on the inertia of the crankshaft and flywheel to provide the force to inhale and compress the air and fuel mixture. While compression occurs, the mixture heats up and becomes more volatile.

With the piston near TDC at 360º crank degrees, the spark plug ignites the mixture to start the power stroke. Combustion events build pressure above the piston creating a pressure difference between the combustion chamber and the crankcase (at atmospheric pressure)

which serves to drive the piston down in its cylinder. The force on the piston acts through the connecting rod, onto the crankshaft. The induced moment on the crank causes acceleration and a gain in rotational velocity.

Near BDC, at 540º crank degrees, the exhaust valve opens to release the combusted gases from the cylinder. Due to the high pressure differential between the cylinder and the exhaust manifold, a high percentage of the gases in the cylinder evacuate very rapidly, with the rest of the gases being evacuated during the subsequent exhaust stroke as the piston returns to TDC at 720º crank degrees. At this point the exhaust valve closes, the intake valve opens, and the engine is ready to repeat the four-stroke cycle.

One interesting feature of the four-stroke engine is the physical nature of how the camshaft/s are driven at half the crank speed. Due to the piston having to travel up and down the cylinder twice per engine cycle the crankshaft needs to rotate through 720°, but as the intake and exhaust valves only need to open once per cycle the camshaft only needs to rotate 360°. This gear ratio of 2:1 is generally achieved through the use of pulleys and belts or gears and chains.

With the piston nearing TDC (720º/0º) on the exhaust stroke, the intake valve cracks open while the exhaust valve starts to close. This period of time is called valve overlap and is a very important feature of the valve events as it can greatly affect cylinder filling during the intake stroke. Many manufacturers use this period of time to utilise 'exhaust scavenging' where more mixture can be drawn into the combustion chamber from a slight vacuum in the exhaust port (Bell, 2012).

Further research and development into producing a more powerful and efficient engine has produced modified combustion cycles based on the Otto cycle. The Modern Atkinson cycle is a good example of this. By delaying the closing of the intake valve until past the end of the intake stroke, some of the intake charge can enter back into the inlet manifold. This allows for a lower compression ratio that is smaller than the expansion ratio and therefore producing lower pressures at the end of the combustion stroke – an essential feature of the Atkinson cycle that minimises waste energy (Balmer, 2011).

Forced induction is now commonplace in many automobiles. A turbocharger is placed in the exhaust stream and uses a turbine wheel to convert some of the exhaust gas energy into rotational movement of a shaft, which is then used to turn a compressor wheel and compress the engine's intake charge. With a higher density of air molecules entering the

engine per intake stroke, more fuel can be added, and a larger energy from combustion is achieved. This has meant some manufacturers have downsized the engines in some of their models as a smaller turbocharged engine can produce more torque and power than their naturally-aspirated engines.

The Miller cycle is a modified version of the Atkinson cycle that uses boosting from a supercharger or turbocharger. The reasoning behind this setup is to recover the lost charge resulting from the smaller displacement on compression and keep BMEP levels stable (Naber & Johnson, 2014). In this context, the Brake Mean Effective Pressure is the measurement of an engine's capacity to do work, with a higher BMEP indicating higher pressures acting on the engine's pistons. It is common to see engines with BMEP's of 7 bar or higher in naturally-aspirated forms and even higher in forced-induction applications. This measurement is based on the average pressure 'seen' by the pistons in an engine to produce the specified power output.

Variable valve lift and duration, as well as variable valve timing are other methods of improving aspects of four-stroke engines. The idea behind this principle is to primarily improve economy, but can also benefit power as cylinder filling and evacuation properties can be changed.

While the concept had been around previously, in 1989 Honda Motor Co. produced the first mass-marketed variable valve lift and timing device on their B16a engine. The system is controlled via the engine control unit with a solenoid opening an oil passage in the head to supply cavities behind pins in the camshaft rockers with pressurised oil. The oil pressure then pushes these pins into a central rocker which rides on a larger camshaft lobe. When the engine reaches a certain rpm and load scenario, the VTEC system activates, locking in the higher lift and duration camshaft lobes and increasing the amount of air and fuel entering the cylinder – producing more power. This meant that below the crossover point the engine could run on 'economy' mode but could also produce power when needed over the crossover point.

2.4 Other types of engine cycles

In production today there are two main types of reciprocating piston engines, the four-stroke and the two-stroke engine. As their names suggest, the two-stroke engine takes two strokes of the piston (or in terms of crankshaft rotation 360º) to complete its cycle,

where the four-stroke engine requires four strokes of the piston or 720º of crankshaft rotation. A stroke in these terms is based on the relative position and movement of the piston and due to the reciprocating design of an IC engine occurs twice per crankshaft rotation.

In brief, the design of the two-stroke engine makes it a suitable candidate for motorcycles due to its torquey nature and light weight architecture. This engine does not possess the intake and exhaust valves that a four-stroke has, or indeed any pump-driven oiling system as lubricating oil is suspended in the fuel mixture. Instead, reed valves and transfer ports control the flow of the air and fuel mixture into the engine, with the piston uncovering ports in the cylinder walls as it moves down the bore. Due to the crankcase being sealed against any out-flow, the partial vacuum during the piston travelling to up the bore sucks fuel and air through the one-way reed valves into the crankcase where the suspended oil in the fuel lubricates the crankshaft bearings and cylinder wall. When the piston travels back down the bore the crankcase gases are compressed, and when the intake ports are uncovered, this gas rushes into the combustion chamber. At this point both intake and exhaust ports are uncovered, meaning some of the fuel and air exits from the exhaust port.

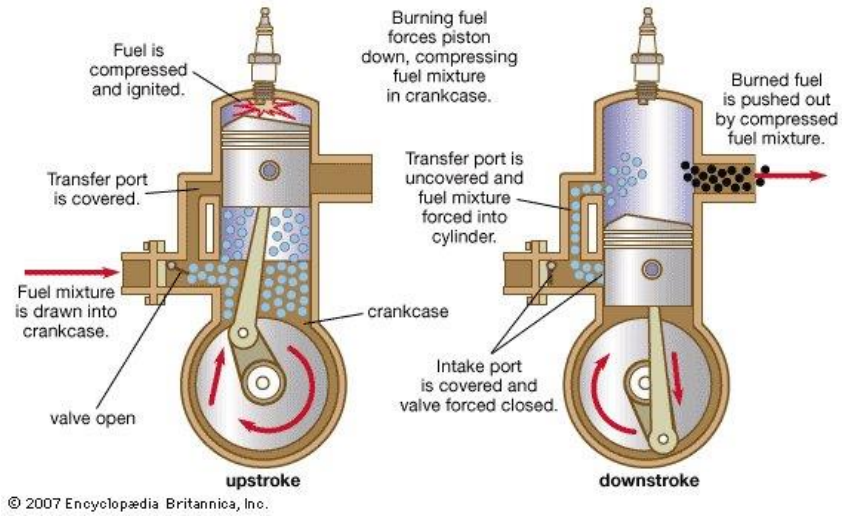

Figure 2-3: Two-stroke engine cycle (Encyclopedia Britannica, 2020).

Clever exhaust design and tuning results in the reflection of a portion of this mixture back into the combustion chamber and increases the pressure slightly, increasing performance. The obvious downsides to this engine are its efficiency and the amount of pollutants given off due to the need for lubrication oil for bearings and seals to be in the fuel. It however has fewer rotating parts and a lower weight than a comparable four stroke.

Four-stroke engines get around the oil-burning issues of their two-stroke counterparts as their crankcase contains oil and lubrication that is provided from an oil pump. The design also means much less fuel is allowed to enter the exhaust (if any) and combustion occurs on a 'fresh' charge of fuel and air. While they may have more valve train components that increase the rotational load on the crankshaft, they are more efficient as well as being more environmentally-friendly.

Another type of engine that made its way into select production vehicles was the Wankel or 'Rotary' engine. Much like two-stroke engines do not have intake and exhaust valves, the rotary engine does not either.

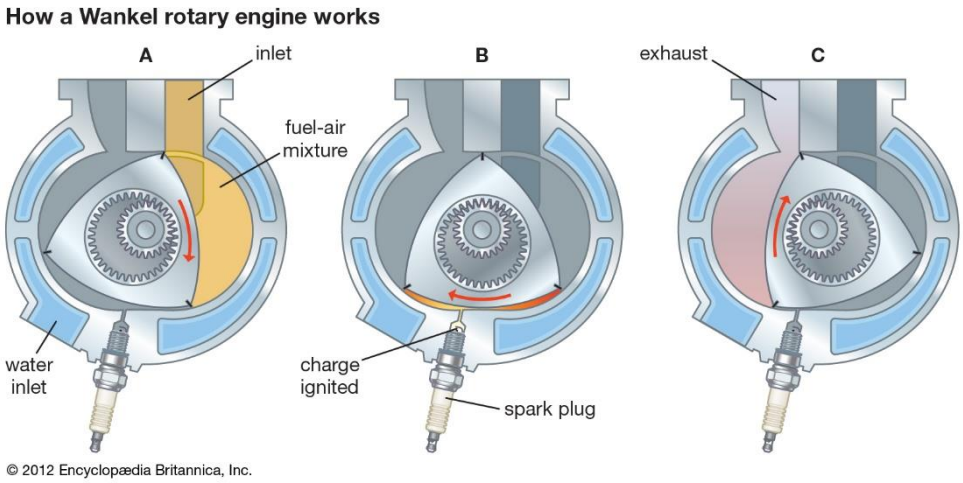

Figure 2-4: Rotary engine cycle with single spark plug (Encyclopedia Britannica, 2020).

The eccentric nature of the triangular-shaped rotor covers and uncovers intake and exhaust ports, eliminating the need for any valve train components. However, like the two-stroke engine, a lubrication oil is needed for the apex seals on the rotor to prevent wear. This meant from the factory these rotary engines burnt oil – producing pollutants. The design of this engine also meant the capacity of these engines was small, but high-revving, producing little torque but capable of large power at high rpms with the result that efficiency suffered and turbochargers were often employed.

2.5 Single vs multi-cylinder engines

While this is not a ‘one size fits all’ situation, many manufacturers of small to medium size vehicles do tend to favour the inline-four engine over others. This is largely due to their ‘smoothness’ and simplicity.

While inline-four cylinder engines are predominantly smoother than singles, twins, and triples, they still require balancing counterweights on the crankshaft to offset the mass of the pistons and part of the connecting rod. This is overcome by ‘flat’ engines such as those produced by Subaru or Porsche where two banks of cylinders oppose each other and the mass of the opposing pistons and rods act as counterweights. Due to this feature the engines utilising this technology typically run more smoothly than inline engines as well as having a lower centre of gravity and less overall height at the expense of width.

For a motorcycle this layout can be problematic where the heads can create a relatively significant protrusion – as exampled with the BMW ‘GS’ series of bikes. This is one of the main reasons why most motorcycle manufacturers stick to the inline engines that neatly fit within or are slung below the chassis.

To counteract some of the vibrations produced by their large single-cylinder engine, KTM have employed two ‘balance shafts’ in their LC4 690cc engine from 2016 onwards. One resides in the crankcase and the other is in the head, where the exhaust camshaft would normally reside. While this design increases the rotational inertia of the engine, it provides a smoother ride and power output. Many manufacturers employ balance shafts to counteract some of the problematic vibrations from inline engines and it is commonplace to see two balance shafts driven off the crankshaft.

2.6 Engines and exhaust noise

One of the downsides of internal combustion engines is their low efficiency and how they dispose of their waste energy. The product of combustion is energy in the form of heat and most of this energy is absorbed by the gases in the combustion chamber, causing expansion and pressure in the combustion chamber. While some of this pressure is used to drive the piston down its bore, most of what is left is wasted out of the exhaust pipe.

2.6.1 Exhaust Blowdown and effects on noise

There are two parts of the process of how the exhaust gases react leading up to and during the exhaust stroke. An initial pressure wave is formed when the exhaust valve opens (pre-BDC) which is followed by the ejection of the remaining hot exhaust gases on the exhaust stroke. Figure 2-5 is a good indication of how the waves follow each other, with the pressure wave travelling ahead due to its sonic velocity plus the velocity of the particles, followed by the particle flow of the exhaust gases which only has its own, lower, velocity.

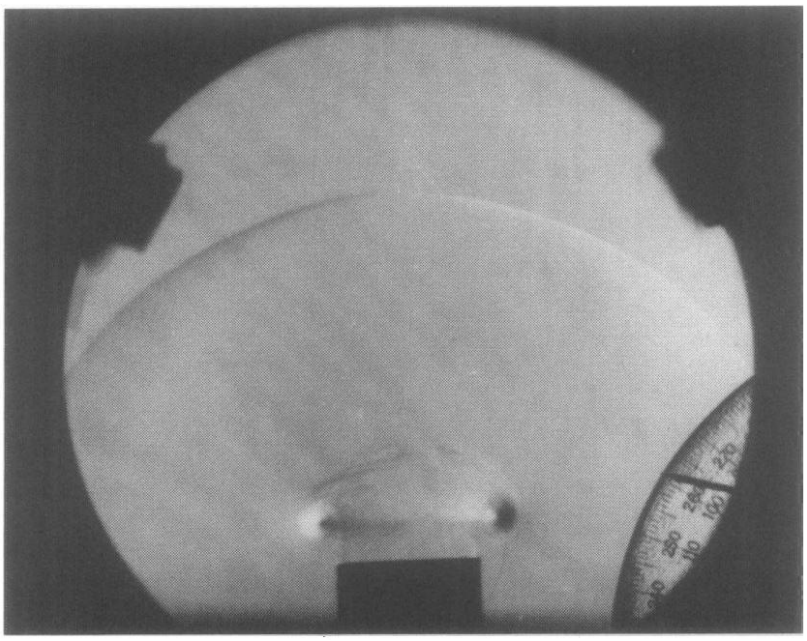

Figure 2-5: Sonic pulse followed by vortex of gas particles (Blair, Design and Simulation of Four-Stroke Engines, 1999, p. 156).

In a typical four-stroke engine the exhaust valve opens pre-BDC on the power stroke to bleed off excess pressure before the exhaust stroke to lessen the pumping loses associated with forcing the exhaust gases out of the cylinder. When the exhaust valve first opens, the in-cylinder pressure is still well above atmospheric pressure and can be 7 bar or more. With the exhaust port at atmospheric pressure a large pressure differential is set up across the exhaust valve. This causes some of the exhaust gases to rush out of the cylinder and cause a sudden "spike" in pressure in the exhaust port. (Kane, 2015)

The only major limiting factor for this sonic pulse is the acoustic velocity in the medium, therefore it will continue to travel through the port and downstream at this velocity. If the pressure differential across the exhaust valve is high enough, the pressure wave can cause a shock wave that propagates faster than the acoustic velocity of the exhaust gases.

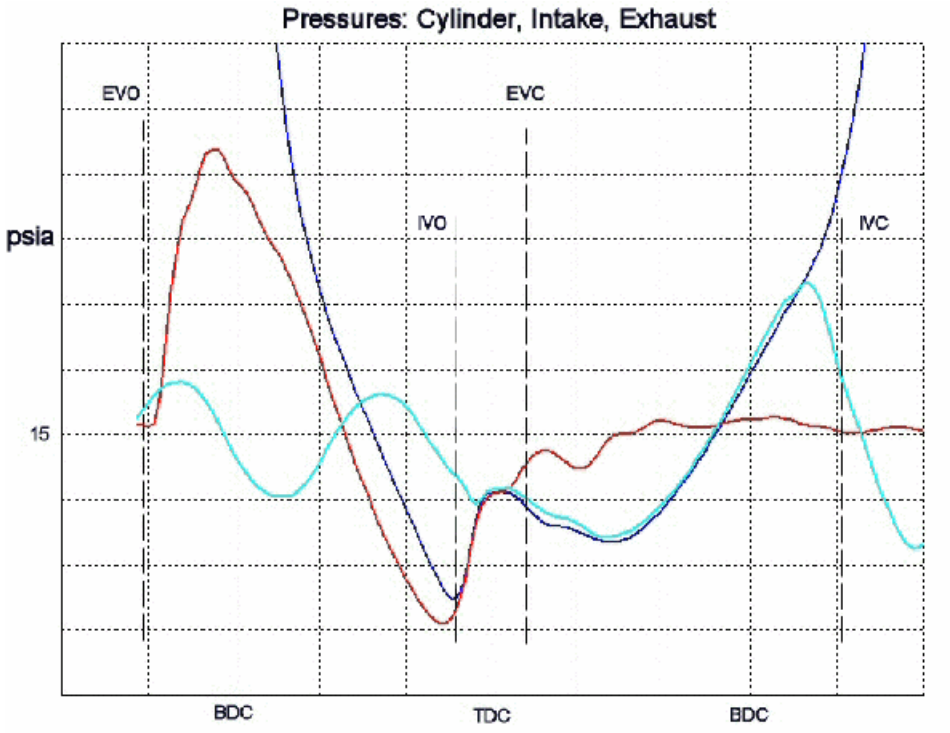

Figure 2-6: Cylinder pressure (blue), Intake Port pressure (teal), and Exhaust Port pressure (red) as a function of crank rotation (Kane, Exhaust System Technology, 2015).

Using Figure 2-6 as a guide, upon the exhaust valve opening the exhaust port pressure rises from atmospheric as the cylinder pressure is released into the exhaust system. The sharp spike seen in exhaust port pressure is due to the extensive pressure differential across the exhaust valve which causes a large instantaneous exhaust particle velocity. This sudden release of pressure induces movement on the exhaust gases while also causing a compression wave that travels at the acoustic velocity (or faster for higher amplitude waves) down the port and into the headers.

The negative pressure seen afterwards in the cylinder and exhaust port is due to resonance tuning as a rarefaction pressure wave has arrived back in the port to assist in removing unwanted exhaust gases from the cylinder. In this instance the length of the exhaust tract has been designed efficiently to produce an expansion wave that arrives back to the exhaust valve on the intake valve opening to draw more air into the cylinder.

As the released pressure wave travels down the exhaust pipe it produces an acoustic wave or potentially a shock wave. Typically this wave has a large amplitude (or volume) as the pressure differential between the cylinder and the exhaust pipe is substancial. The speed at which this pressure wave travels is the sum of the sonic velocity and the particle velocity of the gas flow, however for approximations into exhaust length tuning the

particle velocity can be ignored due to cancelling itself out during the pressure wave's roundtrip back up the pipe to the cylinder.

As discussed by Johan Wall in his Thesis on "Dynamics Study of an Automobile Exhaust System, the excitation from an automobile engine is usually in the frequency interval of 30-200Hz, directly related to the rotational speed and number of cylinders. Typically, these pulses are between 0.1 and 0.4 atmospheres in amplitude with a pulse duration from 2-5 milliseconds, with the frequency spectrum directly correlated to pulse duration. It is not uncommon to see engines producing 100 to 130 dB of noise, with the geometry of the engine having a large effect on the volume produced (Sharmin, Hassan, Rahman, & Al Nur, 2005). While other road noise is discussed in this report, this frequency interval is determined from the number of cylinders of the engine and the rpm range involved.

In its simplest form, the frequency of the wave pulses produced by a four-stroke engine is:

$$f = \frac{RPM * number\ of\ cylinders}{60 * 2}$$

This equation stands for most crankshafts. Subtle differences come into play when dealing with three-cylinder, odd-fire, or offset crankshafts where the frequency will remain the same, however the spacing between pulses will differ. This creates a different tone to the exhaust and can affect the tuning of a muffler or resonator. To get around this issue, many manufacturers run crossover tubes between header pipes to allow any excess in pressure in the tube to bleed off into the other set of pipes and provide a more even flow of exhaust gases to the muffler.

2.7 Engine design and tuning implications on noise levels

The exhaust flow of an engine has a very large part on the noise being produced. This stems from the characteristics of exhaust waves between engines. Where a four-cylinder engine produces an exhaust pulse of ¼ the total exhaust volume for every 180° of crankshaft rotation, a single-cylinder produces a single exhaust pulse for every 720° of crankshaft rotation. This means a four-cylinder will typically sound a lot smoother where the single-cylinder will pulse or 'thud' more.

Simply put, the exhaust pulse frequency for a four-cylinder engine at 5000 rpm will be four-times that of a single-cylinder engine at the same rpm (166.6 Hz vs 41.6 Hz). For certain applications this could mean two completely different silencing techniques are employed between the two engines.

This pulse characteristic also has an effect on the flow needed from a silencing device so as not to choke the exhaust gas flow from the engine. Any choked flow in the exhaust system causes a rise in backpressure and a sub sequential loss in power output.

An easy method by which to demonstrate this effect is to compare the backpressure on the engine with blowing air through a straw. The volume of air in this test is one litre which is expelled over four seconds. A four-cylinder engine has a much smoother exhaust flow which can be likened to blowing consistently through the straw for the complete four seconds, whereas the single-cylinder engine wants to expel all the air in the first second and then rest for the remaining time. While little resistance is felt for the first scenario, you could well 'pop' your ears for the second one.

Some characteristics of an exhaust system need to be specifically tailored to the design of the engine. While the capacity of the engine plays an important role in influencing the diameter of the system, the physical dimensions of the rotating assembly also play a large part in how the gases are expelled.

Take the geometry of the connecting rod and crank for example where an engine with a low connecting rod-to-stroke ratio tends to have more torque at low rpm due to the geometry affecting the piston's acceleration and angle of force acting on the crank. Low rod-to-stroke ratios have the effect of increasing angles between the rod and the bore (which is bad for increasing piston and cylinder wear) and give more dwell at BDC but less at TDC. This inherent feature of a short-rod engine means that it will pull more air in at the beginning of the intake stroke and exhaust more gas towards the end of the exhaust stroke. Bearing in mind we want the maximum force exerted by combustion to occur around 16 degrees after TDC, therefore timing with this engine will need to be advanced compared to a long-rod motor.

The effect of a short-rod motor on the exhaust characteristics is therefore defined by how the exhaust gases are expelled. With an increase in volume nearing TDC on the exhaust stroke a better or larger port will be needed to flow the increasing velocity of gases that occur later in the stroke. A longer rod engine on the other hand can get away with a

smaller or less refined port as the exhaust is expelled in more of an averaged flow rate. In terms of noise being produced, the short-rod motor would have a higher intensity of the exhaust pulse as there is more compression in the sound wave from more gases being expelled in a shorter time, thereby causing a louder volume.

Adjustable ignition and fuelling setups can have an effect on the noise output of the engine. By running an engine lean and/or with retarded timing, the BMEP in the cylinder can be lowered. The lower cylinder pressure causes less of a pressure differential at blowdown, and a lower volume sound wave is produced.

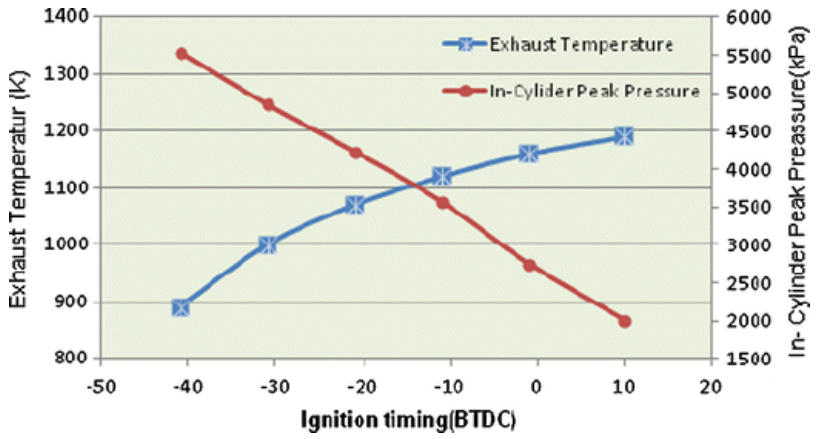

Figure 2-7: Results from testing ignition timing vs torque output (Zareei & Kakaee, 2013).

The graph shown in Figure 2-7 was produced using a test engine set up at 3400 rpm and shows how cylinder pressures drop when ignition timing is retarded. A lower cylinder peak pressure results in a decreased driving force across the exhaust valve which lowers the velocity and energy of the exhaust wave. The outcome of lower energy in the exhaust wave is a lower volume and less noise that needs to be attenuated by any silencing device. Applying a retard to the ignition timing generally causes a decrease in the torque output of the engine and an increase in exhaust temperature (which can damage the exhaust valves) due to any unburnt or still burning gases exiting the combustion chamber. As the gases have not burned in the combustion chamber, their energy has not been used in heating to produce pressure, and this energy is then directed down the exhaust pipe.

The negative issue with retarding timing is the exhaust temperature will rise with more retardation. The extra heat in the gases can be enough to affect the velocity of the exhaust pulse travelling through the medium as the speed of wave propagation changes with a

change in temperature. The same effect could be seen if a muffler designed for the back-end of a vehicle was moved closer to the engine where exhaust gas temperatures are higher.

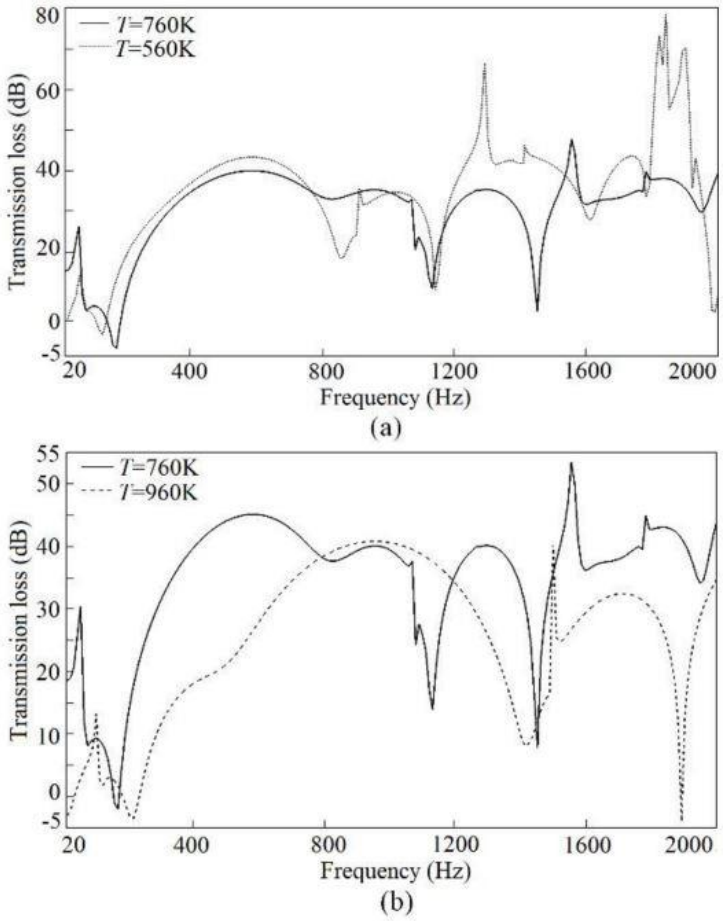

Figure 2-8: Muffle noise attenuation change with regards to gas temperature (Zhang, Fan, & Guo, 2018)

.

Based off the transmission loss graphs above, as the temperature rises in graph (b) the attenuation curve moves to a higher frequency and the acoustic attenuation is reduced at most frequencies. An example of this is in graph (a) where a valley at 850 Hz is moved to 1160 Hz in graph (b) with an increase in temperature from 560 ºK to 760 ºK. Similarly, a peak moves from 1240 Hz to 1560 Hz, while their corresponding TL values are reduced by 10 dB and 20 dB, respectively (Zhang, Fan, & Guo, 2018).

This can be further discussed by using the equation for the speed of sound and varying the temperature of the gas.

$$v_{sound\ in\ gas} = \sqrt{\frac{\gamma R T_a}{M}}$$

As the absolute temperature in the equation is part of the numerator, an increase in temperature would cause a larger acoustic velocity. Another part of the equation is the molar mass where an increase in weight of the gas would lower the velocity of the sound wave. While a minor difference could occur, running the engine rich and producing more hydrocarbons could potentially increase the molecular weight of the gas due to a larger portion of the gas containing CO_2 which weighs in at 44 grams per mole versus oxygen weighing 32 grams per mole.

2.8 Purpose of an exhaust system

An exhaust system functions as a method of safely expelling the combusted gasses from an engine. As the IC engine has advanced through research and development, the exhaust system has improved its functionality to minimise noise levels and lower hydrocarbon emissions, while also improving performance.

Standard exhaust systems on production vehicles are normally designed for power in the rpm range used for day to day driving. They are focused on lowering emissions using catalytic converters and improve on noise suppression using devices such as silencers, mufflers, and resonators. These parts of the system function to attenuate noise levels and produce lower carbon emissions and are requirements that must be followed as part of mass production of vehicles.

In keeping to emissions standards, many road-based engines must incorporate a catalytic converter into the exhaust system. The aim of the catalyst is to convert a proportion of the hydrocarbon emissions into NOx emissions in order to contribute towards the lowering of greenhouse gas emissions from transport based sources. Unfortunately, in terms of functionality the use of a catalytic converter has a negative effect by causing a large rise in backpressure and in addition, it must be located close to the headers to ensure heat gets into the catalyst. However, while this lowers performance of the engine, it does have the helpful feature of quietening the exhaust volume down from the gas travelling through the catalyst matrix.

An important part of the exhaust system is the exit to atmosphere. Typically, the exit is located at the lower rear-end of the vehicle to minimise any drafts or routes that exhaust gases could take to enter the occupants cabin. In most cases for passenger vehicles the exhaust system is a couple of metres long (assuming the engine is in the front of the vehicle) so will increase the weight and complexity of the vehicle. On the other hand, the extra length aids in decreasing the exit temperature of the exhaust gases and allows more space for mufflers or silencers to be placed inline.

2.9 Tuning an Exhaust System

Pipe diameter and length are important factors when designing an exhaust system. As these dimensions set the parameters for the velocity and tuned pipe length, the correct measurements should be as accurate as possible to achieve proper function.

As the exhaust valve opens, high pressure exhaust gas exits into the exhaust runner. This gas has a high velocity which sets up a compression wave in the pipe. By adjusting the pipe to be a certain diameter, the velocity of the exhaust particle flow can be set. From here, the length of the pipe can be tailored to provide a returned inverted wave arriving back at the open valve. This acoustical resonance can create a low-pressure state on the back side of the exhaust valve which helps remove the last of the exhaust gas from the cylinder if timed correctly.

These particular dimensions of the exhaust system will also have an effect on any noise attenuation device through the changing of inlet parameters. An example of such a change could be explained by changing to a larger diameter header or mid-pipe, meaning a larger inlet diameter to a muffler. This larger inlet has an effect on the noise cancelling properties due to the expansion ratio of the muffler changing, as well as the inlet velocity.

Looking at the other side of the engine, intake tuning also relies off these principles but with lower temperatures and pressures. The major difference experienced with exhaust gases are the temperature and velocity involved as the exhaust gas is around 700°C and initially supersonic on blowdown of the cylinder. This makes modelling difficult until the gas slows down and becomes laminar in flow, by which stage most of the wave energy has dissipated (Davis M. , 2015).

2.10 The engine for testing

The engine being used for this research is a 0.223 litre Yamaha engine from their SX-4 Scorpio motorcycle. It is an air-cooled, single cylinder, four-stroke IC engine. The selection of this engine was influenced by its simplicity and reliability, while having readily accessible replacement parts.

The engine's layout is a cross flow head with a single intake and exhaust valve. The single exhaust port helps in simulation as there are no merges or colliding wave fronts upstream, just a single exhaust pulse every two crank rotations. Design is also greatly simplified as there is a single pipe from the head to any silencer or muffler.

While noise tests in FSAE competitions are measured under no-load scenarios, this engine has been attached to a Dynomite water-brake dynamometer to simulate loading conditions that can be found in real-world applications. This allows the effectiveness of the chamber to be understood for different mass flow rates of exhaust gases.

2.11 Types of mufflers for automotive applications

In an automotive application, there is generally three distinct types of sound attenuating devices being used; absorptive silencers, reactive mufflers, and a combination of both.

Absorptive silencers attenuate noise levels by converting the pressure pulses of the exhaust gas into friction, therefore heat, in a fibrous matrix. Typically these silencers are a straight-through design where the fibrous mat is wrapped around a perforated core which the gases flow through. The whole unit is encased in a shell to keep the fibres in while also providing absorption of the frequency pulses from a calculated volume, density, and elasticity of the medium.

Reactive, reflective, or resonant chamber mufflers are designed to use the reflective properties of waves to superimpose and interfere with each other. By reflecting a wave such that it arrives back during the next pulse entry to the muffler, superposition can occur and cancel out some of the incoming wave. The area ratio of the muffler also plays a large part of the noise attenuation where the pressure pulse loses some of its amplitude on expansion into the chamber and will lose more energy by propagating the wave front over a larger area inside of the muffler. Designs will typically have multiple chambers

and passageways to target multiple frequencies, but will be contained in one casing. Most mufflers manufactured nowadays are a combination of both absorptive and reactive style attenuators. This will typically require more space to implement the design, and need closer attention to calculations, but reduces complexity when it comes to manufacturing as every part needed is contained in one unit.

2.12 Muffler Selection

Considering similar engines available is a reliable starting point for selecting a silencing technique. This shows a list of different methods available for silencing a single cylinder engine that are currently in production.

Daniel Potente's study into the design principles for an automotive muffler provide a good introduction into muffler design and advantages of each design. He outlines that reactive (or reflective) mufflers generally consist of a series of resonating chambers and use the phenomenon of destructive interference to reduce noise versus absorptive mufflers that have a perforated core wrapped in insulating material and convert the energy of the sound waves into heat in the absorptive material (Potente, 2005).

Many manufacturers have produced a muffler that incorporates both absorptive and reflective mufflers in one unit. Many late model bikes have a series of reflective-style chambers and an absorptive part incorporated into their design. The chambers target lower-frequency pulses at problematic areas, and the absorptive part takes some volume off the higher frequencies.

Mahindra 2 Wheelers undertook research into improving the transmission loss of the silencer designed for their motorcycle, the Mojo. Their muffler is part resonant chambers, part absorptive silencer. By increasing the length of one of the internal passageways, the Helmholtz resonant frequency of two chambers was modified to work better with the third chamber and increased the transmission loss across the muffler.

Road-based motorcycles generally have to meet more stringent noise and emissions standards so a catalytic converter is common-place for the first component after the headers. The KTM Duke 690 is a prime example of this where the large primary pipe enters the baffle box through a catalytic converter, passes through a reflective muffler, and exits the system via an absorptive muffler with a baffle. This system is designed to

attenuate low frequency noises in the baffle box, then attenuate volume further in the silencer, while still passing emissions by making use of the catalytic converter

Off-road based bikes are different where spark arrestors and perforated core silencers are more commonly found as emissions are less stringent. In general, the smaller capacity of these engines coupled with higher dB limits mean less muffling needs to occur – which allows for a lighter and less restrictive system. A study prepared on trail-bike exhaust noise by Derek Thompson reviewed noise regulations for various regions of the world and compared the noise levels of trail bikes to competition bikes. His results found off-road based bikes to be on average 14 dB louder than the approved level for certification to ride on the road, and those fitted with aftermarket exhaust pipes to be on average 6 dB louder still. This is problematic for countries where trail-based bikes are required to be registered as the bike would not be certifiable for road use (Thompson, 2010, pp. 4-5).

2.13 Selection for a single-cylinder engine

Single-cylinder engines are unique when it comes to noise suppression. Due to a low exhaust pulse frequency and high volumetric flow rate of the exhaust pulse, selection of a design of muffler is quite straight-forward.

"The proper selection of a muffler is performed by matching the attenuation characteristics of the muffler to the noise characteristics of the source, while still achieving the allowable muffler power consumption caused by muffler pressure drop." (Sharmin, Hassan, Rahman, & Al Nur, 2005, p. 1373). This statement outlines the issue with installing a muffler that is not designed for the specific characteristics of the noise source or volumetric flow rate– i.e. installing a reflective muffler onto a race bike designed for high frequencies and high volumetric flow rates. Not only will the flow be impeded, but very little attenuation will occur for any high-frequency noise. It is therefore much more practical to install an absorption based muffler which attenuates noise better at these frequencies and flows better.

This is confirmed by Potente where he states *"As a general rule, reciprocating or positive displacement machines should be attenuated with reactive silencers, and centrifugal equipment should use absorptive silencers."* (Potente, 2005, p. 1373). This statement covers the fact that most rotating or centrifugal equipment operate at higher frequencies and therefore suit absorptive mufflers better, however this is not always true as there are

plenty of domestically-available reciprocating piston engines that produce a high enough exhaust pulse frequency to fall into the absorptive muffler category.

As part of Rolf Jebansinski's study into absorptive mufflers, he undertook testing to confirm whether the theoretical results of a simple perforated-core muffler matched with the real-world results from testing the same muffler. His findings using an engine as a noise source show absorption mufflers attenuate the middle to high frequencies quite effectively but below 250Hz no attenuation is visible for transmission loss. (Jebasinski, 2000). This aligns with the previously discussed literature as at 250 Hz a single-cylinder four-stroke engine would need to be revving at 30,000 rpm to produce this frequency, but a four-cylinder would only need to be at 7500 rpm.

These results in relation to a single-cylinder engine lead to the need to use a reflective-style muffler to best match the exhaust pulse frequency of the engine. In our case the Yamaha engine runs in the 18-80 Hz range, quite low frequencies for muffling. Even second and third harmonics would be muffled by a reflective muffler designed for those tones.

One of the biggest issues presented in Formula SAE and Formula Student teams is how to effectively silence their engines while retaining minimal flow losses in their exhaust system. This task is easier for teams who choose to run a four-cylinder engines as opposed to single-cylinder engines as the characteristics of the exhaust waves favour the readily-available absorptive perforated core silencers. On the other hand, single-cylinder engines have exhaust wave characteristics that suit mufflers made from reactive resonant chambers. To use a perforated core absorptive muffle on a single cylinder would require unusably-long lengths of tube and would lead to packaging and weight issues.

2.14 Conclusion to Chapter 2

Contained in this chapter are the principles on how a four-stroke Otto-cycle engine operates and how this process of converting chemical potential energy to heat leads to producing exhaust noise. Included is the discussion of different engine cycles and in what way variations in geometry can affect the noise being produced by the engine. A description of the Formula SAE competition and how this thesis relates to the event is also explained to show how this style of engine relates to issues faced by teams who enter.

3 Changing the volume – sound waves and their properties

3.1 Introduction to sound waves

For thousands of years, music has been made using some of the most basic wave principles. A relevant example of a musical instrument is the trombone.

A trombone produces sound by setting up an acoustic wave inside a pipe. It is the job of the musician to adjust the length of this pipe to create a resonating wave of a certain frequency or 'note'. At these frequencies the pipe is tuned such that the resonance of this wave produces a note on a scale, and by stringing notes together music is made. To create this acoustic wave the trombone player must vibrate their lips while exhaling to induce vibration in the air inside the instrument. These waves produced oscillate in a similar cyclic fashion to the exhaust pulses from engines.

An exhaust system effectively produces the same result as the trombone where the tuned length and diameter of pipes produce waves at a certain-frequencies to help with performance via scavenging but also quietens the noise made by the engine via interference or absorption.

3.1.1 What is an acoustic wave?

An acoustic or sound wave is the transmission of vibrations through a medium. It is a disturbance of the equilibrium state of that medium and translates via compression and rarefaction pulses from the vibrating source. This infers that sound waves are a longitudinal wave with the direction of travel being parallel to the displacement of the medium, unlike a transverse wave that displaces the medium perpendicular to that of travel (Brown, 2004).

Sound waves only occur in mediums that have particles that are free to vibrate and move, hence sound waves will not travel through the vacuum of space – unlike light or similar electromagnetic waves.

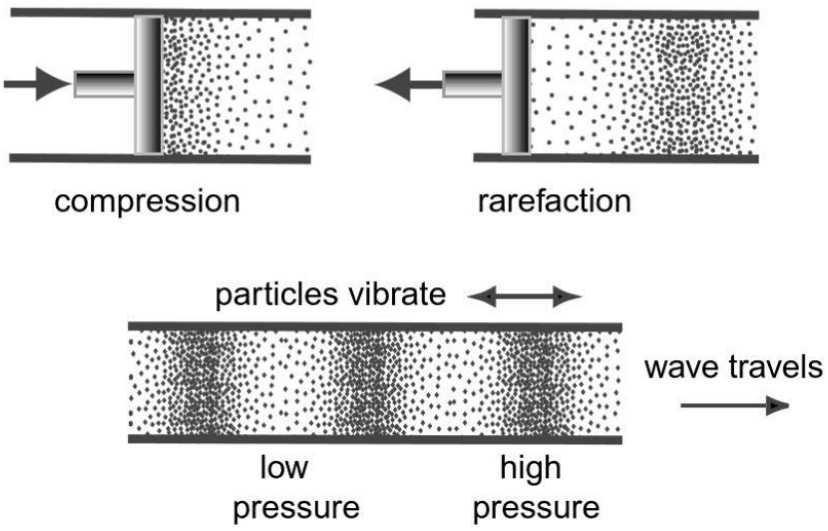

Figure 3-1: Pressure regions of a sound wave (Montwill & Montwill, 2013).

"In low pressure regions, particles are more easily displaced than in high pressure regions, so low pressure means high displacement, and the converse." (Montwill & Montwill, 2013).

A sound wave will travel through a material at the speed of sound of that medium. If the sound wave is forced to travel at higher velocities a 'shock wave' will occur where the medium's molecules are pushed along with great force, creating a shock wave when the bulk of the particles catch up to the wave front. At the velocities needed for a shock wave to occur air acts like a fluid, and while short in length, the sudden change in pressure makes the shock wave followed by a sonic boom audible (Dunbar, 2017).

Another factor to note is the relative velocity of the medium that the sound wave is travelling through. In a piping system a sound wave can travel faster than the speed of sound inside the pipe if taken relative to the system outside of the pipe. This can occur due to the medium or particles in the pipe having a velocity, which can be added or subtracted to the acoustic velocity (speed of sound propagation) within the medium depending on the direction of travel of the wave. Generally the fluid will be at much lower velocities, such as 40m/s, compared to that of the speed of sound. Over long distances this will make a difference in time at which the wave arrives at the end of the pipe.

The frequency (f) of a wave is a measure of the number of repetitions over a timeframe, commonly being measured in Herts (Hz) which is the number of cycles per second. The period of the wave is simply the inverse of the frequency ($T = {}^{1}/_{f}$) and is used to quantify how long one cycle lasts for (typically in seconds). These parameters are very important to wave theory as they are used to find the wavelength (how long the wave is).

$$Frequency\ (f) = \frac{Velocity\ of\ wave\ (v)}{Wavelength\ (\lambda)}$$

3.2 Resonance in pipes, frequency, and wavelengths

As part of basic wave theory, we know that a length of pipe will resonate under certain conditions. A pipe of length L will resonate differently if both ends are open versus if one end is closed. These parameters set the points at where in the pipe the fluid is constrained or can move freely, thus setting nodes and antinodes in the system.

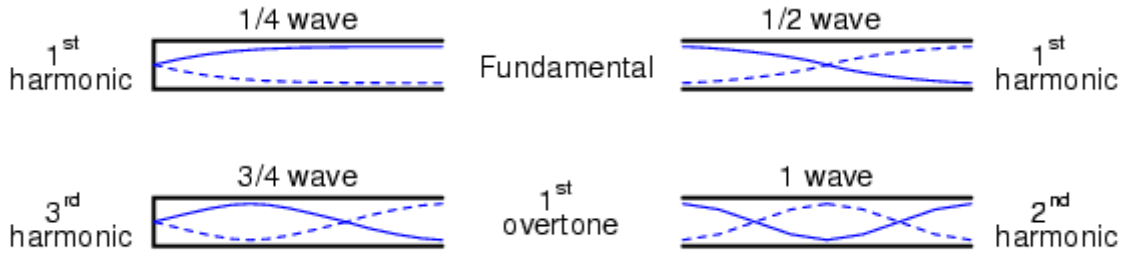

Figure 3-2: Resonance in pipes showing displacement nodal lines (pstir2, 2015).

Displacement nodes occur at a point of zero displacement with their opposite, antinodes, occurring at areas of maximum displacement. As displacement nodes are areas of no displacement, these points are areas where pressure occurs as molecules bunch up.

In an open-open ended pipe, the air molecules at each end are free to vibrate or move, with their only constraint being the elasticity of the medium. These points can be considered as displacement antinodes and are at the location of maximum displacement.

For a wave travelling along an open ended pipe, the returned wave in is inverted due to the nature of the antinode at the end of the pipe. "*Consider a low-pressure region travelling along the tube towards the open end. The air outside is at atmospheric pressure,*

so when the low-pressure region hits the end of the tube air from the atmosphere rushes in and creates a compression wave heading back down the tube. The opposite happens when a high-pressure region hits the end of the tube and rarefaction occurs and travels back down the tube." (Rennie, 2012).

As displacement antinodes occur at either end of the open-open ended pipe, basic symmetry occurs and any whole number of half wavelengths can occur – producing first, second, third, and subsequent harmonic frequencies ($n = 1,2,3, ...$). This leads to the equation for the wavelength in a pipe of length (L) to be:

$$\lambda = \frac{2L}{n}$$

For a pipe with one end closed and the other open, a displacement node occurs on the fixed (closed) end and a displacement antinode occurs on the open end. The shape as seen in Figure 3-2 for an open-closed end pipe shows how the wavelength (λ) is four times the pipe length for the first harmonic frequency. A second harmonic frequency cannot occur in these pipes as the open end will always act as an antinode of maximum displacement. This leads to only odd harmonics being formed ($n = 1,3,5, ...$) in an open-closed pipe, with the equation being:

$$\lambda = \frac{4L}{n}$$

If the end of the pipe is closed, the wave cannot have any particle displacement here and can be considered as a displacement node or a fixed point with no displacement. Pressure will be at a maximum from the incident wave arriving at the wall and reflecting thus making this point also a pressure antinode. If the incident wave is in compression, this compressed region will reflect off the end of the tube and travel back down the tube as a compression wave – the opposite to the previous case. This is the classic echo situation where the reflected pressure wave is an exact image of the incident wave, but travelling in the opposite direction, with a velocity of zero at the closed end (Blair, Design and Simulation of Two-Stroke Engines, 1996).

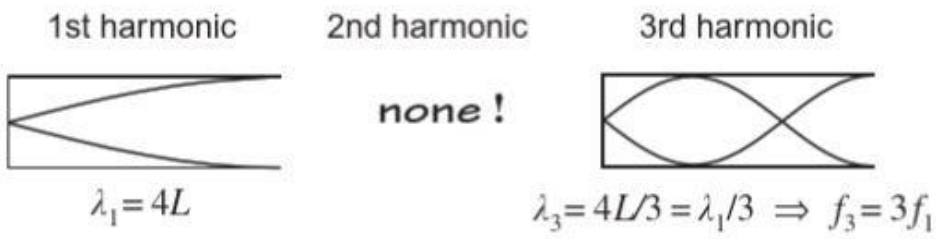

Figure 3-3: Standing waves in an open-closed end pipe (Montwill & Montwill, 2013).

Pipes with a closed-closed end resonate in a similar fashion to the open-open ended pipes where symmetry occurs but have displacement nodes at either end of the tube – little or no movement but high pressure. The equation for the wavelength in terms of harmonics is also the same as the open-open ended pipe.

Figure 3-4: Resonance with nodes at each end (Moebs, Ling, & Sanny, 2016).

This is the same case as a fixed-fixed end string and can be used to model the closed-closed end tube.

For this study, we want to use this characteristic of resonance in pipes to reflect an inverse wave such that it arrives back to the beginning of the pipe when the next wave comes along. The idea of having an inverted wave arrive back at the beginning of the pipe when a wave enters the entrance can be used to cause interference and partially or wholly cancel out the incoming wave – and for the case of sound waves, lower the volume.

An interesting part of the resonance of open-open and closed-closed pipes is the same harmonic resonant frequencies yet opposite nodes and antinodes. If both these resonant characteristics were to be seen in a chamber with a small opening for the inlet and outlet, then interference will occur.

Resonance in a cone is the same as an open-open pipe where $\lambda = 2L$ but acts like an open-closed pipe where pressure is a maximum at the tip of the cone. This special case

is due to the pressure at the tip of the cone acting as a pressure antinode and the open end acting like a displacement antinode – the same as an open-closed tube, but as a sound wave travels down the cone towards the tip, the pressure amplitude increases.

3.2.1 Superposition and interference of waves

Superposition of waves is a phenomenon that occurs when waves interfere and add or subtract from one another to create a larger or smaller amplitude than the individual parts. While it is said the waves can add or subtract, this is physically a change in the medium of which the waves are travelling through – in this case sound waves are travelling through air. As sound waves are a compression and rarefaction of the medium, when two compression waves interfere the pressures are added such that the two pressure waves superimpose and have a higher resultant pressure. In areas where a compression and rarefaction occur, the resultant pressure would be the addition of the two waveforms.

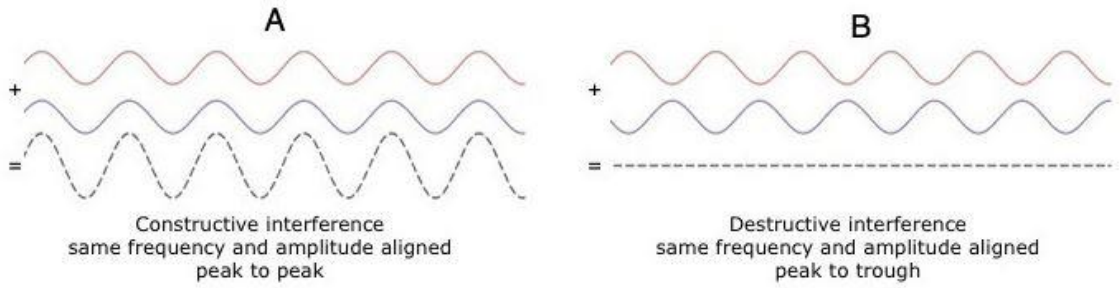

Figure 3-5: Constructive and Destructive interference of sound waves (Science Learning Hub, 2013).

Noise cancellation can occur when destructive interference occurs to a wave. Complete cancellation can occur when identical waves superimpose exactly at 180º out of phase and are of the same amplitude.

A pilot's headset has inbuilt noise cancellation where a microphone converts noise to electrical signals that are then inverted and fed into the headset, producing substantially lower sound levels than that in the cockpit (Montwill & Montwill, 2013). This technique is usually effective for low-frequency noises produced by airline engines.

3.2.2 Sound intensity and volume

The intensity of a wave is measured as transmitted power over an area with the level of intensity being expressed as the dimensionless unit, the Decibel (dB). For acoustic waves, the Sound Pressure Level is a measure of volume relative to a reference value – the Auditory threshold $p_0 = 2 * 10^{-5}\ Pa$. The Sound Pressure Level can then be calculated using the following equation.

$$SPL = 20log_{10}\left(\frac{p}{p_0}\right)\ dB$$

Substituting in a pressure of 0.02 Pa, such as found emitting from your TV at home, a SPL of 60 dB is found.

While high pressures can be created in air, an area of vacuum following a wave cannot be lower than zero Pascal. This sets a limit to the maximum volume for acoustic waves. This level is 194 dB peak as the pressure deviation is equivalent to one atmosphere or 101325 Pa, therefore, for a compression wave at this pressure above atmospheric, the following rarefaction wave will be of the same magnitude but below atmospheric. Any larger pressure and the extra energy begins to distort the wave, creating a shock wave that typically propagates from high-energy impacts or explosions (Staab, 2016).

The pressure ratio (P) for an acoustic pressure wave is a measure of the pressure difference from atmospheric pressure (p_0) to that of a sound wave (p). For a wave with a pressure of 2000 Pa, the pressure ratio would be:

$$P = \frac{p}{p_0} = \frac{103325.2}{101325.2} = 1.02$$

This acoustic wave would propagate at a velocity of c and is dependent on the reference temperature (T_0), reference density (ρ_0), ratio of specific heats for the medium (γ), the gas constant (R), and reference pressure (p_0). For air at 20ºC (293.15 ºK) and atmospheric pressure, the velocity of the acoustic wave is:

$$c = \sqrt{\gamma R T_0} = 343.2\ m/s$$

For larger 'finite amplitude waves' in the region of $P = 1.5$, such as those produced by some engines, the velocity of the shock wave can surpass the local acoustic velocity if the amplitude is high enough and the exhaust tract is long enough.

3.2.3 Shock waves

Shock waves are a high-energy disturbance that occur when the source of the wave propagates faster than the speed of sound in a medium. They propagate in a different manner to regular sound waves with their velocity being a function of their amplitude, but also decay faster as some of the wave energy is dissipated as it travels through the medium. This rate of decay is almost the inverse square of the distance travelled, and when a lower energy is reached, the disturbance will behave as a regular acoustic wave (Grady, 2017).

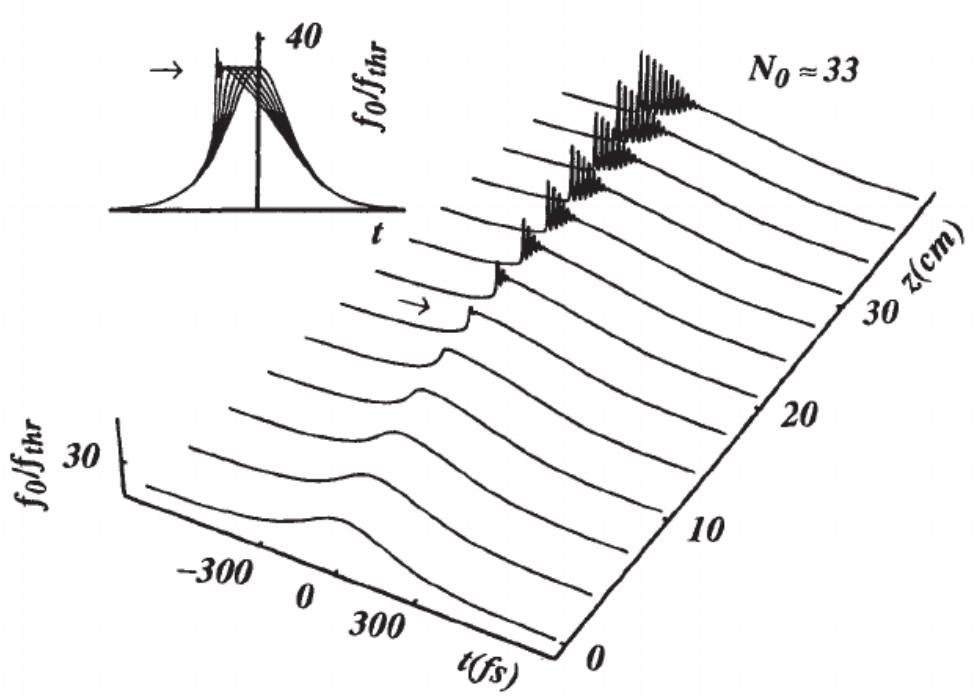

Figure 3-6: Shock waveform showing steepening of wave front (Kaplan, Straub, & Shkolnikov, 2002).

A good analogy of this phenomena is the cresting then breaking of a wave at the beach where some of the water surpasses and rolls over the wave front. This water that rolls over does not continue for long at the increased velocity as its energy is rapidly depleted For a shock wave in air, the head and tail of the wave propagate at the acoustic velocity, but due to the large amplitude of pressure at the peak of the wave the medium behaves differently to normal and the peak propagates faster. After a certain period of time the peak catches up to the head of the wave and overtakes it, causing a shock front to form. While sound waves use little energy during their propagation, shock waves use more energy as the violent propagation of the wave now induces heating of the medium. (Blair, Design and Simulation of Two-Stroke Engines, 1996). In some performance engines at

high compression ratios, shock waves can form in the exhaust pipe, producing loud bangs or pops. This report, however, will focus on using the speed of sound in exhaust gases at 500ºC (as tested) to calculate any wavelength or length of exhaust section.

3.3 Flow losses in pipes

An important part of any fluid flow through a pipe system is how the fluid interacts with the pipe it is travelling in. Different surface finishes, geometry, and temperatures can affect the fluid flowing through the pipe. While most of the affect is upon the velocity of the fluid, the temperature and pressure of the fluid can also be influenced. This literature is not directly studied in this thesis but an overview is important in describing some of the flow features that occur in the exhaust system of an engine.

The pressure losses faced by a fluid travelling through a pipe system can be divided into two categories, major (frictional) losses and minor (local) losses. Sometimes this is called the pressure head and is a measurement of how many vertical units of pressure the fluid has.

$$\Delta p = \left(f_d \frac{L}{D_H} + \sum K \right) \frac{\rho V^2}{2}$$

$$friction\ loss = f_d \frac{L}{D_H} \quad , \quad local\ losses = \sum K$$

Fluids with a higher density or velocity will experience more head loss through a piping system, with longer pipes, smaller diameters, higher roughness, and more local losses causing pressure loss in the major and minor loss categories.

3.3.1 Major losses due to wall friction

One of the restrictions to flow in pipes is the friction between the fluid and the wall of the pipe.

While there can be many values assigned to different surface finishes, in general smoother pipe walls will have less friction and less restriction on flow. The smoother walls of the pipe produce fewer and smaller eddy-currents in the flow of the fluid, creating less restrictions and a smaller boundary layer on the surface of the pipe.

For simplified flow in a pipe, the pressure loss form of the Darcy-Weisbach equation can be used.

$$\frac{\Delta p}{L} = f_D * \frac{\rho}{2} * \frac{v^2}{D_h}$$

This equation is solved to find the pressure loss due to friction ($\Delta\rho$) in Pascals. While some of the parameters from the equation are measurable such as the length, density, velocity, and hydraulic diameter of the pipe, the friction factor is dimensionless and is dependent on the Reynolds number (Re), relative roughness, and the cross section of the pipe if flow is turbulent. For laminar flow, the friction factor can be simplified to $f_D = {}^{64}/_{Re}$ as this flow is independent of roughness. For turbulent flow, relative roughness plays a large factor in flow losses.

In some cases, it has been found that dimpled or rough surfaces are better suit for the task. An example of this is the intake port of an engine. As the mixture entering the intake port is comprised of air containing suspended fuel droplets, a smooth port lacks any turbulence and therefore any method of agitating any fuel that has settled or 'wetted' the walls. The turbulence formed from rough ports helps to remove some of the fuel off the walls and put it back into suspension in the intake charge.

This is contradictory to the work done by Robert N. Wenzel whose theoretical model states that an increase in surface roughness translates into a higher wettability of the surface from a lower contact angle of the droplet if the liquid penetrates into the roughness grooves. (Wensel, 1936). This is due to the geometry of the roughness affecting the plane the contact angle is taken from. This means that the port walls need to be smooth but shaped to induce turbulence, but not rough as the fuel droplets will stick to the walls.

In an exhaust system, a too narrow of a pipe diameter can cause many flow issues. If the diameter is too small, pressure will build during the exhaust stroke of the engine and the exhaust gas will not be expelled fully from the cylinder – causing contamination of the fresh intake stroke and having an effect on combustion.

3.3.2 Minor losses due to bends, fittings, and other flow irregularities

Flow can be interrupted by many irregularities in the surface of a piping system. Flanges, fittings, bellows, and other inline features of piping systems will affect the flow of fluid through them.

Take for instance, a mismatched alignment between the exhaust port and the header pipes of an engine where the exhaust port is partially blocked by the header flange. When the exhaust valve opens and the exhaust gases start to flow out of the port, they encounter a contraction where the flow of these gases is suddenly restricted. This causes a pressure build up on the port side of the flange as the small orifice now does not flow adequately to expel the exhaust gas. This restriction to flow along with its associated flow loss can greatly affect the performance of the engine by not allowing the cylinder to evacuate all its exhaust gas.

Another restriction on the flow of a fluid is an entry to a pipe involving a contraction, such as flowing from a plenum into a runner. The entry coefficient for a protruding tube is much higher than the smooth entry of a bell mouth so it makes sense that vehicle manufacturers use some form of trumpet on their intake runners to keep loses to a minimum. For an exhaust system, the exit of a chamber might be a sudden contraction to a smaller diameter pipe where the flow of the gas encounters the associated flow loss with the step. Minimising the entry coefficient would create less of a head loss on the exhaust gas, and minimising backpressure on the engine.

3.3.3 Enthalpy, entropy, and assumptions

To describe the energy of a fluids system, the terms enthalpy and entropy are used. The enthalpy of a thermodynamic system is defined as the sum of the internal energy and the pressure multiplied by the volume of the system and is used to show how much internal energy a system has plus the amount of work required to make room for it. While the total enthalpy of a system cannot be measured, a change in enthalpy can be – such as work done by pumping or heating will result in a change in enthalpy (ΔH) (Guggenheim, 1959).

Entropy is described as a measure of order or disorder in the universe, with a qualitative measure of being energy dispersal at a specific temperature. In regards to thermodynamics, a lower entropy can be regarded as a measure of the usefulness of a particular quantity of energy, with a low entropy indicating a higher temperature and

therefore more useable energy (Saary, 1993). If a process is assumed to be isentropic it describes the process as being reversible and adiabatic – no heat or mass is transferred to the surroundings. This is an idealised scenario to assist in simplifying problems, and for basic calculations this assumption can still produce accurate results.

3.3.4 Insertion loss vs Transmission loss

Insertion loss is a term used to measure how much noise is attenuated by inserting or modifying a muffler or other sound deadening device in a system, with measurements comparing pre and post modification. Measured in Decibels, this reading is typically taken at the end of an exhaust system to show an end result of the change in a system.

While the Transmission loss of a silencing device is very similar to the Insertion Loss, it is expressed as the measured work on the source side to the silenced side, such as a 20 decibel drop in volume across a muffler, with the value being calculated by the equation:

$$TL = 10log_{10}\frac{W_i}{W_o}$$

This equation is based for a Transmission loss through a cylindrical shape, whereas if the propagation of the wave was spherical, the transmission loss would have a factor of 20 at the beginning which signifies the change in area as the wave propagates.

3.4 Changes in area

Changes in area account for a large part of the attenuation of a reflective-style muffler and for steady-state mass flow rely largely on Bernoulli's principle where the large velocity of the inlet stream is converted to pressure with a lower velocity (assuming no height change of the fluid occurs) during an expansion.

$$p_1 + \frac{1}{2}\rho {v_1}^2 = p_2 + \frac{1}{2}\rho {v_2}^2$$

Applying Bernoulli's equation to a fluid (with a velocity) travelling from a pipe into a chamber of a larger diameter (with negligible velocity), the velocity of the wave is converted into pressure due to the sudden loss of velocity.

This principle works with steady-state flow of a fluid to describe how pressures and velocities change with changes in pipe diameter, however in the case of an oscillating wave such as in an exhaust system, this method is inadequate to describe the properties of both the fluid flow and the acoustic wave. In these scenarios, the velocities of both the acoustic wave propagation and the medium need to be investigated as waves with high energies can dramatically affect the flow of the medium.

3.4.1 Entries and Exits

As discussed earlier, the entry of a pipe can be in many shapes with each design having different flow losses attached to them. It is important to accurately predict the flow loss and find if any major flow restriction will occur as a high entry coefficient can cause backpressure issues. An exit of a pipe can be considered anechoic where the change in pipe diameter is large or the fluid is exiting the system. This is the case for a tailpipe exit out the back of a vehicle as the fluid in the pipe is exiting into atmosphere, essentially a large reservoir. There is less of an exit coefficient present with exits when compared to inlets, so designs such as protruded exits can be used to help reduce reflected pulses from entering back through the exit.

3.4.2 Sudden changes in area

Sudden changes in area occur where the area of the pipe system changes rapidly, such as the exit or entry of a pipe to a plenum. As the diameter of the plenum is generally much larger than that of the connected pipe, a sudden change in diameter occurs that will affect the parameters of the wave travelling through it.

A CFD study into the flow field and pressure loss of a truck muffler had an interesting conclusion that the inlet velocity of the muffler has a great influence on the pressure loss of the muffler whereas the pressure loss of the muffler increases with the increase of the inlet flow rate (Xu, Zhou, & Li, 2015). Based on the finite volume method of designing a muffler with boundary conditions set as the muffler shell, this result indicates that a faster inlet velocity creates a larger ‘vortex’ in the initial expansion of the muffler, causing a snowball effect that reduces the noise levels exiting out the tailpipe.

As most reflective style mufflers have at least one chamber the exhaust has to pass through, the higher inlet velocity would dissipate more energy and have lower pressures

when exiting the muffler. Using Bernoulli's equation for an inlet pipe to a chamber, a higher velocity in would result with a larger pressure wave within the chamber but still maintain velocity in the chamber if the same mass flow rate was maintained between tests.

The basic difference between calculating pressures and flow rates for a sudden enlargement or contraction is the flow in the duct is considered as one-dimensional where in the plenum or volume it is considered to be three-dimensional, and where the velocity in the plenum is low, a change in the amplitude of the transmitted wave and a reflection will occur (Blair, 1996).

Sudden changes in area with included angles greater than 45º have different flow properties to low angles, but still have a pronounced impact on the flow losses when it comes to steady state flow.

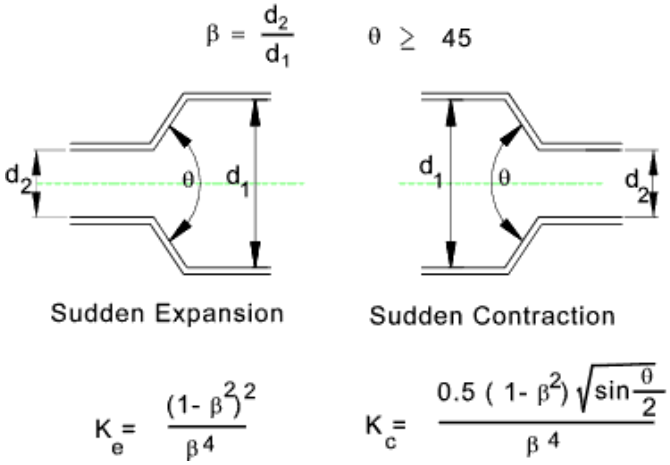

Figure 3-7: Losses for diameter changes in pipe systems (Beardmore, 2013).

A sudden expansion can act like an exit of a pipe if the second diameter is large enough and is not reliant on the angle of the exit. By changing the area ratio of the pipe from two to three times the inlet diameter will see a loss coefficient jump from 0.5625 to 0.7901, showing (theoretically) a larger chamber will have a larger effect on the flow of the fluid.

This is not the case for the opposite end of the muffler where the contraction of a pipe can cause a great effect, as seen by a change from an area ratio of one- half to one-third increases the loss coefficient from six to 36.

In pulsed exhaust flow where the level of noise attenuation needs to be obtained, the pressure changes in each section of the pipe need to be calculated. If the area ratio ($A_r = \frac{A_2}{A_1}$) of a sudden expansion or contraction is in the band of

$$\frac{1}{6} < A_r < 6$$

Then the superposition pressure at the plane of the junction can be assumed to be the same in both pipes at the instant of superposition, inherently being an isentropic process. While limited, this model is "remarkably effective in practice" (Blair, 1996, p. 98).

This method is based on Benson's theoretical solution for junctions where the plane in-between the runner and plenum, or any two locations, has the same superposition pressure. Benson's theory assumes the process is isentropic, so can be limited for more complex problems.

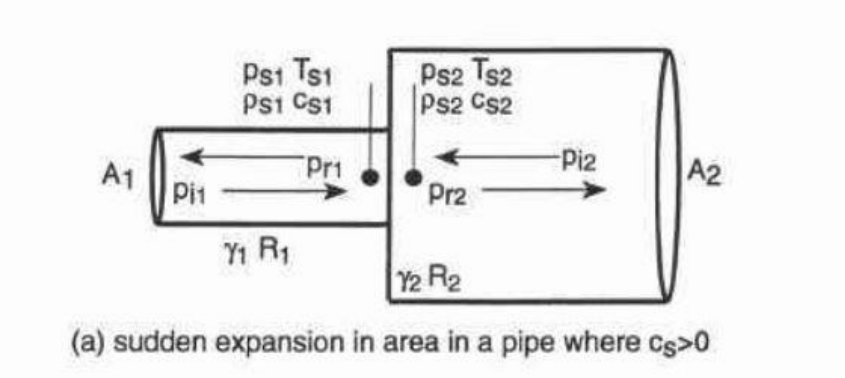

Figure 3-8: Sudden expansions in a pipe (Blair, Design and Simulation of Two-Stroke Engines, 1996, p. 98).

For example, consider an incident pressure wave, p_e, of pressure ratio of 1.2 reaching a sudden expansion of $A_r = 2$. Assuming the gas is air and under normal conditions, the pressure amplitude ratio of the incident compression wave is $X_{i1} = 1.02639$.

By using the following equations, the pressure amplitude ratios of the reflected waves at the boundary can be found.

$$X_{r1} = \frac{(1 - A_r)X_{i1} + 2X_{i2}A_r}{1 + A_r} \quad and \quad X_{r2} = \frac{2X_{i1} - X_{i2}(1 - A_r)}{1 + A_r}$$

These values are $X_{r1} = 0.9912$ and $X_{r2} = 1.01759$.

This leads to pressure ratios for the reflected waves of $P_{r1} = 0.940$ and $P_{r2} = 1.130$ which show the sudden enlargement acting like a slightly less effective open-end (at $P_{r1} = 0.8293$). In this scenario, the incident pressure wave reflects a rarefaction wave

back up the pipe, and propagates a compression wave of a smaller pressure ratio into the larger pipe. The difference in pressure between the incident wave and the wave post expansion is in the region of 7100 Pa, a significant loss in sound pressure. Converting to a sound pressure level, the sound level has dropped from 160 dB to 156 dB.

Working on from this, now assume the incident wave is travelling to a sudden contraction. This scenario is different as the loss coefficient of the inlet to the contraction needs to be factored in to the calculations and is due to the assumption of non-isentropic flow of the gases. In reality, isentropic flow occurs and losses are formed at the inlet and outlets of the pipes. Once factored in, the pressure loss of the wave can be found through the change in area, and following a similar process to the previous one we can find an estimate for the pressure at the plane of the contraction. From here we are able to use loss coefficients on the entry based on the mass flow rate and applicable geometry to find the pressure head loss from the contraction (Blair, 1999).

This example shows that an incident pressure wave arriving at a sudden expansion into a plenum will reflect a rarefaction wave of a lesser pressure ratio back up the pipe, while also propagating a compression wave, also of a lower pressure ratio, into the plenum.

3.4.3 Volume attenuation for sudden changes in area

The sudden expansion and contraction in a chamber-style muffler causes sound waves to reflect and interfere with each other. This is an efficient method to attenuate low frequency sounds that have large amplitudes. Results show that larger expansion ratios in chamber mufflers result in larger transmission loss (Potente, 2005).

This is shown through the following plane-wave equation:

$$Attenuation = 10log_{10}\left[1 + \frac{1}{4}\left(\left(A_r - \frac{1}{A_r}\right)^2 sin^2(kl)\right)\right]$$

Where A_r is expressed as the area ratio from the pipe to the chamber, l is the length of the chamber, and $k = \frac{2\pi f}{c}$ is the wave-length constant, wave frequency divided the speed of sound of the medium. This equation is just a simplified version of the transmission matrix for a simple resonant chamber and is only designed for low frequency calculations

below the cutoff frequency, the value of which can be found by substituting in the speed of sound and the diameter of the largest pipe in the system into the equation:

$$f_c = 1.84\frac{c}{\pi D}$$

Substituting in a larger value of A_r into the attenuation equation yields a larger transmission loss of the muffler. Varying the length of the chamber or the frequency simply changes where the bulk transmission loss is occurring as the attenuation curve is a function of the muffler length.

A requirement for a larger attenuation value is a large value for the area ratio, with the effect of muffler length having little effect on the peak attenuation - but moving the frequency at which it occurs. The cyclic nature of attenuation is also apparent where a muffler length is the integral multiple of one-half the wave length (Davis, Stevens, Moore, & Stokes, 1953).

3.4.4 Gradual changes in area

As opposed to sudden changes in area, gradual changes in the area of a pipe or duct can be done via tapered sections to promote different properties to the expansion of particle flow or wave propagation.

By definition, the process in a tapered conical section is more gradual and efficient from being spread out in terms of both length and time, and has a more pronounced effect in performance over a larger speed range. A practical method of analysing the geometry of tapered pipes is to divide the nozzle or diffuser into sections of equal length and take the area at that point to be the mean value (Blair, Design and Simulation of Two-Stroke Engines, 1996).

Conical sections have been studied before, with the noise attenuation of convergent and divergent cylindrical ducts being tested by Amit Kumar Gupta of IET-Devi Ahilya University.

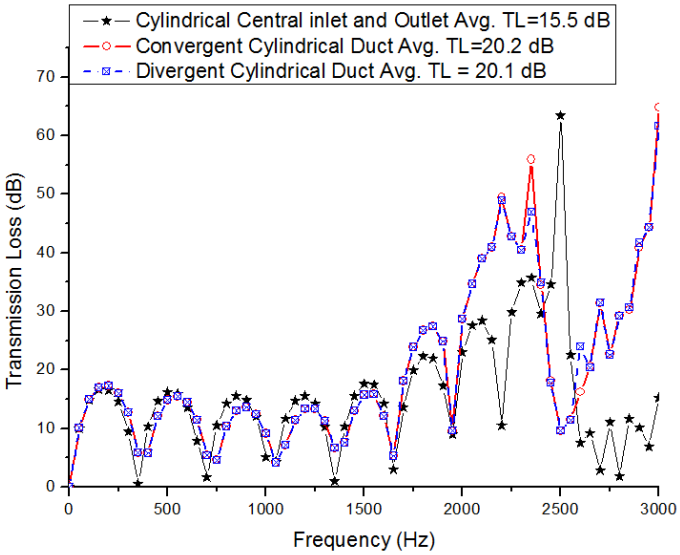

Figure 3-9: Transmission loss for different shape changes in a duct (Gupta, 2016).

By using an amplifier and speaker setup to create a load and by testing from a range of 1-3000 Hz, Gupta's results show that both conical sections have up to a 6 dB transmission loss over a standard cylindrical section.

The transmission loss is evaluated for the three different duct shapes which have the same gas volume. The result shows that the maximum attenuation is achieved by the convergent duct as compared to the two other cases. The transmission loss curves show that the taper muffler is able to attenuate the noise level from mid to high frequency zone while in the low to mid frequency zone the behaviour of all the ducts are similar (Gupta, 2016, p. 781).

These results show that conical sections have a pronounced effect on the transmission loss of an exhaust system at higher frequencies. This could have been due to the way the waves propagate into the conical sections tested versus into a chamber where flow separation could occur and muffle the noise in different ways. Another interesting point is how the conical sections also provide similar muffling to a regular non-tapered chamber.

These results are in contrast to a study conducted at the Langley Aeronautical Laboratory where *"Tapering either or both ends of the chamber has little effect on the muffler performance except for some loss of attenuation near 700 cycles per second"* (Davis, Stevens, Moore, & Stokes, 1953, p. 14). At lower included angles the conical sections could act as a horn, decreasing the effectiveness of the muffler at higher frequencies.

3.4.5 Volume attenuation for gradual changes in area

An applicable equation for tapered sections on noise attenuation can be used under the assumption that the length of the muffler is measured from the longitudinal centre of the tapered section. This equation is, again, a simplified version of the transmission matrix solely for tapered chambers, based off the four-pole method.

$$Attenuation = 10log_{10}\left\{\left[1 + \frac{\left(\sqrt{A_r} - 1\right)^2}{\sqrt{A_r}}\left(\frac{1 - \cos\sigma}{\sigma^2}\right)\right]^2 + \left[\frac{\left(\sqrt{A_r} - 1\right)^2}{\sqrt{A_r}}\left(\frac{1 - \sin\sigma}{\sigma^2}\right)\right]^2\right\}$$

Using the same notation for the area ratio, A_r, and $\sigma = 4\pi\frac{l^t}{\lambda}$ where l^t is the length of the conical (tapered) section and λ is the wavelength, an approximation for the attenuation of the muffler can be calculated.

Another method of finding the transmission loss through a conical section is by looking at the pressure change through dividing the cone into different sections.

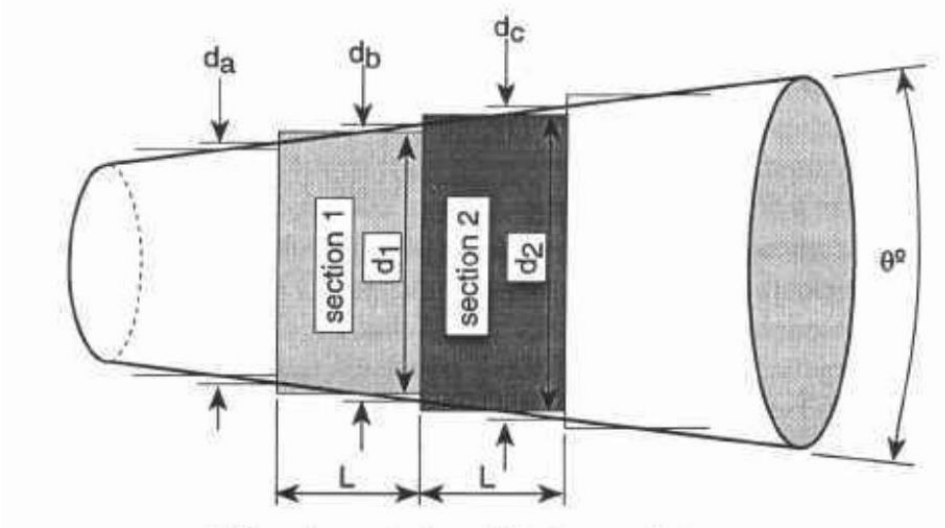

Figure 3-10: Dimensioning of a tapered pipe (Blair, Design and Simulation of Two-Stroke Engines, 1996).

The area and effective diameter of section 1 can therefore be shown as:

$$A_1 = \frac{A_a + A_b}{2} \quad and \quad d_1 = \sqrt{\frac{{d_a}^2 + {d_b}^2}{2}}$$

The process from this point is just an iterative version of the sudden expansion equations for each smaller step. This shows that many lower expansion ratios occur at smaller steps when a compression wave enters the taper when compared to a sudden expansion. Depending on the length selected for each section, this method can require a lot of processing power and a robust model to work from. Another effect on the calculations is if flow separation occurs from the walls of the conical section where the process should be amended to replace the momentum equation for the constant pressure equation in an attempt to simulate a greater entropy gain from separated flow.

3.5 The four-pole method.

Based on acoustic filter theory, the four-pole method simulates an acoustic system combining a volume chamber with inlet and outlet tubes.

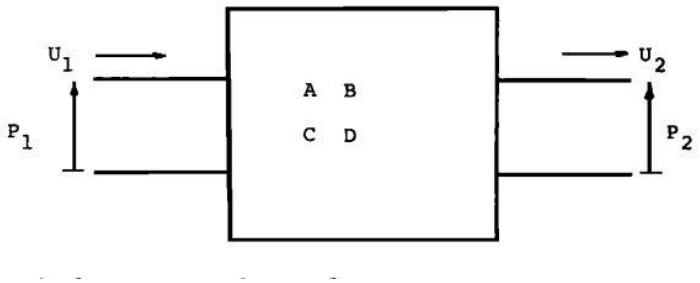

Figure 3-11: Acoustic four-pole network analogy (Young & Crocker, 1975).

The input side of the system has gas particles that vibrate sinusoidally with a velocity amplitude of U_1 in response to an applied pressure amplitude P_1, where the outlet side asserts a pressure amplitude P_2 on the input side of some further system, sharing with it a common particle velocity of amplitude U_2. The four-pole equation is then formed where $A, B, C,$ and D are known as four-pole parameters.

$$\left\{\frac{P_1}{U_1}\right\} = \left|\frac{A\ B}{C\ D}\right|\left\{\frac{P_2}{U_2}\right\}$$

Of advantage are the four-pole parameters that only characterise the system for which they are determined. This allows for inline multi-chamber systems to have each element calculated individually. At the equilibrium condition, the four-poles are

$$A = \left.\frac{P_1}{P_2}\right|_{U_2=0} = 0, \qquad B = \left.\frac{P_1}{U_2}\right|_{P_2=0} = \left. -i\frac{\rho\omega P_1}{\partial P_2/\partial n}\right|_{P_2=0},$$

$$C = \left.\frac{U_1}{P_2}\right|_{U_2=0} = \left. i\frac{\partial P_1/\partial n}{\rho\omega P_2}\right|_{U_2=0}, \qquad D = \left.\frac{U_1}{U_2}\right|_{P_2=0} = \left.\frac{\partial P_1/\partial n}{\partial P_2/\partial n}\right|_{P_2=0},$$

The subscript $U_2 = 0$ indicates a blockage of the outlet tube and $P_2 = 0$ indicates zero pressure at the outlet.

For a simple muffler, there are three major portions to the boundary surface.

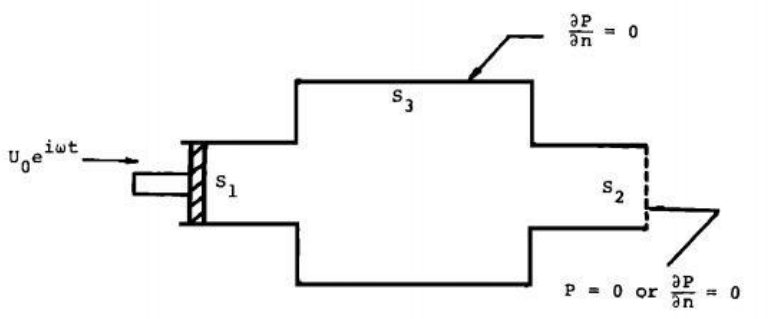

Figure 3-12: Boundary surfaces for a simple muffler.

In Figure 3-12, S_1 is a kinematic boundary where the acoustic velocity U_0 is prescribed; S_2 is a geometrical boundary when blocked, but a dynamic boundary when opened; S_3 is a geometrical boundary which covers all the rigid walls of the system (Young & Crocker, 1975). By connecting both ends of the chamber to a non-reflective impedance, ρc, the transmission loss equation can be derived.

$$TL = 20\log_{10}\left\{\frac{\left|A + D + (\rho c)C + \frac{B}{\rho c}\right|}{2}\right\}$$

Then by substitution of the four-pole constants under the equilibrium state the basic four-pole equation based on the finite element idealisation is formed. Proof of this theorem is

provided in many acoustics and mufflers textbooks, with many research papers being published about modelling using this method.

While the four-pole finite-element approach is able to be applied to more complex shapes, this research focusses on simple chambers of which plane-wave theory will satisfy the graphing and theoretical calculations. For mufflers designed with multiple parts internally, evaluate each part piece by piece along the direction of flow.

3.6 Resonant Chambers

For many years mufflers and silencing devices have used resonant chambers to assist in attenuating noise. As discussed earlier, there are two main parts to this chamber; the resonant interference and the compressible gas inside.

3.6.1 Resonant frequency

As discussed earlier, a resonant chamber acts as a closed-closed and open-open end pipe where displacement nodes lie at either end of the pipe. As the pressure antinodes in this case are areas of high pressure, we can use these points to help attenuate incoming waves. The theory behind this is by reflecting a pressure wave off the end wall that arrives back at the start of the chamber the same time as a rarefaction wave enters, the waves destructively interfere and lower the output volume. This would mean the returning wave needs to be 180º out of sync, or return have travelled half the wavelength. This can be accomplished by setting the length of the chamber be equal to one quarter of the target wavelength, such that the wave travels to the end and back.

"The cyclic nature of the attenuation curve is evident with the attenuation dropping to zero for frequencies at which the muffler length equals an integral multiple of one-half the wave length $\lambda/_2$" (Davis, Stevens, Moore, & Stokes, 1953, p. 13).

If a target frequency for muffling was at 6000 rpm for a four cylinder four-stroke engine, this would indicate a frequency of 200 Hz. If we take the speed of sound in the medium to be 343 m/s then we know the wavelength will be 1.715 m, then the chamber needs to be ¼ of the wavelength, so a chamber of 0.43 m would be a good starting point.

3.7 Quarter Wave Resonators

Like the resonant chambers, side-branch resonators or quarter wave resonators rely on the principle of noise reduction through destructive interference. These resonators are mounted to the side of an exhaust pipe and return a wave of inverse phase to the main pipe to interfere and cancel some of the original wave out. As the chambers are effectively a length of pipe with a closed end, by making the length of the pipe equal to $\lambda/4$ an inverse wave will return to the source at the start of the next peak.

$$TL = 10log_{10}\left(\frac{tan^2(kl) + 4(\frac{S}{S_B})^2}{4(\frac{S}{S_B})^2}\right)$$

One important part of these resonators is placing them at nodes along the length of the exhaust system so that they can affect the areas of highest pressure. Their effectiveness is influenced by the ratio of the main tube area to the side branch area (S/S_B).

3.8 Helmholtz Resonators

The Helmholtz resonator is a style of chamber that relies on the compressibility of a fluid to resonate a mass. It is typically seen as a side-branch connected to a chamber on exhaust or ducting systems where a specific frequency is targeted for attenuation.

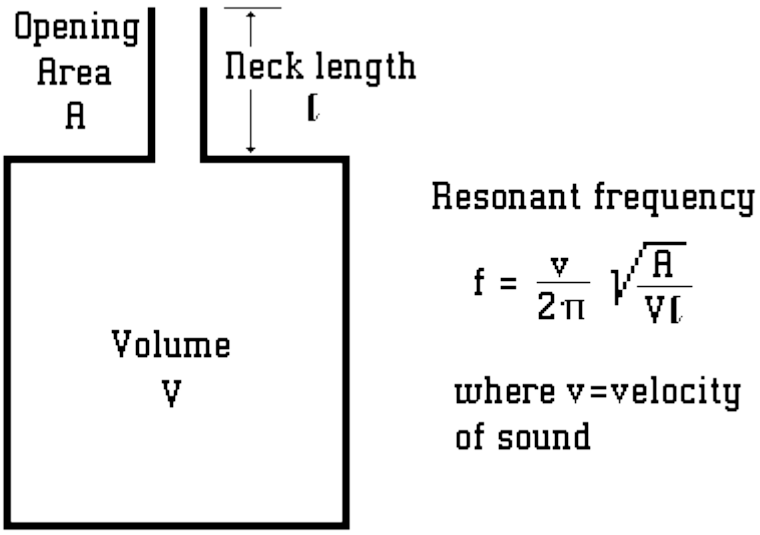

Figure 3-13: Helmholtz resonator formula (Russell, 2019).

A basic example of a Helmholtz resonator is a bottle. By blowing across the top of the bottle, a resonating frequency can be established. The principle behind this resonance is the mass of the air in the neck of the bottle is acted upon via the air being blown across the top of the bottle. The resonance occurs as the air in the body of the bottle acts as an oscillating spring system, drawing air in and out of the neck of the bottle and producing a note. Varying the volume in the body of the bottle acts to change the effective spring rate of the compressible air. By filling the bottle up with some water to decrease the volume of the chamber, the pitch will increase accordingly from the higher spring rate. Empty the some and the pitch of the note will drop due to the larger volume of air in the chamber imitating a softer spring.

$$TL = 10log_{10}\left[1 + \left(\frac{{}^{c}/_{2S}}{{}^{\omega L'}/_{S_B} - {}^{c^2}/_{\omega V}}\right)^2\right]$$

Once again, the transmission loss is a function of the main tube area to the side branch area, but includes an effective length of the side branch, L', to account for the length of the neck before the body.

One important aspect of a Helmholtz resonator is its location of attachment on the pipe it is acting on. Like a side-branch resonator, it should be placed on an antinode of the pipe to achieve better attenuation and be tuned precisely for a set frequency, or multiple resonators used for a band of frequencies (Forouharmajd, Nassiri, Monazzam, & Yazdchi, 2015).

3.9 Mufflers and noise attenuation

Many mufflers have been designed using multiple chambers and resonators to attenuate noise at the target frequencies of the source, while being packaged into one unit. During the design process there are numerous functional requirements that should be considered when transferring the calculations into a physical object. Such functional requirements may include adequate insertion loss, backpressure, size, durability, desired sound, cost, shape and style (Potente, 2005). These features should be examined as most are important parameters that will directly affect the design.

3.9.1 Grades of Mufflers

A generic guide for grades of mufflers was published by the Electrical Generating Systems Association which groups silencing devices by their decibel reduction. At the time of publishing there was no standard for how much noise should be attenuated by a muffler so this standard attempted to group the effectiveness of each muffler into groups. EGSA Classes 1-8 cover the decibel reduction range with Class 1 ranging from a 10-15dB reduction and Class 8 ranging from a 45-50dB reduction (Electrical Generating Systems Association, 2014). While mainly used for industrial equipment, this guide can be applied for most pieces of equipment needing a muffler of a certain transmission loss – typically for Health and Safety precautions. Selection is simple using this guide as once the spectrum of noise for the engine has been plotted and the target frequency and sound level found, a grade is selected that will bring that volume down to a certain standard.

3.9.2 Backpressure

Backpressure is a measure of how much resistance occurs through a system when a fluid flows through it. In our case this system is considered to be the exhaust system with the inlet coming from the exhaust valve and the outlet being the tailpipe exiting to atmosphere, but generically is considered as the restriction to fluid flow through a system, causing a rise in pressure, resisting the flow of the particles.

In its simple parts, backpressure is the resultant friction and other flow losses experienced by the exhaust gases as they travel through the exhaust system causing a rise in pressure as their velocity drops. While based on geometrical features, this parameter is also

dependent on volumetric flow rates where frictional losses increase with larger velocities and smaller hydraulic diameters.

3.9.3 Size, shape, and style

While most mufflers are primarily dictated by function, most will need designing to fit within certain space constraints. This can cause issues when it comes to the performance of the silencing device as lower target frequencies generally require longer or larger dimensions to be effective.

In a study done by Eastern Mediterranean University into maximising the transmission loss of a muffler, the results showed that the variation in the out-take area of muffler had no distinctive effect on the Transmission loss, however the variation of the inlet tube was more effective at attenuating noise (Kermani, 2015). Further findings from this study indicated that increasing the lengths of all inlet, outlet, and muffler body combined with a larger outlet diameter would result in a larger transmission loss.

"It was found that among various geometrical factors, the ratio of change of the silencer cross-sectional area is the most important for effectively attenuating the shock wave and supressing the noise" (Sekine, Kudo, Onodera, & Takayama, 1995).

An increase in the perforated-core length will equate to a larger transmission loss across the muffler, with a larger perforated-area of pipe allowing for a lower turbulence intensity than the fewer perforations present in a shorter length (Saeid, 2013). This study also suggests that larger perforations will do a similar effect to increasing the length.

"Based on our study, it was found that the intermediate pipe diameter and tail pipe diameter have higher influence in the lower speed range compared to the number of baffle holes in the end of the muffler having an influence in the higher speed range." (Chikurde & Mihnish, 2013, p. 10).

3.9.4 Durability

Over time an absorptive muffler will get clogged from carbon particles or the material will burn off and require repacking, meaning a lower insertion loss. Reactive mufflers are generally more durable due to the lack of packing material. (Potente, 2005)

Given the conditions of a typical exhaust system found on vehicles and machinery, it must be constructed from a resilient material. Commonly, stainless steel or other grades of

steel that can be aluminised are used for this purpose. This is due to their resistance to rusting, durability, and cost.

3.9.5 Sound quality

Most instances that require a silencing device are required to remove volume over the whole spectrum of frequencies. Select cases require volume to be attenuated in specific frequencies, or certain frequencies to be let through. These qualities can all be adjusted by the designers of the selected silencing device, with many high-end vehicle manufacturers opting for specific sound characteristics from their vehicles.

3.9.6 Cost

Among many things, cost is a very important factor for many manufacturers. While a polished 304 grade stainless steel exhaust system with multiple tuned resonators fits well in a performance car, your archetypal grandmother would not need this exhaust on her Swift. Instead, a cheaper aluminised or 400 grade steel that is relatively light, durable - and long-lived is used. Recent trends seem to indicate manufacturers are moving towards sheet metal parts and/or doping in elements such as silicon for better mechanical properties. (Rajadurai, Afnas, Ananth, & Surendhar, 2014). Keeping machining processes simple also helps with the cost of manufacturing, and manufacturers choose to use pressed or folded sheet metal parts to construct their mufflers and silencers.

3.10 Research aims

After reviewing the available literature on engines, mufflers, and acoustic properties of audio waves, the aim of this research is to evaluate the effectiveness of the transmission loss equations to predict acoustic attenuation and their applicability on real-world situations. With previous studies focussed on sharp tapers and sudden changes in area, an aspect that would be beneficial is looking into shallow tapers and their effectiveness on attenuating noise. Another point of difference will be evaluating the equation's validity when compared to audio recordings from a test engine with exhaust chambers installed, and making a prediction as to the design of a muffler for the KTM engine run in WESMO's WP-18 car.

4 Methods and Experimental

This chapter focusses on calculating and modelling the Transmission Loss equations, followed by building an exhaust test rig capable of testing mufflers of different parameters. Modelling of the exhaust chambers is done based on the Transmission loss equation for a chamber with tapered ends, with results plotted and compared with the recorded values from testing with exhaust chambers.

4.1 Modelling

Before moving on to real-world situations, the Transmission Loss equations need to be calculated and graphed.

4.1.1 Calculations for acoustic velocity

Simple modelling of the exhaust chambers can be done by using the plane-wave transmission loss equations found in Chapter 3 for a resonant chamber and tapered sections. These equations can be used for each of the designed chambers in 20 rpm intervals with not much processing power needed. The results can also be compared to chambers of sudden increases in area to see the effect the taper has on the attenuation curves.

Along with this simplified transmission loss calculation, rearrangement of the variables will allow for the length of the chamber to be found if target frequencies and the attenuation amounts are known.

Firstly, the speed of sound in the exhaust gas is needed. Following the example provided by Gordon P. Blair, the properties of exhaust gas are as follows:

$$R_{exh} = \Sigma\left(\varepsilon_{gas} R_{gas}\right) = 0.125\left(\frac{8314.4}{44.01}\right) + 0.141\left(\frac{8314.4}{18.015}\right) + 0.734\left(\frac{8314.4}{28.013}\right)$$
$$= 307\ J/kgK$$

Next, C_P, C_V, and γ values for the exhaust gas are calculated,

$$C_P = \Sigma\left(\varepsilon_{gas} C_{P\,gas}\right) = 0.125(1154.43) + 0.141(1765.36) + 0.734(1129.13)$$
$$= 1222\,J/kgK$$

$$C_V = \Sigma\left(\varepsilon_{gas} C_{V\,gas}\right) = 0.125(965.51) + 0.141(1303.83) + 0.734(832.33)$$
$$= 915\,J/kgK$$

$$\gamma = \frac{C_P}{C_V} = \frac{1222}{915} = 1.33$$

Then the acoustic velocity of the exhaust gas can be calculated.

$$c_{exh} = \sqrt{\gamma RT} = \sqrt{1.33 * 307 * 773} = 563\,m/s$$

This value assumes the exhaust gas is near the stoichiometric ratio for petrol, 14.7:1, and at 500ºC or 773ºK. From here, we can find the cutoff velocity for the transmission loss equation. As testing will be on chambers of both 100mm and 120mm in diameter, the cutoff frequency calculations for each are as follows:

Cutoff frequency, 100mm diameter chamber,

$$f_{c,100} = 1.84\frac{563}{\pi 0.1} = 3296\,Hz$$

Cutoff frequency, 120mm diameter chamber,

$$f_{c,120} = 1.84\frac{563}{\pi * 0.12} = 2747\,Hz$$

Both these frequencies are much higher than the exhaust pulse frequency that a single-cylinder can produce, and even for some of its harmonics. This indicates keeping the frequency studied to below 2000Hz would be safe in terms of cutoff frequencies of either muffler.

4.1.2 Substitution and graphing

Now that the velocity of sound in the exhaust gas is known, it can be substituted into the transmission loss equation for a simple chamber with tapered ends. As the tapered acoustic loss equation only accounts for one taper angle on both ends of the muffler, an average of both taper lengths will be used. While this may produce results that are slightly

off, they should not affect the results by much as the exhaust cones chosen are generally close in taper.

Two values for the area ratio will be used, 8.16 for the 100 mm diameter chamber, and 11.76 for the 120 mm chamber. It is worth mentioning that the initial testing of the engine rig to determine if audible differences could be heard was done with a 100 mm versus a 130 mm diameter pipe of area ratio of 13.80. This was solely done to test 'extremes' for an audible difference to make any changes before controlled testing occurred. The 130 mm chambers were not used due to their lack of correlation with the 100 and 120 mm chambers. Remembering that $\sigma = 4\pi\frac{l^t}{\lambda}$ where l^t is the length of the tapered section, and $\lambda = {}^{v}/_{f}$, we can plot the attenuation curve for frequencies from 0-2000 Hz for each of the tapered chambers.

$$Attenuation = 10log_{10}\left[1 + \frac{1}{4}\left(\left(A_r - \frac{1}{A_r}\right)^2 sin^2(kl)\right)\right]$$

By starting out with the attenuation for a simple chamber, then substituting the loss from tapering each end, curves can be found. While the equation below for a taper produces a positive attenuation when graphed, it should be read as a loss in attenuation where the loss is a minimum at lower frequencies and a maximum higher up.

$$Attenuation = 10log_{10}\left\{\left[1 + \frac{\left(\sqrt{A_r} - 1\right)^2}{\sqrt{A_r}}\left(\frac{1 - \cos\sigma}{\sigma^2}\right)\right]^2 + \left[\frac{\left(\sqrt{A_r} - 1\right)^2}{\sqrt{A_r}}\left(\frac{1 - \sin\sigma}{\sigma^2}\right)\right]^2\right\}$$

When processing data, this factor is accounted for where each tapered attenuation values are subtracted from the maximum tapered value, to produce a loss in terms of frequency. These tapered values are then subtracted from the attenuation values of a regular muffler at each corresponding frequency interval. This reduction in each curve can be seen as a decay of sorts. For comparative reasons, we can also plot this modified attenuation curve against the curves for regular chambers to see the difference a taper will make to the noise levels.

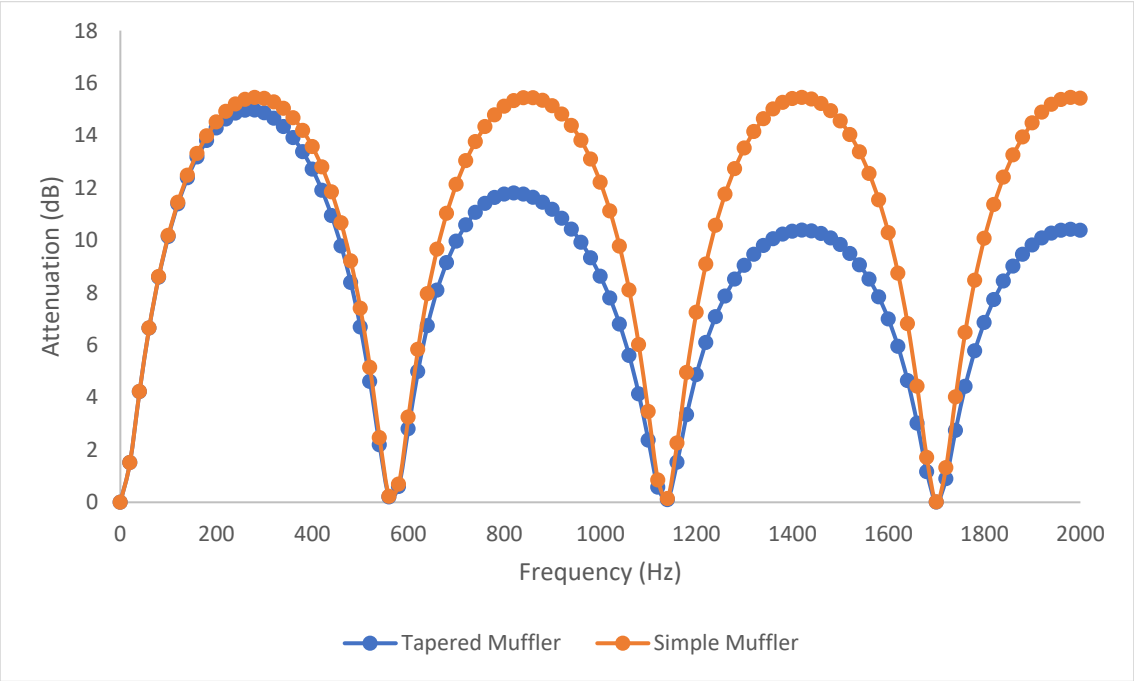

Figure 4-1: Modified attenuation curve taking into account tapered entry and end effect.

If simple chambers of a full length are plotted against the same chambers with tapered ends a visible reduction in the attenuation in higher frequencies is visible. As mentioned before, this phenomena could be due to the tapers acting like a horn where some of the higher frequency noise simply passes, or 'beams' through the central region of the muffler (Davis, Stevens, Moore, & Stokes, 1953).

An assumption made here for the reasons of graphing the data is based around subtracting the attenuation loss from a tapered end from the attenuation curve of the simple muffler. If subtraction alone were to occur at each frequency interval, the final attenuation curve would go into the negative region of the graph, not modelling the attenuation curve in the slightest – i.e. the muffler would start producing more noise. This is why the attenuation loss values from the tapered ends had to be scaled relative to each point on the simple muffler attenuation curve then subtracted from the simple muffler equation. While this modifies some of the points, it closely matches the correct values as the attenuation loss at and near the peaks are not changed by much. It would also not make sense if there was an attenuation loss from a tapered end on an area of no attenuation.

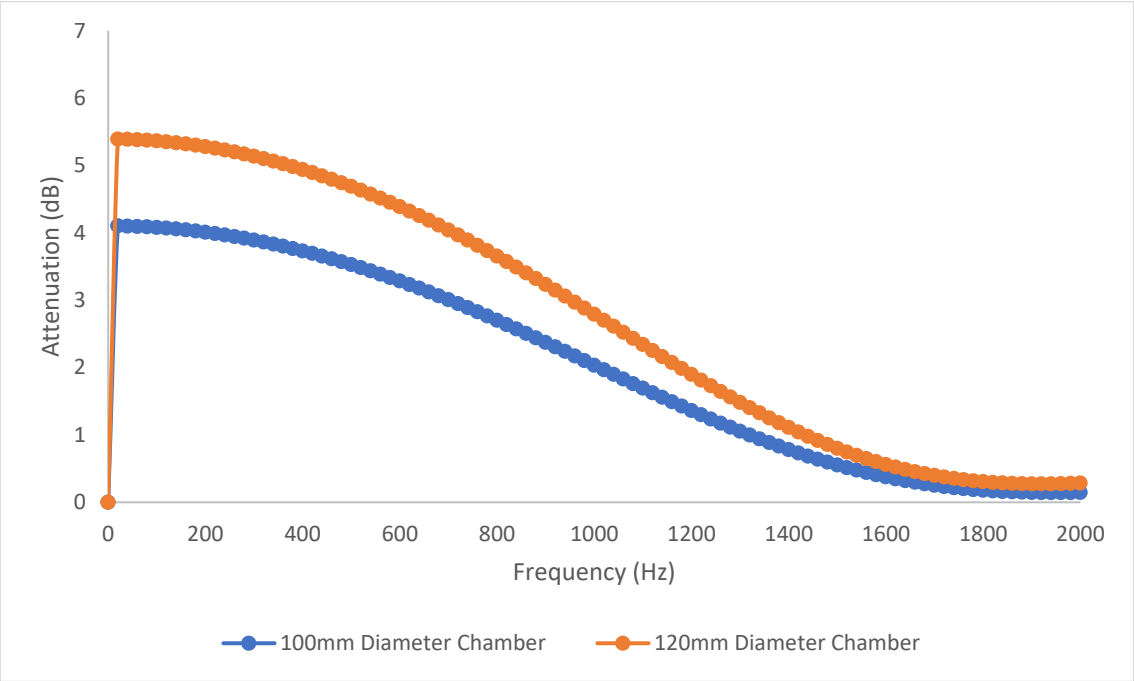

Figure 4-2: Attenuation curve due to the area ratio of a tapered conical section.

In much the same way a larger Area ratio increases the attenuation of a muffler, the taper attenuation is also affected where a large ratio will have a larger attenuation loss then a smaller ratio. The attenuation curves of each Area ratio will all converge after a certain frequency with a longer taper losing attenuation characteristics more rapidly. The result of this would be that at higher frequencies a muffler with a larger area ratio would behave the same as a smaller area ratio. This also highlights the issue with tapers where for any taper or area ratio, the high frequency attenuation is poor.

While this is the case, a taper in a pipe, especially at the entry to a pipe, will greatly reduce the flow loses on entry. For exhaust systems with high flow rates, designing with tapers could drastically lower backpressure seen by the engine as pumping loses when compared to a sudden step.

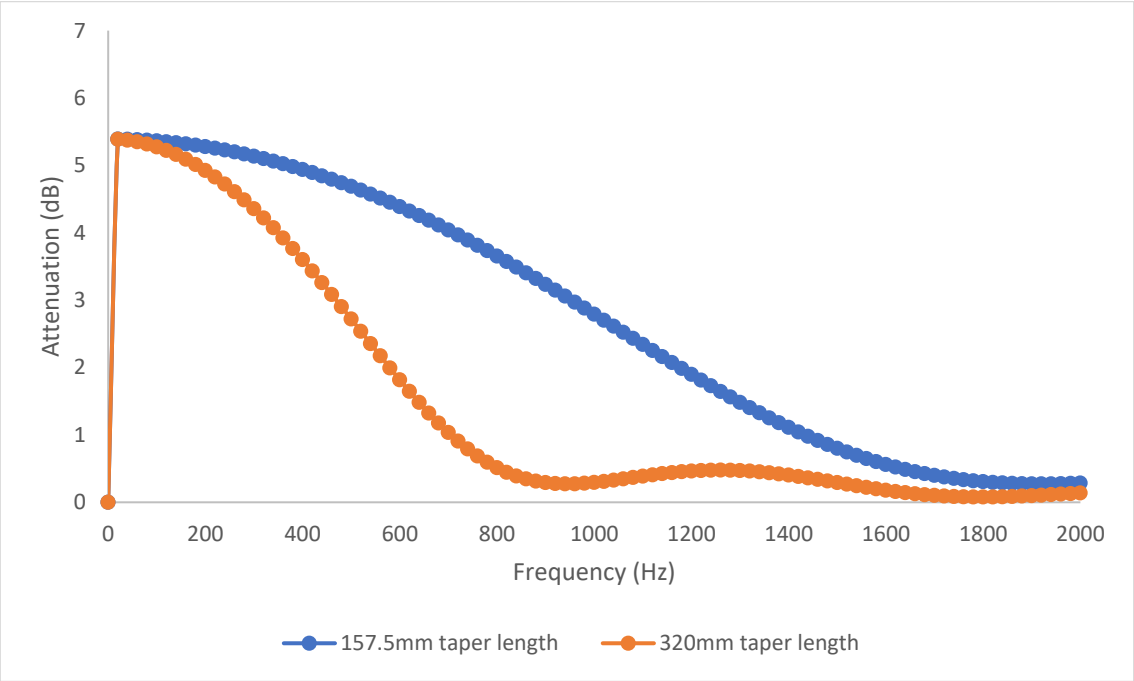

Figure 4-3: Shorter tapers provide more acoustic attenuation higher in the frequency band.

The attenuation characteristics of two of the tapers are shown in Figure 4-3 where a noticeable 3 dB in acoustic attenuation lost around the 800 Hz frequency. In this case, the shorter length taper would attenuate the medium and higher frequencies better than the long taper.

Once the simple chamber attenuation equation has been combined with the tapered attenuation equation, evaluations can be made between each configuration of chamber. The first comparison is that of the area ratio.

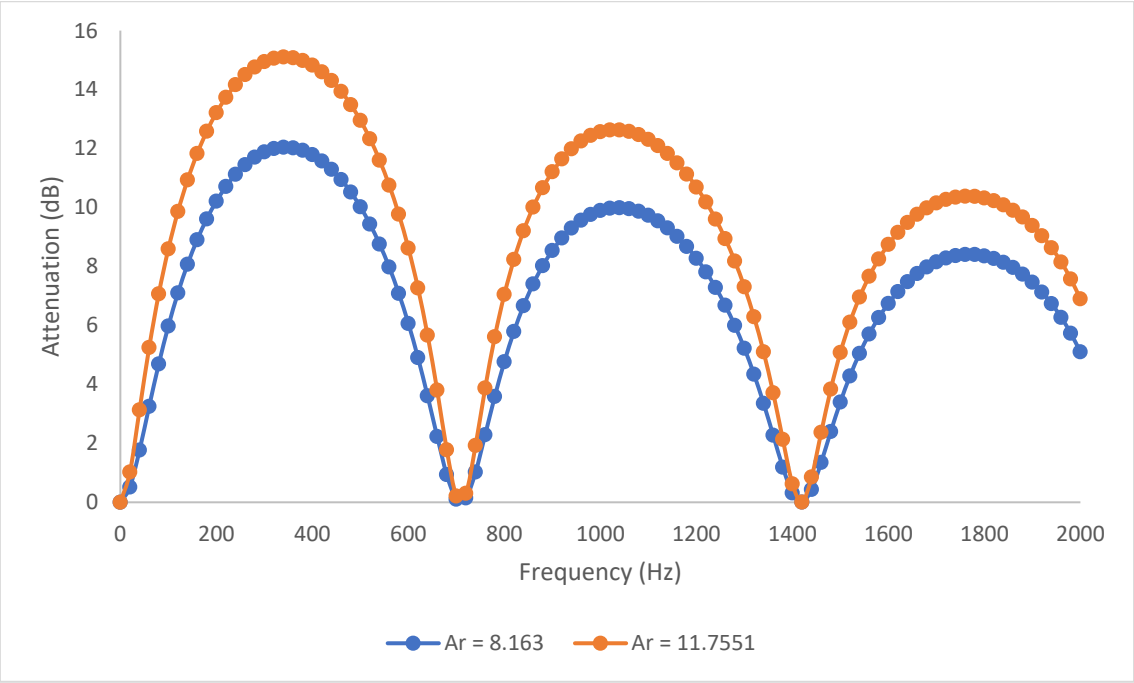

Figure 4-4: Attenuation characteristics between different area ratios with a tapered end factor applied.

One feature of Figure 4-4 is the decay of the attenuation for the higher area ratio. While the larger expansion in this muffler will attenuate more noise, the attenuation will decay faster than a smaller muffler. In a combined space a change in area ratio could be the difference between two chambers or one large one, so a comparison would need to be made.

A longer muffler will rock the frequency that the attenuation occurs at while also modifying the attenuation bands. Shown below in Figure 4-5 where the area ratio is kept constant, the longer muffler used in configuration 13 has shorter attenuation bands but an increased number of them. On a coincidental note, having these two mufflers inline would work rather well at attenuating noise due to the semi-additive nature of attenuation in mufflers where the attenuation curve would cover most frequencies. The correct method of proving this would be using the four-pole equations for each step of the exhaust system.

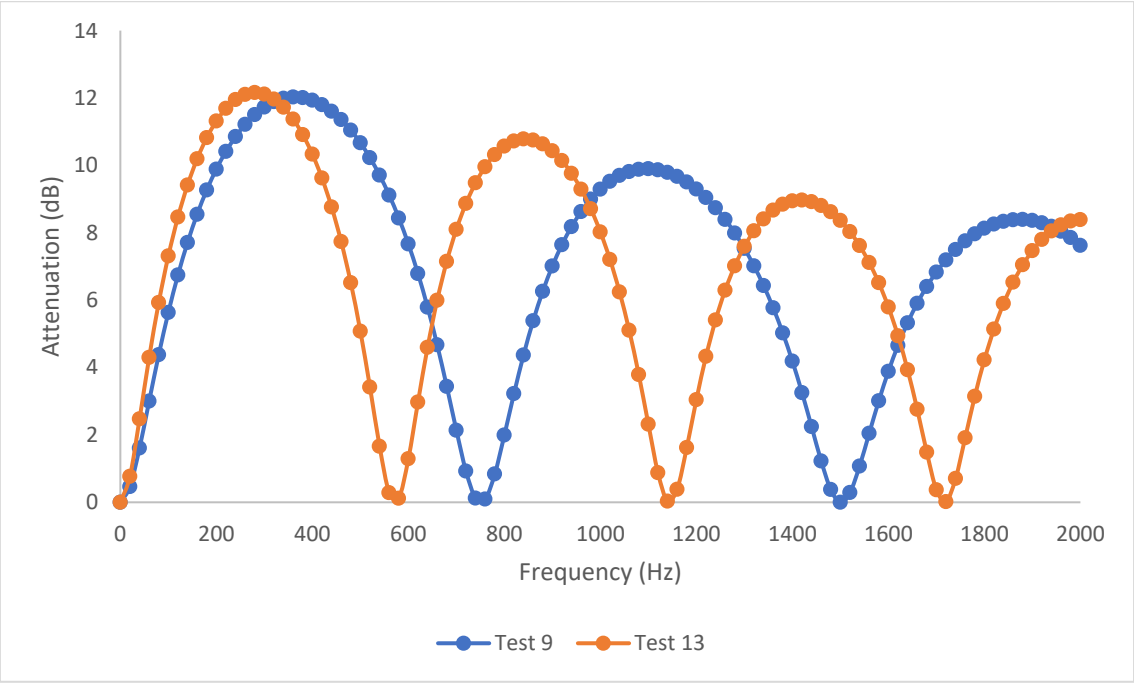

Figure 4-5: Attenuation characteristics of a longer muffler are shown as a closer sinusodial pattern.

Another important part of these graphs is the effect of the acoustic velocity on the attenuation bands where an increase in temperature or density will be shown through widening of the attenuation bands. If the exhaust gas is cooler than the measured values, the attenuation curves would narrow and shift down in frequency.

While not shown here, graphs for each of the exhaust chambers that are being tested have been plotted and are found in the results section of this thesis.

4.2 Engine measurements and setup

As mentioned earlier in this report, the engine being used for testing is a Yamaha Scorpio 223cc motorcycle engine. Its SOHC layout and twin-valve head simplifies the modelling and calculations involved with tuning resonant chambers.

The engine has a 70mm bore and 58mm stroke, with a connecting rod of 105.5mm long. This under-square engine likes to rev freely, and the high rod-to-stroke ratio of 1.82 provides a peak torque and peak power valve that are close in rpm – 17.5Nm at 6500 rpm and 13.4kW at 8000 rpm respectively. A relatively low compression of 9.5:1, pent-roof head, and base timing of 5° means this engine can be happily run on 91 octane fuel. As this testing will only be focussing on the exhaust side of the engine, the factory carburettor has been retained to supply fuel for ease of operation and reliability.

The single intake and exhaust valves of 34mm and 28.5mm are located in the same longitudinal plane of the engine, with the single spark plug being located off to the left-hand side of the head. This minimises swirl in the combustion chamber and instead focuses the mixture in the centre for the spark plug to ignite.

Using the given data, this little engine has a BMEP of 9.86 bar (3sf).

Camshaft specs were not readily available so were measured using dial indicators on the back of intake and exhaust valve spring retainers. This process was straight-forward as the engine had large maintenance covers on both sides of the head to gain access for valve lash adjustments. Without removing the cam chain and camshaft from the cylinder head, measuring the cam profiles from the lobes was not possible.

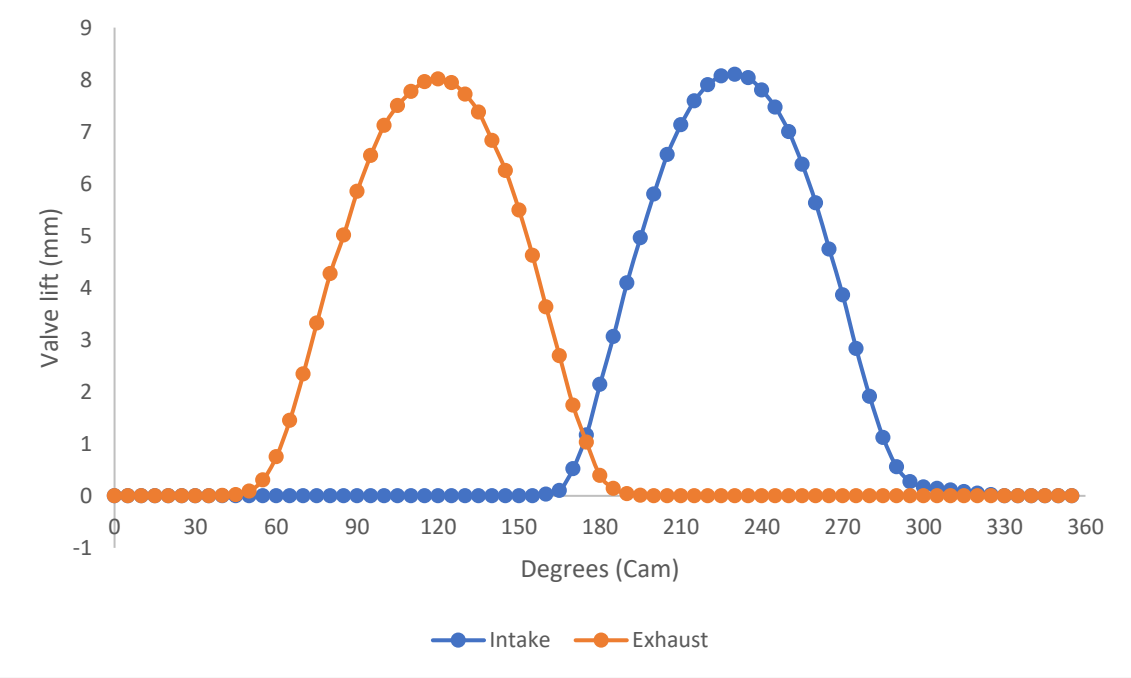

Figure 4-6: Test engine valve lift profile showing timing and lift properties.

Exhaust valve lift measurements show that over the 720° duration of the engine's cycle, the exhaust valve is open 145° (cam), or 290° (crank). Taking this in terms of exhaust valve open duration, 290° crank degrees at 8000 rpm is the equivalent of 0.006 seconds. If 100% volumetric efficiency is assumed, 0.223 L escapes over a 0.006 seconds – almost 37 L/s. If this volume travels down the 31.8 mm (ID) exhaust pipe, it will exit at almost 150 m/s. This quick calculation does not assume gas lost from blowdown which due to the pressure differential between the cylinder and the exhaust pipe, will be at an even higher velocity. While 150 m/s is fast, this is still less than half the velocity of the speed

of sound in air, let alone for heated exhaust gases. For scavenging effects of the header, we would use these values to predict a time where we would want a rarefaction wave to travel back to the cylinder, preferably at the end of the exhaust stroke, 0.006 seconds after the initial pulse. This would suggest a length of 0.45 m for the primary header pipe if the target for scavenging was 8000 rpm.

4.3 Test rig setup

From early on in this project, a method of mounting and running the engine was needed.

This came in the form of a frame made from Maytec aluminium extruded framing. This decision was influenced by the availability and versatility of the framing that allows for adjustments or modifications at any stage of the build.

Figure 4-7: Dynamometer rig showing remote throttle and start button (on left).

Based around the shape of the Yamaha engine, a dual-width frame extends around the perimeter of the rig, with internal lengths cut to allow adjustment for different engine widths, lengths, and mounting points. The engine is secured to the framing using 3 mm steel mounts in three of the factory mounting locations. Supports for the fuel tank, intake,

and exhaust were installed along with a tray and upright for a control panel with remote throttle lever. To make the setup portable, the framing is mounted to a small laboratory workbench with locking caster wheels on every corner.

One of the first items on the list when setting up the engine was to rebuild the carburettor and give the engine an oil change. By doing these two maintenance issues, the engine should be reliable for the entirety of testing. The factory carburettor and ignition system were kept for these tests as it was deemed a sensible decision. Setting up fuel injection and electronic timing would not benefit the test enough to justify the added complexity and time required to wire up the system and tune. The result of this is the air-to-fuel ratio might vary in testing depending on the flow of each of the exhaust chambers, however as the carburettor operates off the volumetric flow rate through its port, it will slightly compensate for a higher or lower airflow into the engine.

The engine wire harness also needed piecing together and terminating to get the engine running. The regulator/rectifier, ignition coil, and the CDI box were all rubber-mounted to one of the engine support frames to keep them away from heat and safe from vibrations.

In addition to wiring up the engine, a starting system and battery were installed to allow for remote starts and for ease of use. Along with a remotely mounted throttle lever, this setup protects the operator from the engine while it is running. An acrylic sheet was also installed between the motor and operator to protect the user in case of failure of the engine or auxiliary equipment. Under no-load scenarios the engine can be started in gear and the remote throttle handle is used to control the rpm of the engine. For cold starts the engine was started in neutral and warmed up with the choke to make idling easier.

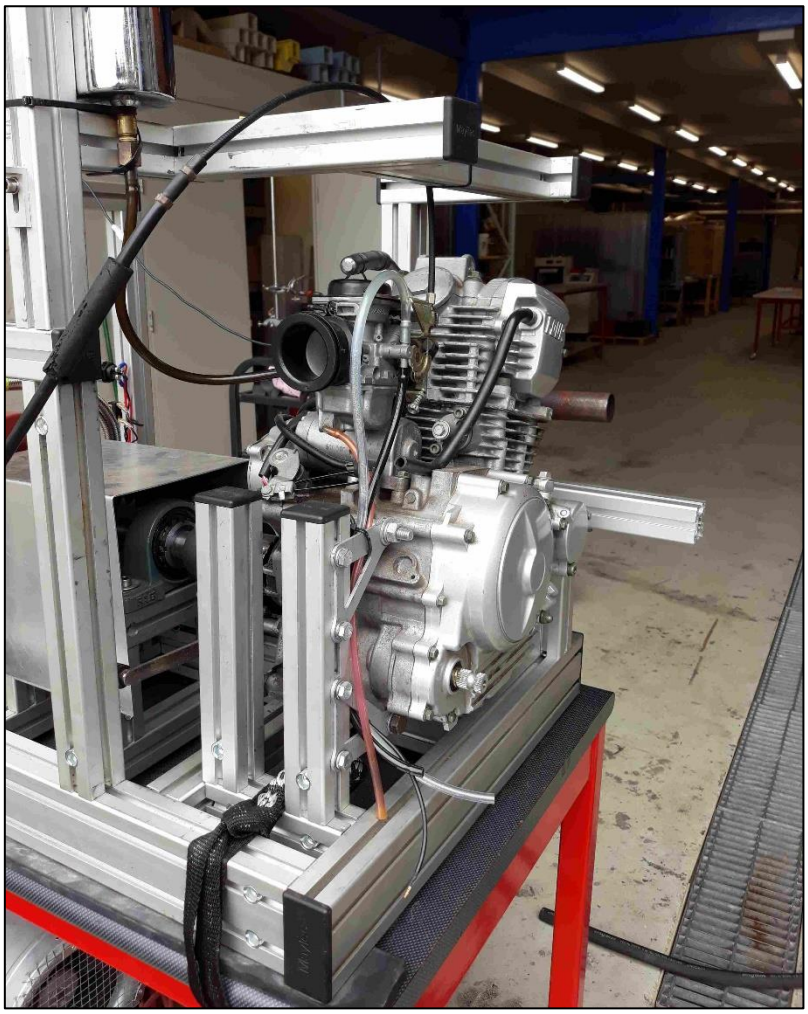

Figure 4-8: Rear side of dynamometer rig showing the engine mount setup and orientation of exhaust pipe.

To apply a load in a controlled procedure, a Dynomite water-brake dynamometer has been installed. This style of dynamometer is designed to be an inefficient water pump where the engine's power is used to turn an impeller, applying work to the water flowing through the impeller housing. Another benefit of the Maytec framing is the adjustability to allow for alterations in lengths to be made when lining up the output shaft to the dynamometer. This was done to ensure the output shaft of the engine was running true to the input shaft of the water-brake unit, and that the pillow block bearings were not binding in any way. Previously, this dynamometer unit had been used for initial map creation and light-throttle tuning of Waikato Engineering Students' Motorsport Organisation's (WESMO's) KTM Duke R 690cc engine on a different frame. The KTM engine had been mounted differently to the other test rig chassis and used a chain drive to drive the dynamometer. Driving the dynamometer from the Scorpio engine meant using a flexible jaw couplings and an output shaft adaptor while rotating the entire setup by 90 degrees when compared to the last test rig due to width of the framing.

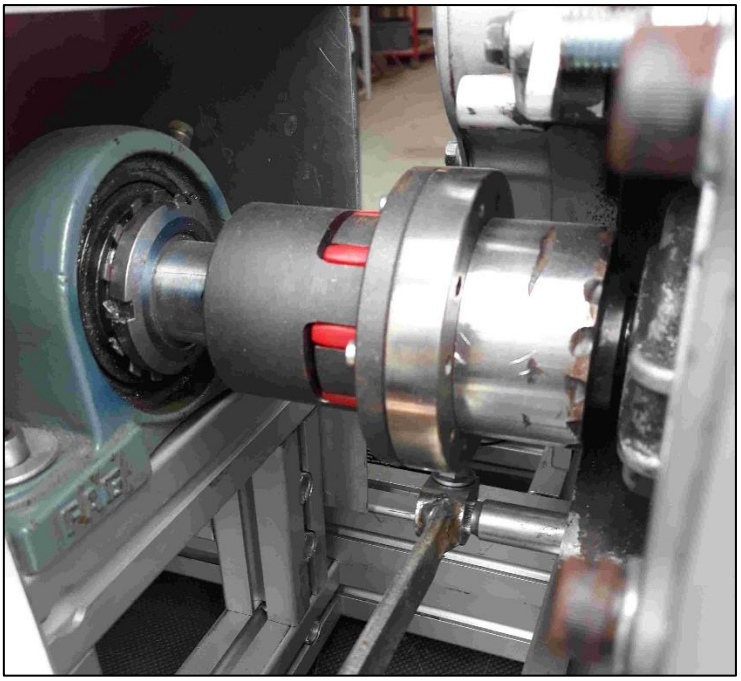

Figure 4-9: Direct drive via a flexible jaw coupling, showing dynamometer support pillow-block bearings and extended gear shift lever below.

Going to a direct drive from the engine to the dynamometer was influenced by the slack in the chain and vibrations caused by the previous setup. As the nature of a single-cylinder engine is to only fire once per 720° of crank rotation, the crank accelerates and decelerates to a higher degree than that when compared to a four-cylinder that fires once per 180°. This leads to the single cylinder having more of a 'rough' output and when any chain slack is factored in, this can affect the output to the dynamometer and increase dynamometer chassis vibrations. This was seen with the KTM engine previously used where it was visible at lower engine speeds that any chain slack would oscillate between the top and bottom sides of the loop when under different loading scenarios and caused vibrations that loosened bolts on the test rig. The chain is also a safety concern and required large shields.

Johan Wall's study on destructive vibrations notes that if a structure is allowed to freely vibrate at one of its natural frequencies, continued vibration at resonance may lead to structural failure, therefore avoiding resonance is usually necessary (Wall, 2003). This is also the case for our dynamometer chassis where the whole unit is mounted to a work bench. To get around some of these issues, 10mm rubber strips have been put under the dyno chassis to absorb some of the vibrations given off by the running engine. This

modification lowers noise levels from less chassis vibration and also stopped the chassis bolts from backing out.

One adjustment made with the tuning in the Dynomite software where the rpm of the water brake can be averaged over a number of cycles. The use of this feature is to remove some of the error by averaging the velocity values when logging the dynamometer data on a computer. The velocity of the internal rotor is very important as the water brake gets its power and torque values from a strain gauge and magnetic rpm pickup. Knowing the strain gauge value, the mechanical properties of the arm, and the rotational velocity of the internal rotor allows the software to find a torque and then multiply by rpm for a power value. Ideally, the high-rpm design of the dynamometer means it should be driven straight off the engine's crankshaft but in this application it would be very hard to do so. For this reason the engine will be run in fifth gear – its highest gear to try and get the output as close to engine speed as possible.

4.4 Exhaust test chambers

From early on in this project, there was a need for exhaust chambers of different dimensions to test how the theory stacked up to measurable results. The system needed to be designed such that the testing pieces could be quickly modified or swapped out in-between runs while being sturdy enough to withstand large vibrations and the heat of exhaust gases.

In early 2018 our Formula SAE team, WESMO, was visited by Graeme Harris who formally owned Harris exhaust pipes and now conducts research and presents Lectures at Ara Institute of Canterbury. Along with providing an informative lecture for the team, Graeme was kind enough to lend us his exhaust chambers and adaptors to test what effect they have on a four-stroke engine.

Figure 4-10: Some of the conical sections used for exhaust noise testing.

His equipment includes conical and straight sections of varying length and diameter. Each part of the cone sections could be clipped together for quick chamber changes and had recessed O-rings for sealing. Coincidentally the factory Yamaha exhaust external diameter of 35 mm was a perfect fit for these exhaust testing pieces, so a short centreline length of 200 mm and a 90 degree bend was left attached to the head and ran outwards from the engine. The outlet was positioned such that any mechanical vibration or noise from the engine induction and dynamometer was minimised.

As the factory 35mm outside diameter pipe of the engine's exhaust matched the internal diameter of the exhaust test chambers, each of the chambers were slipped on and the cap screw tightened to clamp onto the exhaust pipe. This method allowed quick changes between chambers while wearing heat-resistant gloves.

Figure 4-11: Configuration 15, 13, and 14 test chambers ready for testing.

Figure 4-12: Exhaust cone showing the clip system and labelling for each section.

Initially, each chamber setup was supported via a retort stand which was clamped via a rubberised grip to the furthermost end of the exhaust chamber. This was introduced to stop any vibrations from the chambers affecting the noise results while also supporting the mass of the exhaust system hanging off the head of the engine. It was soon found that the vibrations of the engine and exhaust were loosening the retort stand clamps and causing the stands to vibrate. This was overcome by removing the clamps and testing to see if the setup would support itself – which it did. This simplified the setup process as one less item had to be adjusted between tests.

Through these tests the length of the primary header pipe was kept the same by marking where to stop the slip joint on the exhaust cones. A centreline length of 200mm was selected for the primary pipe as having a length this short would minimise any harmonics formed until higher order harmonics were attained.

The two main testing conical sections were 100mm and 120mm in diameter with varying lengths and tapers. These two diameters had the closest selection of parts so comparisons between an expansion ratio of 8.16 and 11.77 could be studied. Other diameter testing pieces were used but the results were predominantly for checking the validity of the experiment – such as that seen in the initial testing.

As each testing setup could simply be clipped into place, recordings were made for each section of test chamber. After the header pipe the divergent cone was added and recorded, followed by the divergent cone and cylinder, and finally by the whole chamber. This data can then be used to study what effect a large exit has on the noise levels.

The list of configurations is as follows

Test Cones	Divergent		Cylinder		Convergent		Configuration
	Diam-eter	Leng th	Diam-eter	Leng th	Diam-eter	Leng th	
Divergent only	100	195					1
	100	110					2
	120	195					3
	120	120					4
Div. with ~80mm cylinder	100	195	100	70			5
	100	110	100	70			6
	120	195	120	82			7
	120	120	120	82			8
Div, cyl, conv	100	195	100	70	100	110	9
	100	110	100	70	100	195	10
	120	195	120	82	120	120	11
	120	120	120	82	120	195	12
100 long cyl vs short	100	110	100	187	100	195	13
120 long cyl vs short	120	120	120	20	120	195	14
120 long taper vs short	120	360	120	82	120	280	15

Table 4-1: Set list of exhaust configurations.

4.5 Recording equipment setup

4.5.1 Volume measurements

Sound waves produced from testing were recorded via a decibel meter located such that met the rules for SAE Noise test regulations. These rules can be found in Appendix 2 and outline what noise levels are permitted and how the sound level meter will be set up in regards to exhaust exit location.

As a precaution, the sound level meter was re-calibrated before each set of runs. As testing was going to occur over a few days, calibrating it this way would account for any variance in the meter or any environmental factors that could happen between sets of runs. Batteries were also replaced at the start of testing to ensure the meter would not run out during a test.

Location of the sound level meter was checked with every change of pipe, ensuring it stayed at a distance of one metre from the outlet, at a 45º angle. The meter was set up on

a retort stand on a small trolley to remove any vibrations that could occur if it was attached directly to any part of the engine or dynamometer chassis. As the separate trolley was also on castor wheels, it could be repositioned and locked into location for each test scenario.

4.5.2 Noise spectrum measurements

Noise spectrum recordings were obtained using a microphone mounted directly below the decibel meter which was plugged into a laptop. The exhaust noise was recorded directly into Audacity®, a freeware audio recording, editing, and analysis software [1]. In the software the audio recordings could be edited, cut, and divided into individual runs.

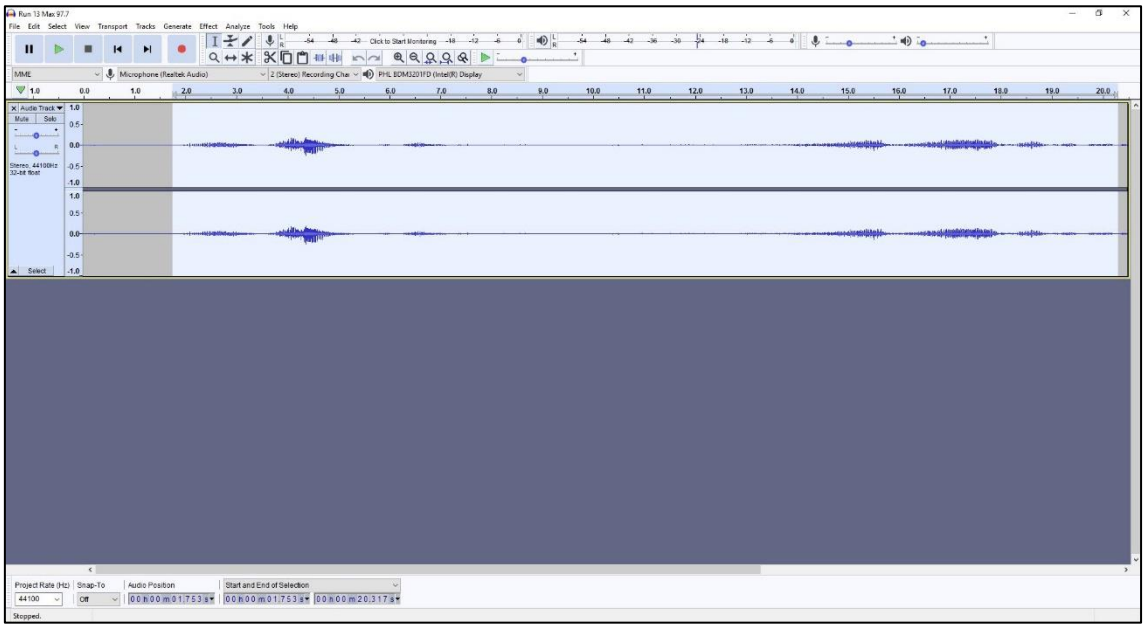

Figure 4-13: Selecting data within Audacity for spectrum analysis.

By selecting areas of audio track with little noise pollution, a better spectrum can be plotted. This method also works for selecting the unloaded and loaded noise recordings to compare whether any difference in noise occurs with the higher mass flow rate.

Audio spectrum analysis was also processed within Audacity. The spectrum analysis was carried out by averaging the volume at each frequency and plotted within the software to visualise the noise given off by each test.

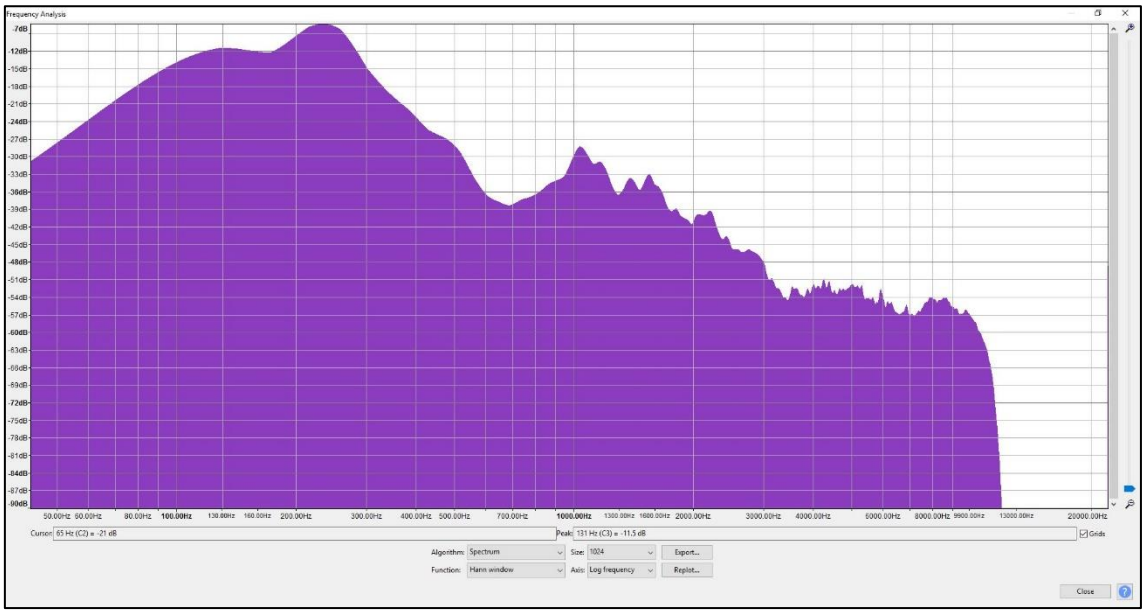

Figure 4-14: Audio spectrum plot from Audacity.

By recording volume measurements for all frequencies seen by the microphone, a full spectrum can be analysed to find any irregularities in higher frequencies that what the engine is producing. The data can later be analysed and shrunk down to frequencies directly related to exhaust pulses and the chambers.

An important part of the spectrum analysis is the ability to export the spectrum as a .txt file for graphing. This allowed the data to be loaded into Microsoft Excel and differences in volume graphed. As we would only be studying frequencies in the range of 50-2000 Hz (limited by microphone sensitivity and engine rpm) this data can be shrunk down, scaled, and compared where needed. While the maximum operating speed of the engine is 10,000 rpm, this produces a maximum frequency of 83.3 Hz which is very low, so higher harmonics are also being considered, hence the 2000 Hz upper-limit to match the computer modelled data.

Another part of preparing for the noise level tests was making sure that the environmental factors stayed constant. The biggest factor that could affect results was any environmental or industrial noise recorded by the microphone. This meant testing could only occur on days and times where noise pollution was below 65 dB – a volume that would not be heard over the running engine at idle and under no load. At times testing proved difficult due to windy or rainy days, and pushed out the timeline for when data was meant to be collected.

4.5.3 Other measurements

Exhaust temperature measurements were recorded via thermocouples placed in the exhaust system. Initially, the temperature of the exhaust gas was measured at the junction between the header pipe and the chamber. As discussed later, this method produced inaccurate results so a change to reading temperatures before and after the exhaust chambers was done. These measured values would also assist in finding any heat lost via conduction of the chamber walls. Due to the relatively short lengths of pipes used and short time each chamber was installed, very little heat was absorbed by the exhaust chambers once the engine was up to operating temperature and running. In comparison the amount of exhaust gas passed through the chambers, the energy gain was infinitesimal compared to the energy released in noise and heated gases.

Humidity and ambient temperatures were also recorded via a basic weather station to monitor any large differences or help to explain any irregularities between days. The biggest issue with this part of the testing was finding appropriate days to conduct tests as all measurements had to be taken outdoors due to a lack of any indoor noise testing facilities. Windy or rainy days meant testing could not occur, which pushed out the testing schedule.

5 Results and Discussion

This chapter focuses on the results from the modelling and testing stages of research, followed by a discussion of what was found. After the initial setup and testing, results from each chamber test are given and contrasted against the theoretical attenuation properties of each muffler. A small study is also undertaken into the effect of a taper on the exit of the exhaust pipe to see if any attenuation occurs due to an expansion step.

5.1 Initial testing

Initial sound measurements were taken with no exhaust chamber installed on the engine. This testing was conducted over a large range of engine speeds and under no load conditions to establish a baseline on the noise produced by the engine. From here, two chambers were tested to test how sensitive the recording equipment was.

From early on in the project the results looked promising as changing the exhaust cones around produced audible differences that could be heard at idle and under different no-load scenarios, with the largest effect on noise coming from the largest and longest chamber.

The first test conducted showed visible differences in the volume of the exhaust noise being produced. This test is based on a comparative study between the shortest and smallest test chamber to the longest and largest chamber to validate if the testing methods would be accurate enough to pick up any difference in volume – comparing extremes.

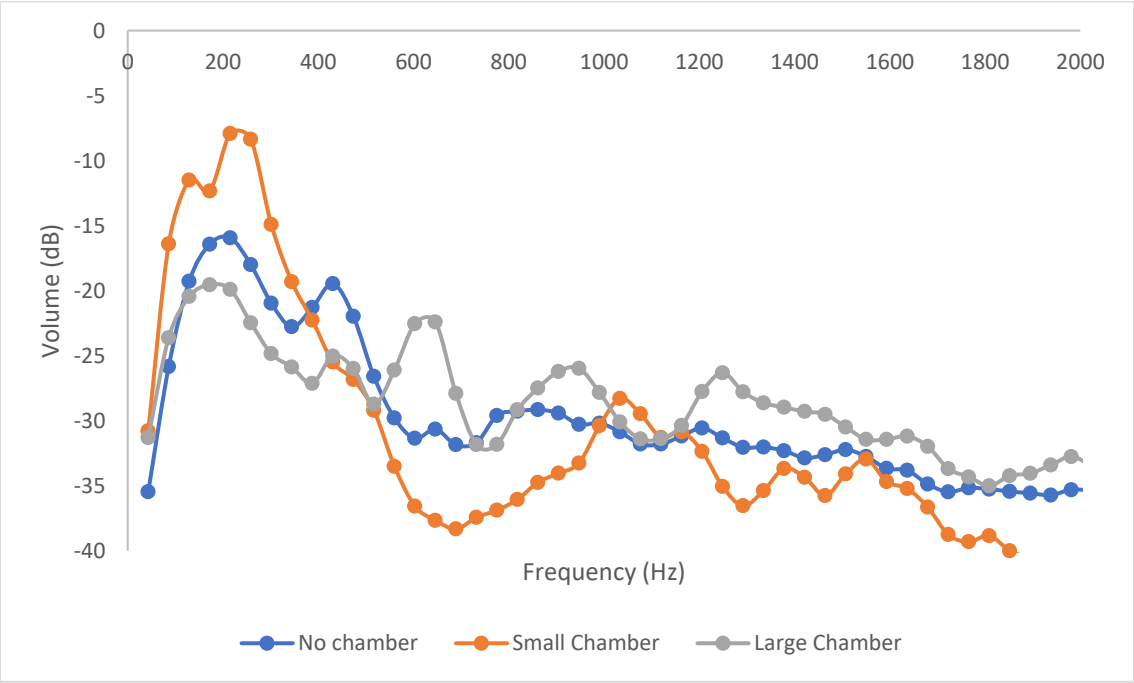

Figure 5-1: Initial testing to validate experimental rig.

A brief analysis of the three setups indicate a clear reduction in lower-frequency noise by the large chamber when compared to the straight pipe and the small chamber. While unknown at this stage of testing, the cause for this lower-pitch reduction in volume could be due to the longer length, larger diameter, larger volume, or a combination of these.

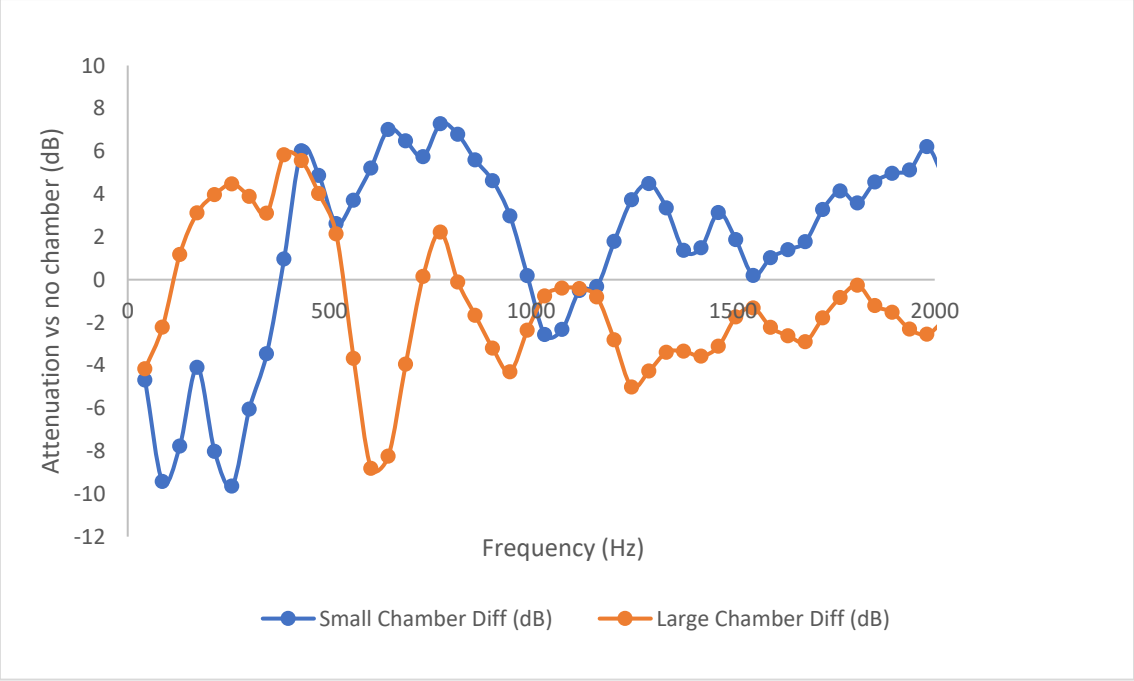

Figure 5-2: Noise attenuation of each initial test chamber showing Decibels lost (+ve) or gained (-ve).

Comparing the difference between lines on the graph, a 12 dB reduction at 215 Hz is seen between the large chamber and the small chamber. Due to the logarithmic nature of the decibel scale, this is over 10 times softer in volume at this frequency. Looking at this relationship at the 645 Hz frequency, it is very much the opposite where the small chamber is 15 dB quieter than the large chamber. The blue 'no chamber' line splits the difference in most cases, apart from a few peaks.

The biggest hurdle faced by this testing was the frequency of the exhaust pulses. Because the microphone setup only recognises frequencies above the 40 Hz range, or 4800 rpm, no lower frequencies could be validated, which meant tuning had to rely on higher harmonics. On the other hand, by 1000 Hz, the engine would have to be either revving at 120000 rpm or be at 8000 rpm and be on its 15^{th} harmonic to be producing frequencies in this range.

One issue with the testing setup was the lack of support for the volume measuring equipment where the software designed for the sound level meter was only available on compact disc for older versions of Windows and would not run with serial converters. This meant a microphone had to be used to record the audio spectrum, then the levels compared to the sound level meter

Initial power measurements from the dynamometer did not look promising. Due to using the large 9" Dynomite water-brake on such a small engine, the power curve showed no difference between any of the three setups chosen. While we had access to a smaller 6" water-brake dynamometer, the fittings and control units would have had to be swapped out, a recalibration done on the torque arm, and a new drive system off the crank would have had to been manufactured. This is due to the near 3:1 gear ratio of the primary drive in the engine's transmission lowering the output shaft speed too much, and causing too much torque at a low rpm for the smaller water-brake to load the engine. The decision was made to continue to run the current setup and in the case of inconsistent readings to disregard the power graphs and use the dynamometer solely as a load source.

5.2 Chamber noise tests

The next stage of testing was directed at which part of the chamber is making the biggest difference to volume levels. By strategically testing the different diameters and lengths

of each configuration, results should be found that indicate resonance is occurring and causing attenuation or rises in noise levels.

The proposed list of tests was set at 15 different configurations under no-load and load scenarios to trial the effect that different shapes, steps, and lengths had on the noise being produced.

The list of tests was constructed to provide the most efficient way of testing with as minimal changes as possible per setup. Starting by bolting on the divergent cone to the header meant subsequent tests using this cone could be run in order, then the chamber detached, rotated, and the reverse could happen.

The results from the audio recordings are as follows. Power level recordings from the dynamometer will be disregarded as there was an inconsequential difference between runs that could simply be due to fluctuations in water pressure or strain gauge error. The dynamometer in these tests was solely used as a load device on the engine to record any difference between the unloaded and loaded sound levels.

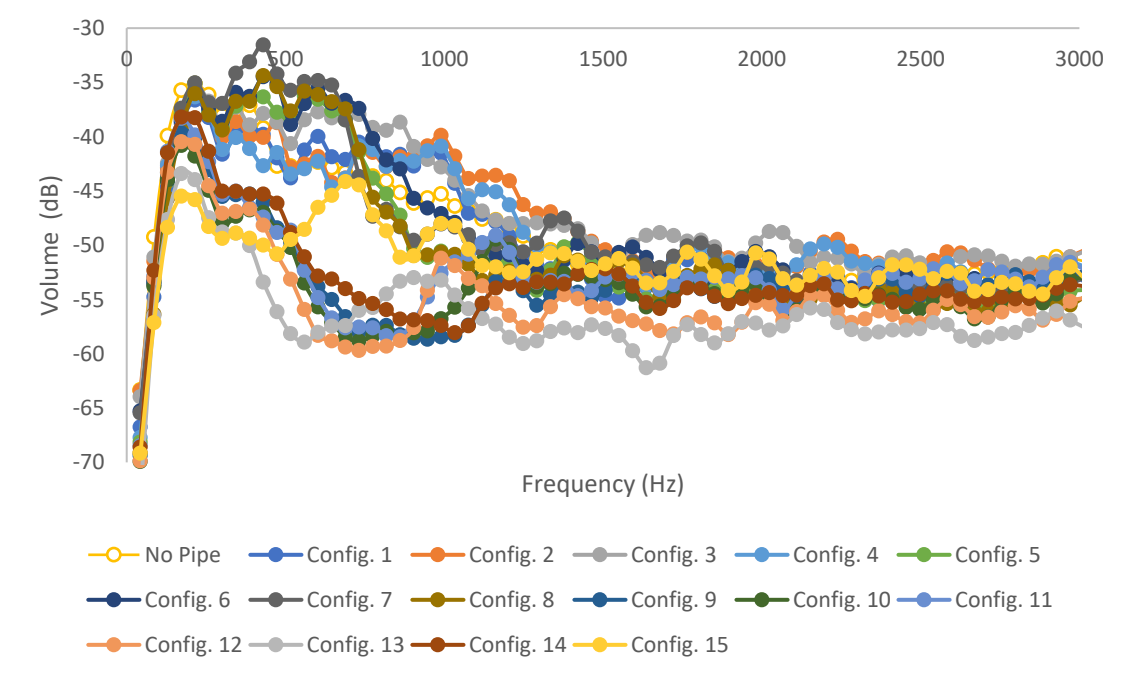

Figure 5-3: Volume levels for all tested configurations

In this initial graph of all the sound recordings, it is clear there are two distinct trends occurring here. While configurations 1-8 are grouped around the 'no pipe' levels, configurations 9-15 are at a much lower decibel level up to 1000 Hz. This difference is

due to the higher configurations being a full chamber design, unlike the lower numbers which are just single divergent cones or conical sections with a cylinder attached.

The negative values for the y-axis on the spectrum graph is due to the nature of the recordings in Audacity where the decibel scale has a zero value at the maximum microphone level, which is common to see in most recording software. When comparing other graphs, we will look at the noise attenuated. To get these values, each configuration's spectrum data will be subtracted from the 'no pipe' data to give the difference. Not only is it more accurate for comparisons, but differences in the attenuation can be read with accuracy. The first instance of this graph will be for the unloaded vs loaded engine condition.

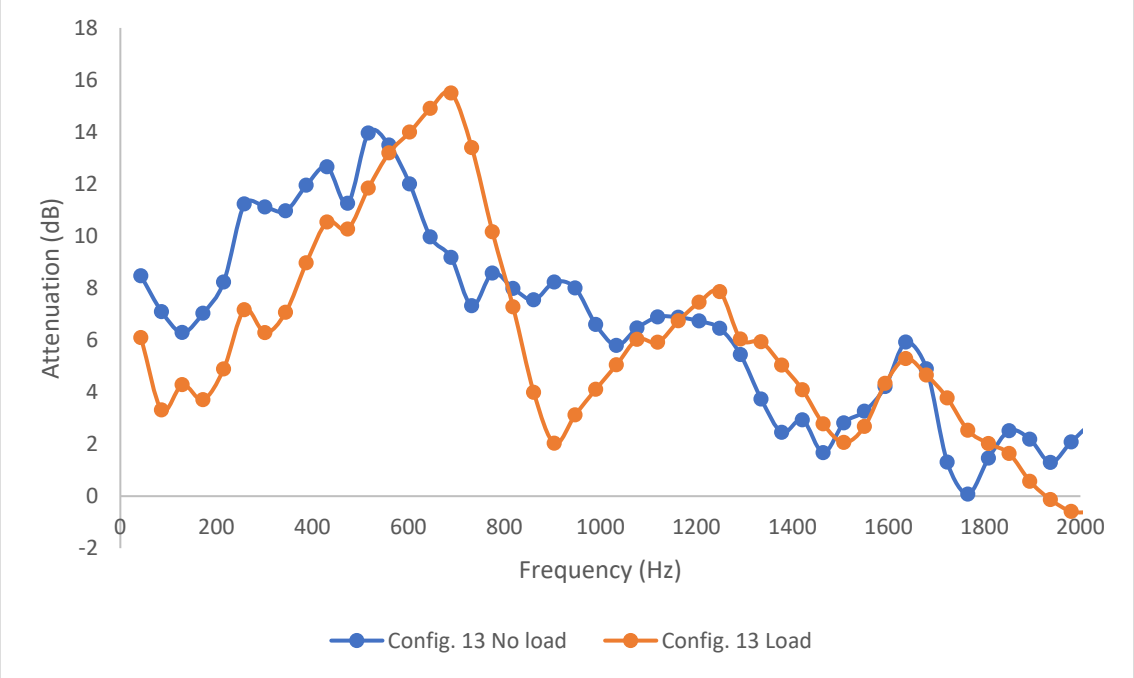

Figure 5-4: Difference in attenuation between unloaded and loaded engine conditions.

An initial point of interest is the difference in noise attenuation between the unloaded and loaded engine for a full chamber. It seems to be that the loaded condition shows a higher attenuation in the mid-range frequencies, where the unloaded condition shows higher attenuation in the lower and higher ranges. The peak and trough of the loaded condition at 700 Hz and 900 Hz are both 6 dB on either side of the unloaded condition, which could show resonance occurring due to a higher mass flow rate through the chamber than otherwise. While there is a difference, combining the two loading conditions should provide an average attenuation condition that can be used to compare the practical results

to the theory. It will also give the spectrum calculations more accuracy due to a higher number of data points to average at each frequency.

During the process of testing, some of the configurations were not a full chamber, with certain setups being a divergent cone, or a divergent cone with a cylinder attached leading to atmosphere. This was a test done to see how much difference in attenuation a chamber would make to each of these other setups. This process led to further results that will be discussed after the chamber noise tests. By selecting configurations that could be easily changed between runs, the time taken for testing was minimised. One series of configurations is shown below in Figure 5-5 where the first test was configuration four, a divergent cone. From here the test was run then a cylinder was clipped on to the cone, the noise measuring equipment repositioned, and the next test (configuration eight) run. To complete this series of tests, a convergent cone was clipped to the end of the cylinder to form a full chamber and the last recording taken.

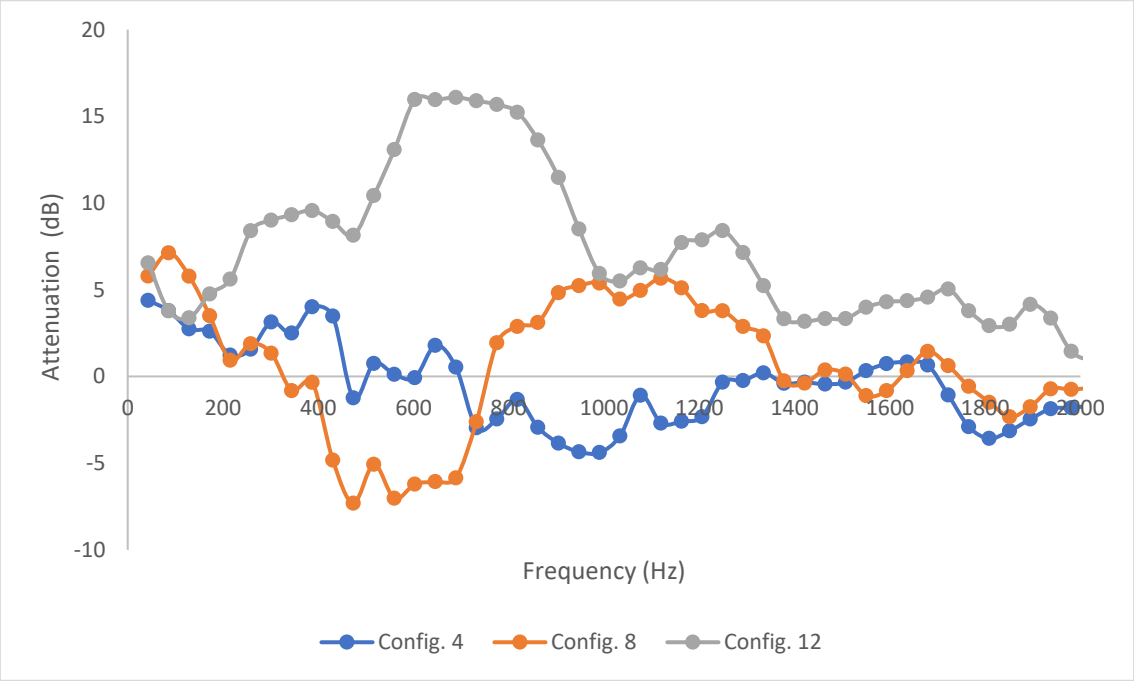

Figure 5-5: Attenuation differences due to configuration changes.

Visible in Figure 5-5 is the large gain in attenuation when configuration 12 is setup. By installing a convergent taper to create a chamber, the noise levels are reduced dramatically. A large peak around the 750 Hz mark shows a loss in volume of 16 dB over the baseline or the other setups. The chamber also has the most attenuation across the frequencies recorded, so is the clear choice for muffling the most amount of noise.

An interesting feature of configuration eight is the gain in volume from 400 Hz to 750 Hz, followed by a 5 dB attenuation up to 1400 Hz. This characteristic could suggest a resonance frequency being met, or the shape of the outlet section is reflecting the sound waves more densely in one direction when compared to a divergent cone or a straight pipe exit on the other configurations. The divergent cone in configuration four seems to direct the noise out of the exhaust pipe and increase the volume over most of the spectrum. This could suggest the emitted waves at the exit of the pipe are reflecting off the tapered surface and being directed, or the taper is allowing for less of an entry flow loss and allowing the rarefaction wave to flow more freely into the pipe – creating a larger amplitude of the exhaust waves.

Part of the reason for testing different exhaust chambers was to see how well theoretical results would compare to real-world situations. Initial graphing of the theoretical calculations saw a sinusoidal pattern occur, as to be expected from the literature. By using some of the data from literature, the data seemed to match their graphs well. This deemed the equation and calculation process to be a success. When graphed against the test data however, instant differences were visible.

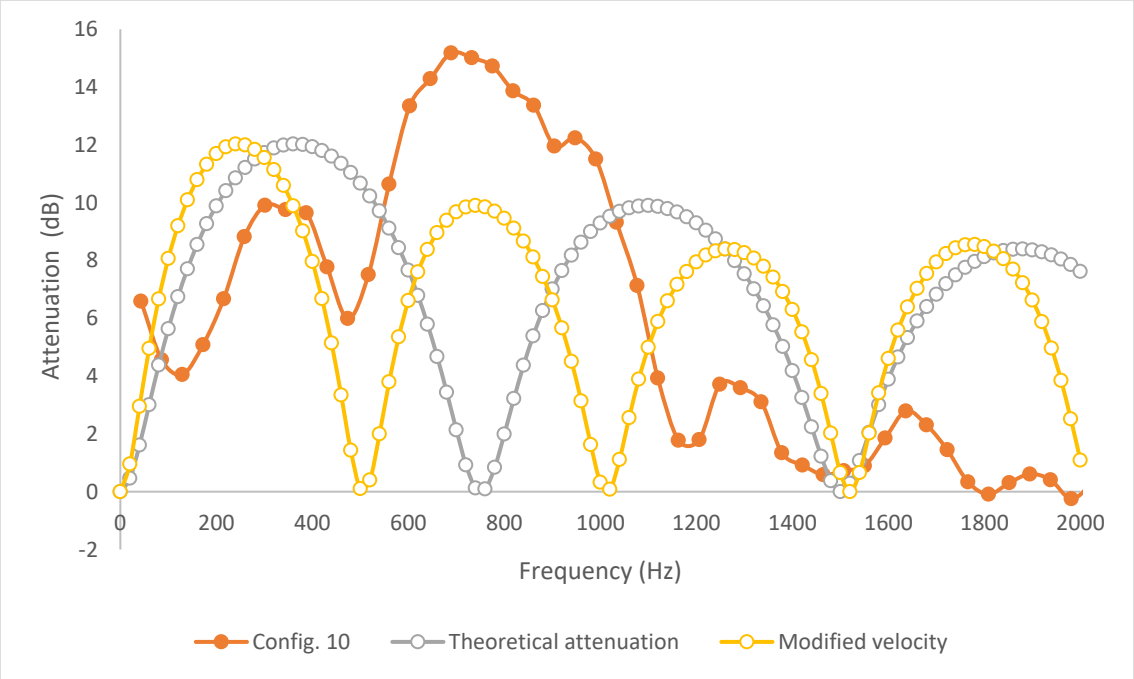

Figure 5-6: Comparisons between the predicted attenuation, the physical attenuation, and the resulting modified attenuation curve.

One issue faced when comparing the expected theoretical data to the data from testing was that none of the attenuation bands lined up. This was unexpected after having tested

the equations against data from literature. A possible cause of this was an issue with the testing equipment, however the attenuation data seemed sensible. This led to a suspicion that the acoustic velocity was off. After going through the calculations for the acoustic velocity in sound, found in Appendix 4, the exhaust gas temperature measurements were taken again. The inlet temperature to the chambers was a little higher, at 540 ºC, but during operation the temperature in the chamber fluctuated due to some of the atmospheric gas being drawn into the chamber through the tailpipe. This saw the temperature of the gas drop dramatically over the length of the chamber, with a hand being able to be comfortably held at a distance of 300mm from the outlet of most chambers where the gas temperature was 50 degrees. Based on these findings, recalculation of the acoustic velocity took the speed of sound down to 380 metres per second. Once the new value was put into the graphs, the resultant change saw the theoretical attenuation bands align more accurately with the measured ones, so the new acoustic velocity was kept.

With the acoustic velocity fixed, theoretical attenuation values can be subtracted from the 'no pipe' recording data and then compared to the measured recording data for those configurations.

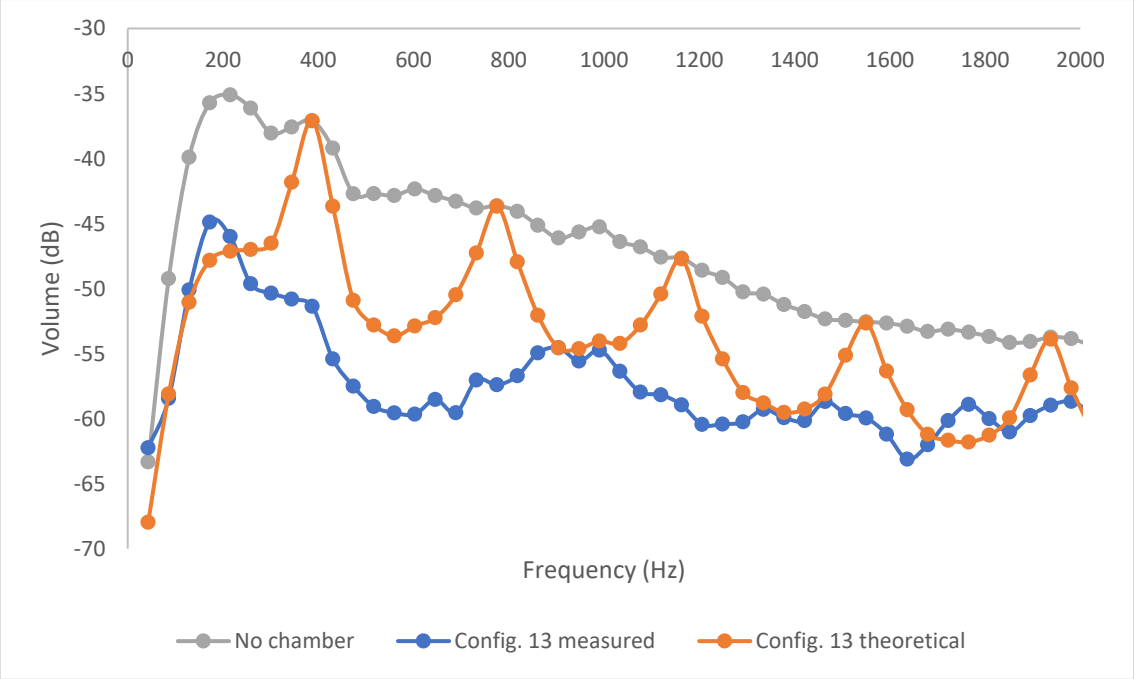

Figure 5-7: Theoretical attenuation of configuration 13 versus measured attenuation of test chamber.

Plotting the recordings of 'no pipe' and configuration 13, along with the theoretical attenuation of configuration 13 on the 'no pipe' levels gives a comparison as to how well the theory predicted the noise level to be. For the third and fourth attenuation bands, the data matches well, with the attenuation peaks showing very similar levels to configuration 13's volume.

There is still a large volume difference around 580 Hz. If the velocity of sound is assumed to be 380 m/s, this would mean an open-open ended pipe resonance of 0.32 m or an open-closed pipe resonance of 0.156 m. Coincidentally, this is close to the length of the exhaust header from the valve to the inlet of the chamber, at 0.315 m. Hypothetically speaking, this resonant system could be the cause for the extra attenuation. It could also be a resonant system involving the tailpipe and the chamber under certain conditions.

The next set of configurations were set out to test the effect of cone taper with regards to flow direction. This test was done with configurations 9 and 10, and 11 and 12, to see if a steeper taper on the divergent cone coupled with a shallower taper on the convergent cone would affect attenuation when compared to opposite configuration. The graph of configuration 11and 12 is displayed as the results are clearer than those of 9 and 10. Configuration 11 has a 34.2º included entry angle whereas configuration 12 has a 53.2º included angle.

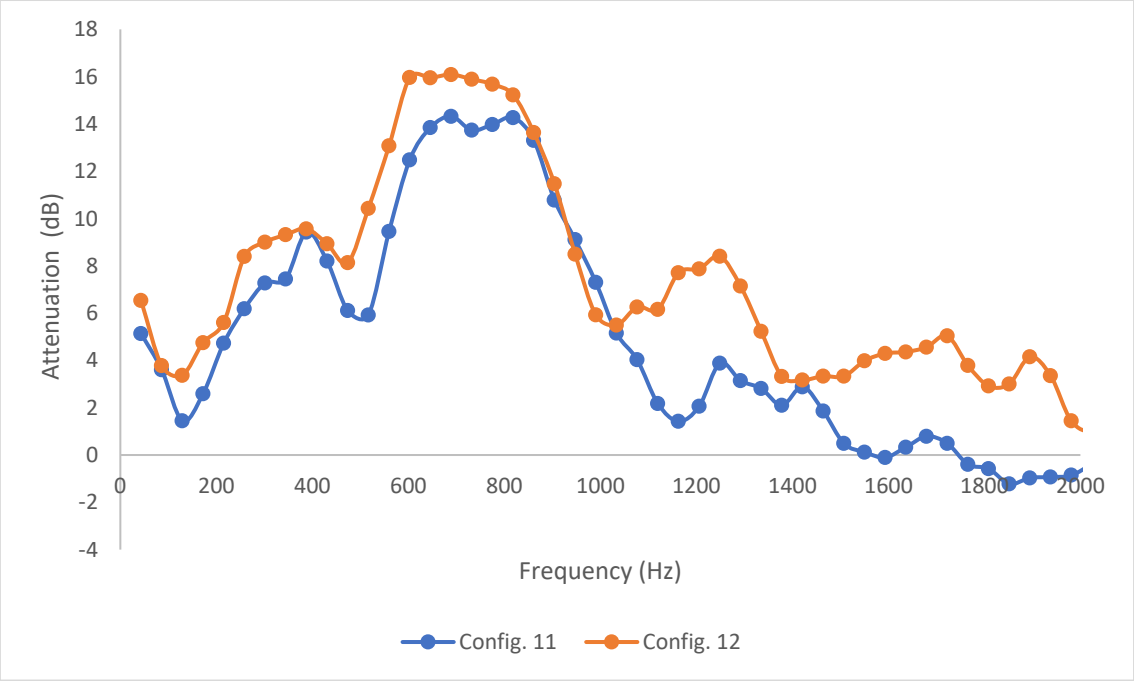

Figure 5-8: Attenuation in a chamber seems to favour a steep entry and shallower exit.

Following the attenuation curves in Figure 5-8, a higher attenuation seems to favour a steeper divergent cone into the chamber with a shallower convergent cone to the tailpipe. This was not a one-off as the same effect occurred on the 100 mm diameter chambers. As was discussed in the modelling section of this thesis, a sharper taper attenuates better into higher frequencies, as can be shown here. The shallower convergent taper on exit could be helping to distribute the reflected pressure pulse over a longer period, with the subsequent reflected waves being of lower energy and spread over more frequencies. The shallower convergent cone could also help to attenuate noise from the reflected rarefaction wave that enters the tailpipe. As the rarefaction wave makes its way into the chamber, it is reflected as a pressure wave due to the increase in diameter, and with a taper, this resultant reflected pressure wave would have its energy reflected over a longer interval – causing lower energy pressure waves and a lower volume.

The next test was the effect of the Area ratio on the attenuation of each chamber. A comparison between the measured noise levels for similar length chambers, configurations 10 and 12, was graphed.

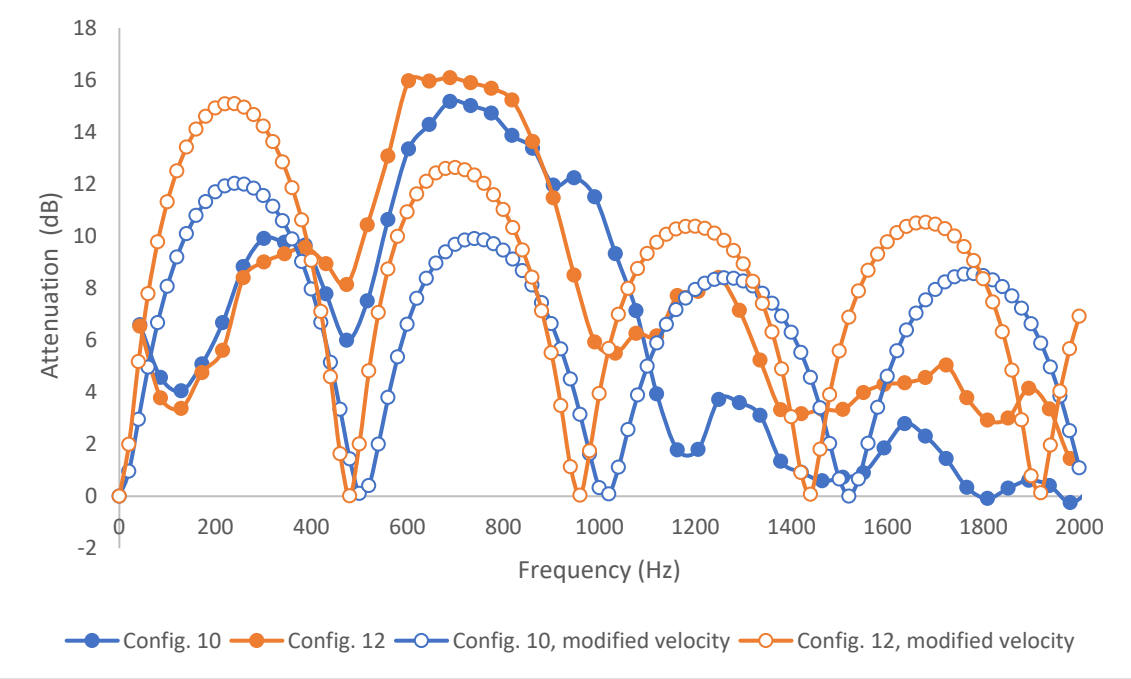

Figure 5-9: As predicted, a larger Area ratio attenuates more noise.

The effect of the Area ratio is clear in Figure 5-9 as the larger 120 mm diameter chambers in both theory and measured values have higher attenuation characteristics. While the difference between attenuation changes between peaks, the location of the attenuation

bands would appear to match the measured data with how the slightly longer 120 mm chamber narrows the bands but has higher attenuation values.

One aspect that is noticeable is how much higher the attenuation for measured values is in the second attenuation band compared to the theoretical attenuation, however for all the other bands the opposite is occurring. Adding to this aspect is the attenuation for the first theoretical band is very similar to the attenuation values for the second measured band. This difference could arise from other harmonics affecting the measured data, such as a Helmholtz resonator being set up, or resonance in the header pipe.

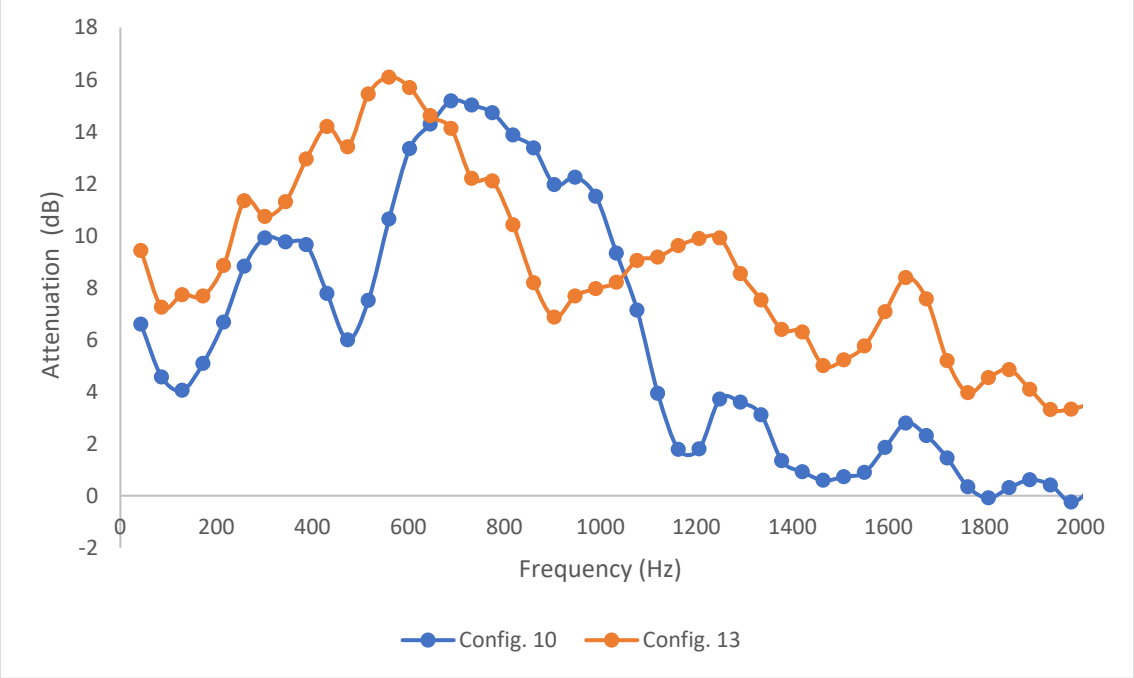

Figure 5-10: A longer chamber acts to lower and narrow the attenuation bands.

This is the situation where chamber length tuning comes into play. The shift of the attenuation band to the left shows the longer chamber is better at silencing lower frequencies, but is also proficient in muffling the higher ones too. The elasticity of the internal volume of the chamber may come into play here as the inlet and exhaust cones have not changed, simply the central cylinder has been substituted for a longer one, a change from 70 mm to 187 mm – 1.68 times the volume.

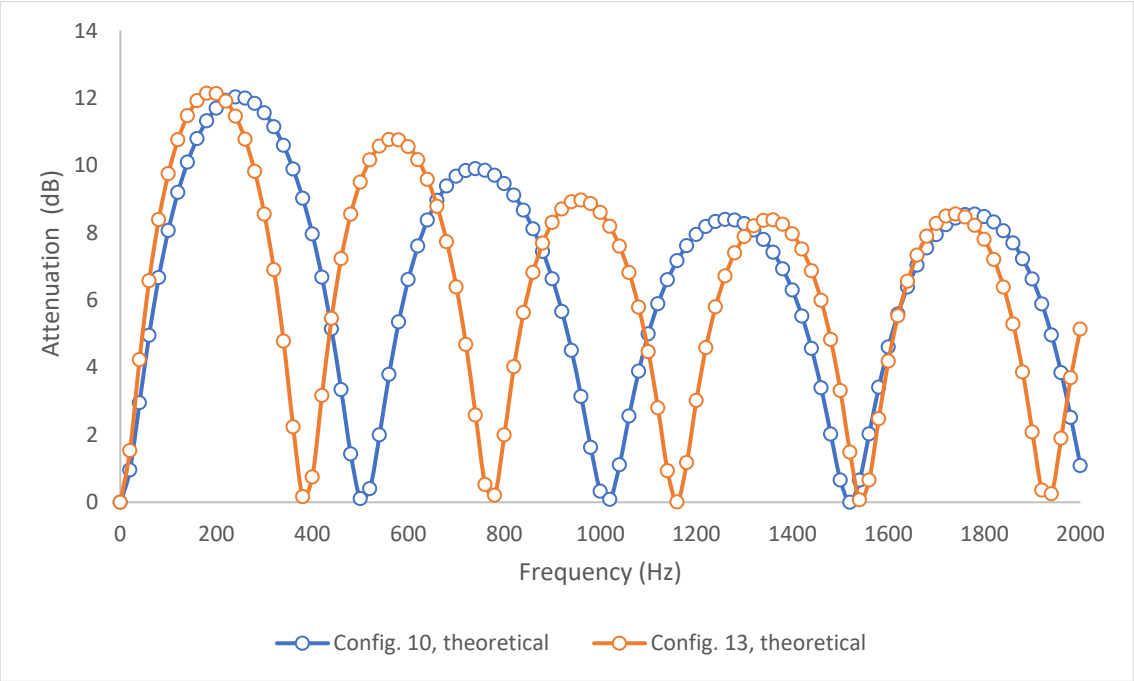

Figure 5-11: Theory showing a longer chamber will lower the frequency and narrow the attenuation bands.

It can be seen on the second attenuation band that the theoretical results match the measured results pleasingly well. The narrow yet taller attenuation band of the longer pipe occurs around the 550 Hz region, matching the test results, with the following second band of the shorter chamber taking over.

This test was repeated with the set of 120 mm sections but now included a super-short central cylinder 20 mm in length and to contrast this, a set of long tapered cones.

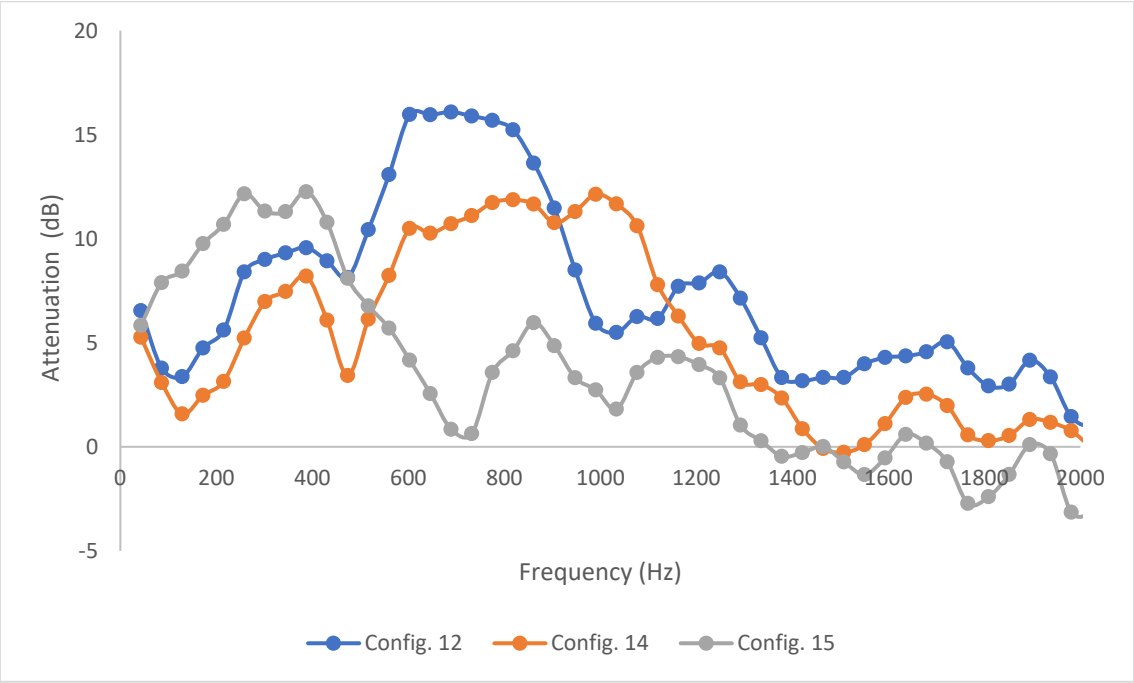

Figure 5-12: Low included angles reduce the chamber's ability to attenuate noise in the higher frequencies.

The result of this series of configurations is an indication of how the difference in length affects the attenuation band location as well as the ability for the chamber to attenuate noise at higher frequencies. The short chamber for configuration 14 shows the wider and higher-frequency attenuation band that was to be expected, but a lack of any other attenuation is visible. The extra-long tapers of configuration 15 also make themselves apparent where the attenuation band is narrow and of a low-frequency, coupled with a poor attenuation in higher frequencies that sometimes increases the volume of the exhaust – similar to that of the first eight configurations. As mentioned in the literature, this could be seen as the higher-frequency waves 'beaming through' the centre of the muffler, having no sound loss.

On a side note, the poor absorption in the low frequencies and the good absorption in the mid-range made the exhaust note of configuration 14 rather pleasing. This sort of chamber tuning is what some manufacturers work with to produce exhausts with certain characteristics that customers enjoy.

A final chamber comparison was done to compare the characteristics of all the chambers involved.

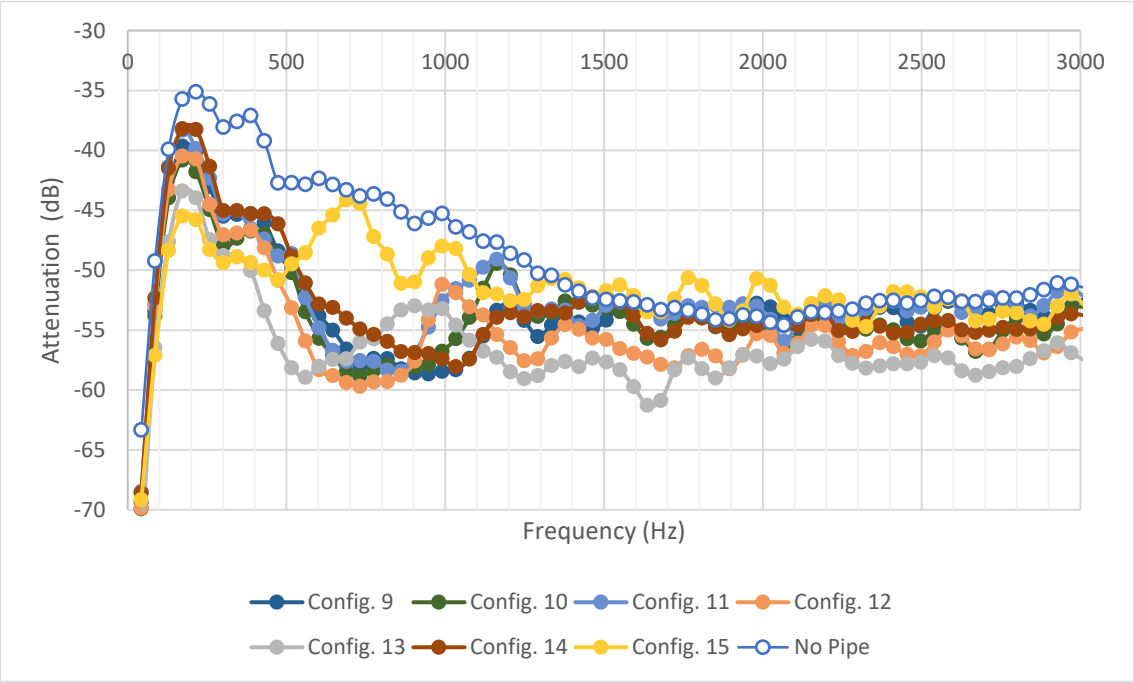

Figure 5-13: All tested chambers showing the most and least effective at attenuating exhaust noise.

Looking at the volumes for each chamber, it is visible that the characteristics of the configurations effectively muffle the volume at lower frequencies as by 1500 Hz, the levels of most are similar to that of no chamber. There are a few outliers and one that stands out is configuration 13, the long-bodied chamber. This 100 mm chamber has the second highest attenuation in the lowest frequency peak, and attenuates the most noise over the higher frequencies. While configuration 13 does loose to the long-tapered chamber, configuration 15, in the lower frequencies by 2 dB, it has higher attenuation elsewhere and would be a much better selection for use.

5.3 Exhaust exit noise tests

The final stage of testing involved changing solely the exit to atmosphere by varying the exit cone and attaching cylinders of different lengths. This test is designed to find any difference in sound that might occur from having a controlled step to atmosphere and could affect the shape of the exhaust's exit.

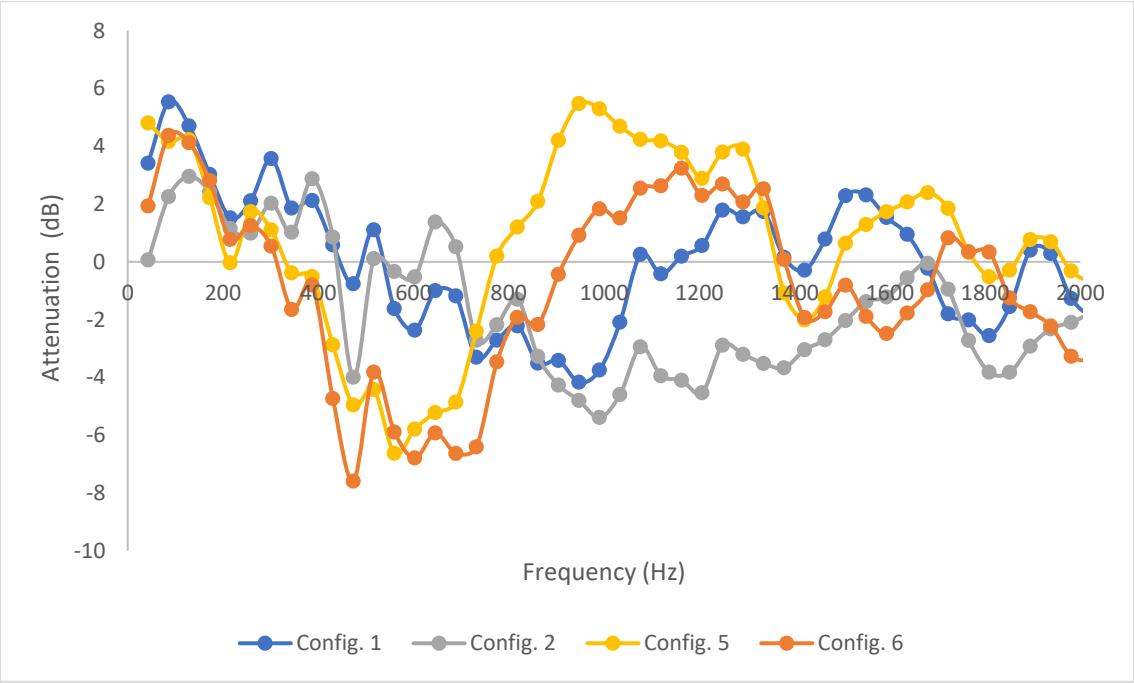

Figure 5-14: Attenuation levels between different shaped exits, relative to no expansion on exit.

The exit of the exhaust is an interesting parameter as it appears that constructive interference occurs around 550 Hz and destructive interference occurs around 1100 Hz for configurations six. Using the acoustic velocity of 380 m/s from testing and a frequency of 550 Hz, coupled with the knowledge that an open-closed tube will resonate at ¼ of the wavelength, we find that the length of the tube is 0.172m. This is coincidentally close to the 180mm length of the divergent cone and tube which could suggest that the addition to the exhaust is resonating and constructively interfering with the exhaust waves to produce a higher volume.

5.4 Discussion of results

Comparing the data to the theory, a strong correlation is seen between the attenuation peaks and the measured noise levels. When the theory suggests lower attenuation is meant to occur, there is still attenuation occurring from some other unknown source. While this is favourable for noise levels, it means further investigation is required into the cause of the attenuation.

Working backwards through the plane-wave equations, if the acoustic velocity and target frequencies for attenuation were known then the user could find an approximation for the

required chamber length and adjust the taper length to help spread the attenuation over a wider range of frequencies.

If more precise volume measuring equipment were to be used, then the effects of the chambers could be seen down to lower frequencies, and in some cases the first harmonic of the engine's speed. This would allow for a better view of the first attenuation band – if any, to see how the chambers attenuated very low frequencies.

5.5 Selection of a reactive muffler for a single-cylinder engine

From the results of the testing combined with the theoretical attenuation of each chamber, it appears that for a single-cylinder engine that has a low exhaust pulse frequency, the best shaped muffler was one that has a taper length of around ¼ the total length of the chamber. Having a steeper taper on the divergent cone followed by a shallower taper would increase the noise attenuation, if the results of the tests are correct, and a larger area ratio would also increase the attenuation.

A good starting point to finding the correct chamber for the engine would be to create an audio spectrum of the exhaust noise and locate target frequencies for attenuation. From there, finding an area ratio that works for the correct amount of attenuation and fits the vehicle should be the next step. This gives all the parameters needed for the simple plane-wave calculations for the chamber length.

5.5.1 Recommendation of a reactive muffler for the KTM LC4 690 engine

Using the results from this research, a recommendation for a muffler fit for WESMO's KTM engine can be found. We know the operating range for the KTM is 2600-8000 rpm, giving a frequency range of 43.3-133 Hz (not including harmonics). Unfortunately the audio data for the KTM has not been recorded so we do not know where target frequencies are on the spectrum, however, readings using the sound level meter at idle of 120 dBC and 127dBC at the engine test speed of 5500 rpm are known. Basing the target levels on the competition rules, we know that the volume at idle has to be less than 103 dBC and at the test speed, 92 Hz, of 110 dBC. Both of these sound measurements are far over the volume limit for the KTM.

To attenuate over 17 decibels at the peak of the attenuation curve would require an area ratio of 16, or 4 times the inlet diameter. For a 38 mm exhaust header pipe diameter, such as that on the vehicle currently, the body of the chamber would need to have a 152 mm internal diameter. Rearranging the transmission loss formula in terms of chamber length, L, we can find a suggested length for the new muffler;

$$l = \frac{csin^{-1}\sqrt{\frac{4(10^{\frac{TL}{10}}-1)}{(A_r-\frac{1}{A_r})^2}}}{2\pi f}$$

Assuming the acoustic velocity of the medium is 380 m/s, the area ratio is 16, and the required transmission loss is 18 dB at 5500 rpm (91.7 Hz), then a length is found of 0.93 m. Packaging a chamber this large would be a nightmare for most Formula SAE teams as the only sensible location would be down the side of the vehicle, covered by heat shielding to pass scrutineering. The same calculation for idle conditions gives an even longer result at 1.99 m in length.

Halving the length of the 92 Hz chamber will double the peak frequency of the attenuation band. Being sinusoidal in nature, the shape of the curve means the attenuation at 91 Hz only drops to 14 dB, while at 43 Hz the attenuation is only 8 dB. This is where a series of chambers would come into play. Using the four-pole method to calculate the transmission loss at each stage of the muffler would be an efficient method of finding a combination of chambers that would be able to attenuate enough noise to bring the engine down to the regulated volumes. Any target frequencies that did not meet noise regulations could then have a side-branch or Helmholtz resonator added later.

While the individual transmission loss values do not simply add together for inline chambers, a good starting point for the KTM would be to use a chamber of 0.465 m in series with a chamber of 0.186 m. The attenuation peaks of the 0.465m chamber are multiples of 200 Hz and the troughs are at multiples of 400 Hz. In contrast, the peaks of the 0.186 m chamber are multiples of 500 Hz, troughs are multiples of 1000 Hz. Areas of low attenuation would be in the region of 2000 Hz, 4000 Hz, and further multiples. Adding a side-branch resonator of 47.5 mm would help to cancel some of the noise out at these frequencies. This unit could be packaged together, albeit a 650 x 160 mm (length by diameter) cylinder is difficult to package, it is not impossible.

6 Conclusion

This thesis conducted a study on attenuating exhaust noise for a single-cylinder Otto-cycle engine destined for use in WESMO's WP-18 Formula SAE vehicle.

A review of literature showed that the issue of muffling engines is a universal problem that requires in-depth calculation and modelling. Selection of an appropriate muffler is an important task as different styles of engines require different attenuation levels and silencing techniques. A four-cylinder engine has different requirements to a single-cylinder mode when it comes to silencing, with different exhaust pulse frequencies and flow characteristics dictating the most appropriate style of silencing device. For a single-cylinder engine, the appropriate style of noise control is based on resonant chambers tuned for the correct peak attenuation at the target frequencies. Basing these chambers on the plane-wave equations proved that the basic theory behind the attenuation in a chamber closely translates into measurable results, even for the chaotic exhaust flow in an engine. Applying this modelling to known shapes, such as the test cones, proved reliable in estimating where the location and shape of the attenuation bands.

The results of the noise test show the research aims have been met by proving the applicability of the plane-wave equations on exhaust noise, while the testing of different conical chambers showed the variance in attenuation between the different geometries. Data from testing proved that an increase in the area ratio of the chamber correlates to an increase in the noise attenuation, a trend that is followed by the theoretical calculations. It is also seen that an increase in length of the chamber affects the locations of attenuation, with the longer chambers attenuating lower frequencies but with a narrower attenuation band width. The shorter chambers would move the frequency higher and flatten out the attenuation bands. The change to an acoustic velocity of 380 m/s saw a significant improvement in the accuracy of the theoretical results, with attenuation bands matching the measured volumes.

The shape of the tailpipe exits did affect the noise levels being produced where a divergent cone would typically increase the volume produced by the engine. By adding a cylindrical length to the end of the cone, the resonant frequencies would change where a loss in attenuation for a few hundred Hertz was followed by a proportional gain in attenuation straight afterwards. This effect could be used where a deeper exhaust pitch is desired but less mid-range noise is needed.

While the location of the attenuation bands align between the theoretical and measured results, the variation from the expected attenuation level could be due to different harmonic frequencies arising or other resonating systems forming in the exhaust. As discussed, the cylinder and header could be forming a Helmholtz resonator, while the chamber and exit pipe could also form the same resonator, all affecting the total attenuation of the system.

Any change in the sound's medium will also affect the noise attenuation results where exhaust gas compositions or temperatures different to those measured will cause variations in density, which can alter the acoustic velocity in the exhaust gas. This condition could cause a sudden rise or fall in velocity, affecting the resonant frequency of such a short section. While the data proved accurate, if a proper indoor facility were to be used, more accuracy could be achieved from the sound level testing. As previously mentioned, the ambient noise for all the tests was below 65 dB but if the tests were done in a purpose built facility then any environmental and noise pollution errors could be accounted for.

Further work into finite volume calculations and multiple resonator systems would benefit this study where complex systems muffler could be calculated and designed, then implemented on future iterations of WESMO's vehicles. Based on the four-pole method, this study should include an accurate representation of the temperature of the exhaust gas in the calculations as a long chamber, such as those for a single-cylinder engines that can have a large temperature gradient across the chamber which greatly affect the acoustic velocity of the gas.

7 Bibliography

Balmer, R. T. (2011). *Modern Engineering Thermodynamics.* Academic Press.

Beardmore, R. (2013, 01 28). *Fluid flow in pipes*. Retrieved from ROYMECH: http://www.roymech.co.uk/Related/Fluids/Fluids_Pipe.html

Bell, A. G. (2012). *Four Stroke Performance Tuning.* California: Haynes North America Inc.

Blair, G. P. (1996). *Design and Simulation of Two-Stroke Engines.* Warrendale, PA: Society of Automotive Engineers, Inc. .

Blair, G. P. (1999). *Design and Simulation of Four-Stroke Engines.* Warrendale, Pa.: Society ofAutomotive Engineers, Inc.

Brown, R. (2004, 04 12). *Sound Waves in a Fluid.* Retrieved from webhome.phy.duke.edu: https://webhome.phy.duke.edu/~rgb/Class/phy51/phy51/node39.html

Chikurde, R., & Mihnish, K. (2013). *Optimization and Validation of Exhaust Tailpipe Noise for a Passenger Car.* SIAT, India: SAE International.

Davis, D. D., Stevens, G. L., Moore, D., & Stokes, G. M. (1953). *THEORETICAL AND MEASURED ATTENUATION OF MUFFLERS AT ROOM TEMPERATURE WITHOUT FLOW, WITH COMMENTS ON ENGINE -EXHAUST MUFFLER DESIGN.* Washington: NATIONAL ADVISORY COMMITTEE FOR AERONAUTICS .

Davis, M. (2015, 03 05). *When Do Exhaust Gas Temperatures Become A Cause For Concern?* Retrieved from Hot Rod Network: http://www.hotrod.com/articles/when-do-gas-exhaust-temperatures-become-cause-for-concern/

Dunbar, B. (2017, August 17). *NASA Armstrong Fact Sheet: Sonic Booms*. Retrieved from NASA: https://www.nasa.gov/centers/armstrong/news/FactSheets/FS-016-DFRC.html

Electrical Generating Systems Association. (2014). *Guide for Rating Generator exhaust silencers.* Retrieved from Electrical Generating Systems Association: http://www.egsa.org/Portals/7/Documents/Standards/EGSA%20Silencer%20Rating%20Guide%20Final.pdf

Encyclopedia Britannica. (2020, January 02). *Two-stroke cycle.* Retrieved from Encyclopedia Britannica: https://www.britannica.com/technology/gasoline-engine/Cylinder-block#/media/1/226592/1386

Encyclopedia Britannica. (2020, January 02). *Wankel rotary engine.* Retrieved from Encyclopedia Britannica: https://www.britannica.com/technology/gasoline-engine/Cylinder-block#/media/1/226592/165449

Fallah, S. (2014). *Electric and Hybrid Vehicles - Technologies, Modeling and Control: A Mechatronic Approach.* Surrey: Wiley-Blackwell.

Forouharmajd, F., Nassiri, P., Monazzam, M. R., & Yazdchi, M. (2015). The estimation of Helmholtz resonator and active noise. *International Journal of Environmental Health Engineering*, 1-6.

Guggenheim, E. A. (1959). *Thermodynamics.* Amsterdam: North-Holland Publishing Company.

Gupta, A. K. (2016). Comparison of Noise Attenuation Level by Convergent and Divergent Cylindrical Duct with Space Constraints. *International Journal of Scientific Research in Science, Engineering and Technology (ijsrset.com)*, 778-781.

Jebasinski, R. (2000). *Absorption mufflers in exhaust systems.* ACOUSTICS 2005.

Kane, J. (2015, April 28). *Exhaust System Technology*. Retrieved from EPI-eng: http://www.epi-eng.com/piston_engine_technology/exhaust_system_technology.htm

Kane, J. (2015). Exhaust System Technology - The Sound and the Fury. *Race Engine Technology Magazine*.

Kaplan, A., Straub, S., & Shkolnikov, P. (2002). Sub-Cycle Pulses and Field Solitons: Near- and Sub-Femtosecond Em-Bubbles. In F. Kajzar, & R. Reinisch, *Beam Shaping and Control with Nonlinear Optics* (pp. 291-317).

Kermani, M. (2015). *Muffler Design by Noise Transmission Loss Maximization.* Gazimağusa, North Cyprus: Eastern Mediterranean University.

Khajepour, A., Fallah, S., & Goodarzi, A. (2014). *Electric and Hybrid Vehicles: Technologies, Modeling and Control: A Mechatronic Approach, First Edition.* John Wiley & Sons, Ltd.

Moebs, W., Ling, S. J., & Sanny, J. (2016, September 19). *Standing Waves and Resonance.* Retrieved from OpenStax: https://openstax.org/books/university-physics-volume-1/pages/16-6-standing-waves-and-resonance

Montwill, A., & Montwill, B. (2013). *Let There Be Light : The Story of Light from Atoms to Galaxies.* Imperial College Press.

Naber, J. D., & Johnson, J. E. (2014). *Alternative Fuels and Advanced Vehicle Technologies for Improved Environmental Performance.* Woodhead Publishing.

New World Encyclopedia, c. (2018, March 04). *Internal combustion engine*. Retrieved from New World Encyclopedia: //www.newworldencyclopedia.org/p/index.php?title=Internal_combustion_engine&oldid=1009502

Nuclear-Power.net. (2019, 10 14). *Pressure Loss Coefficient*. Retrieved from Nuclear-Power.net: https://www.nuclear-power.net/nuclear-engineering/fluid-dynamics/bernoullis-equation-bernoullis-principle/head-loss/pressure-loss-coefficient-plc/

Potente, D. (2005). General Design Principles for an Automotive Muffler. *ACOUSTICS 2005* (pp. 153-158). Busselton, Western Australia: Australian Acoustical Society.

pstir2. (2015, 01 08). *Sound waves in a closed pipe Problem* . Retrieved from Physics Forums: https://www.physicsforums.com/threads/sound-waves-in-a-closed-pipe-problem.790788/

Rajadurai, S., Afnas, M., Ananth, S., & Surendhar, S. (2014). Materials for Automotive Exhaust System. *International Journal of Recent Development in Engineering and Technology*, 82-89.

RAŢIU, S. (2003). THE HISTORY OF THE INTERNAL COMBUSTION ENGINE. *Annals of the Faculty of Engineering Hunedoara*, 145-148.

Rennie, J. (2012, 09 28). *Reflection of sound waves from the open end of an organ pipe & relationship b/w nodes & pressure* . Retrieved from physics.stackexchange.com: https://physics.stackexchange.com/questions/38548/reflection-of-sound-waves-from-the-open-end-of-an-organ-pipe-relationship-b-w

Russell, D. (2019). *Helmholtz Resonators - Basic Analytic Devices*. Retrieved from seas.harvard.edu: https://people.seas.harvard.edu/~jones/cscie129/nu_lectures/lecture3%20/ho_helmholtz/ho_helmholtz.html

Saary, S. (1993). Book Review of "A Science Miscellany". *Khaleej Times*, 14.

SAE, I. (2018). *Formula SAE Rules 2019 (V1.0 25 July 2018).* SAE International.

Saeid, N. H. (2013). Diffuser perforation effects on the performance of a vent silencer. *Noise Control Engineer*, 355-362.

Science Learning Hub. (2013, September 13). *Sound - wave interference.* Retrieved from Science Learning Hub: https://www.sciencelearn.org.nz/resources/2816-sound-wave-interference

Sekine, N., Kudo, I., Onodera, O., & Takayama, K. (1995). *Effects of Shock Waves on Silencer Characteristics m the.* Heidelberg, Berlin: Springer.

Sharmin, T., Hassan, A., Rahman, M., & Al Nur, M. (2005). DESIGN AND CONSTRUCTION OF A MUFFLER FOR ENGINE. *International Conference on Mechanical Engineering 2005* (pp. ICME05-TH-47). Dhaka, Bangladesh: Bangladesh University of Engineering and Technology.

Staab, W. (2016, November 29). *An Upper Limit to Sound?* Retrieved from Hearing Health and Technology matters: https://hearinghealthmatters.org/waynesworld/2016/an-upper-limit-to-sound/

Thompson, D. (2010). Trail Bike Exhaust Noise: Are road-legal trail bikes. *Proceedings of 20th International Congress on Acoustics, ICA 2010*.

Wall, J. (2003). *Dynamics Study of an Automobile Exhaust System.* Karlskrona, Sweden: Blekinge Institute of Technology.

Wensel, R. N. (1936). Resistance of Solid Surfaces to Wetting by Water. *Industrial and Engineering Chemistry, Volume 28, NO.8*, 988-994.

Xu, J., Zhou, S., & Li, K. (2015). ANALYSIS OF FLOW FIELD AND PRESSURE LOSS FOR FORK TRUCK MUFFLER BASED ON THE FINITE VOLUME METHOD. *INTERNATIONAL JOURNAL OF HEAT AND TECHNOLOGY*, 85-90.

Young, C.-I. J., & Crocker, M. J. (1975). Prediction of transmission loss in mufflers by the finite-element method. *The Journal of the Acoustical Society of America* , 144-148.

Zareei, J., & Kakaee, A. (2013). Study and the effects of ignition timing on gasoline engine performance and emissions. *European Transport Research Review*, 109-116.

Zhang, H., Fan, W., & Guo, L.-X. (2018). A CFD Results-Based Approach to Investigating Acoustic Attenuation Performance and Pressure Loss of Car Perforated Tube Silencers. *Applied Sciences*, 545.

7.1 Credits

```
[1]: Audacity® software is copyright © 1999-2019 Audacity Team.
Web site: https://audacityteam.org/. It is free software
distributed under the terms of the GNU General Public License.
The name Audacity® is a registered trademark of Dominic Mazzoni.
```

8 Appendices

8.1 Appendix 1; Test chamber experiment list.

Longest Simple Chamber	120*722L							
Shortest Simple Chamber	120*335L							
Test Cones	**Divergent**		**Cylinder**		**Convergent**		**Test #**	
	Dia	Length	Dia	Length	Dia	Length		
Divergent cone only	100	195					1	
	100	110					2	
	120	195					3	
	120	120					4	
Div. cone with ~80mm cylinder	100	195	100	70			5	
	100	110	100	70			6	
	120	195	120	82			7	
	120	120	120	82			8	
Full Chamber	100	195	100	70	100	110	9	
	100	110	100	70	100	195	10	
	120	195	120	82	120	120	11	
	120	120	120	82	120	195	12	
100 long cyl vs short	100	110	100	187	100	195	13	Use 10 for comparison
120 long cyl vs short	120	120	120	20	120	195	14	Use 12 for comparison
120 long taper vs short	120	360	120	82	120	280	15	Use 12 for comparison
100 long taper vs short taper w. cylinder								Use 1 and 6 for comparison
120 long taper vs short taper w. cylinder								Use 3 and 8 for comparison

Table 8-1: Full list of configurations, including comments.

8.2 Appendix 2; FSAE Noise test regulations

IN.10.1 Sound Level Measurement

IN.10.1.1 The sound level will be measured during a stationary test, with the vehicle gearbox in neutral at the defined test speed

IN.10.1.2 Measurements will be made with a free field microphone placed:

- free from obstructions
- at the exhaust outlet vertical level
- 0.5 m from the end of the exhaust outlet
- at an angle of 45° with the outlet in the horizontal plane

IN.10.4 Test Speeds

IN.10.4.1 The maximum test speed for a given engine will be the engine speed that corresponds to an average piston speed of 914.4 m/min (3,000 ft/min) for automotive or motorcycle engines, and 731.5 m/min (2,400 ft/min) for “industrial engines”. The calculated speed will be rounded to the nearest 500 rpm. Test speeds for typical engines will be published on the event website.

IN.10.4.2 The idle test speed for a given engine will be up to the team and determined by their calibrated idle speed. If the idle speed varies then the vehicle will be tested across the range of idle speeds determined by the team.

IN.10.4.3 The vehicle must be compliant at all engine speeds up to the maximum defined test speed.

IN.10.5 Maximum Permitted Sound Level

- At idle 103 dBC, fast weighting
- At all other speeds 110 dBC, fast weighting (SAE, 2018)

8.3 Appendix 3; Additional Exhaust noise Spectrum graphs

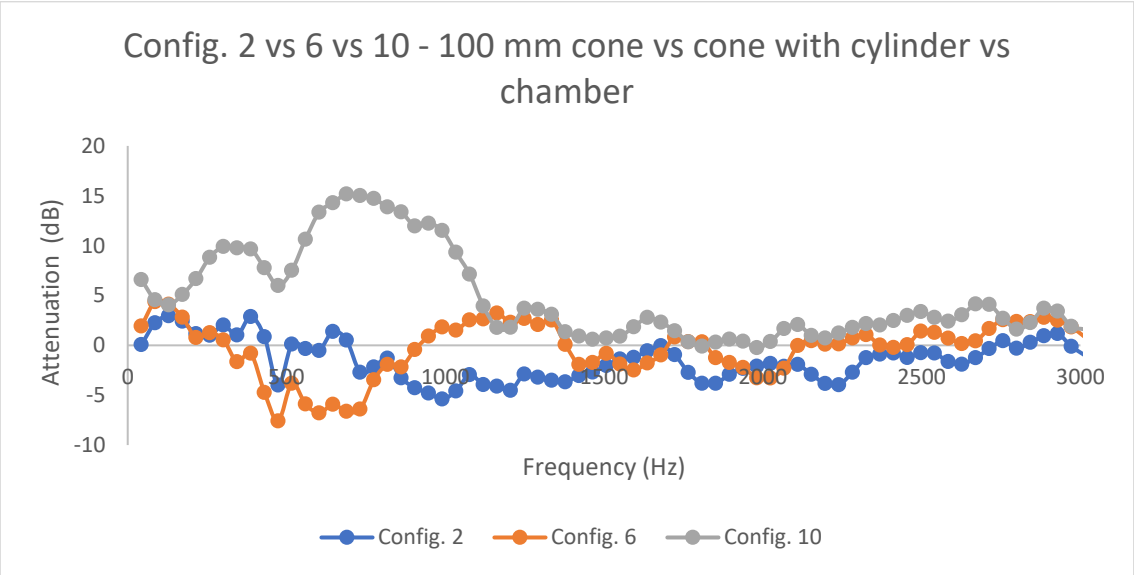

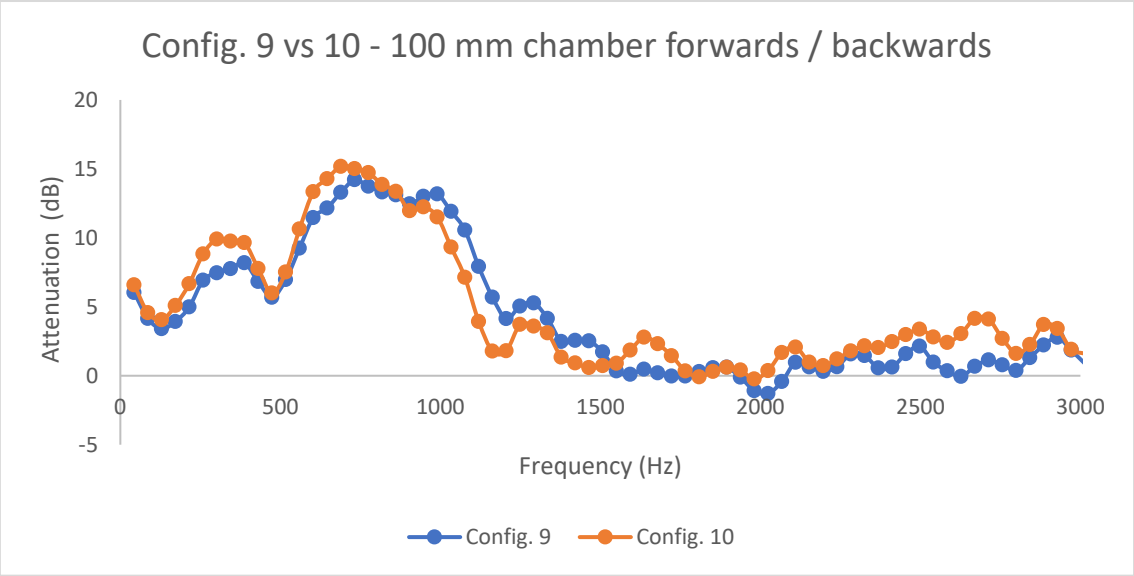

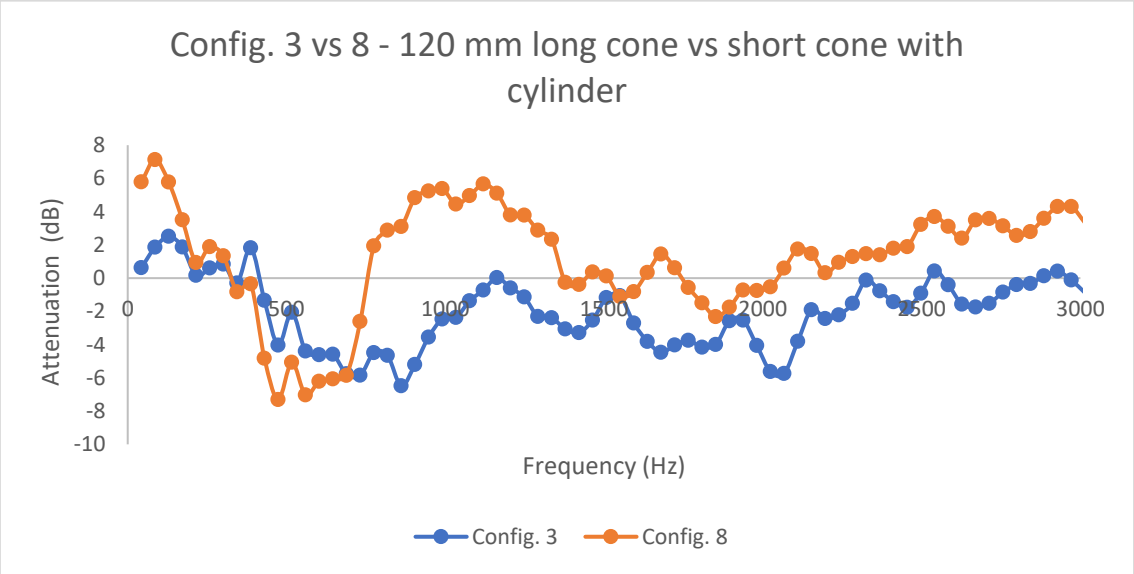

8.4 Appendix 4; Calculation of acoustic velocity of exhaust gas.

TABLE 2.1.1 PROPERTIES OF SOME COMMON GASES FOUND IN ENGINES.

GAS	M	κ_0	κ_1	κ_2	κ_3
O_2	31.999	-9.3039E6	2.9672E4	2.6865	-2.1194E-4
N_2	28.013	-8.503.3E6	2.7280E4	3.1543	-3.3052E-4
CO	28.011	-8.3141E6	2.7460E4	3.1722	-3.3416E-4
CO_2	44.01	-1.3624E7	4.1018E4	7.2782	-8.0848E-4
H_2O	18.015	-8.9503E6	2.0781E4	7.9577	-7.2719E-4
H_2	2.016	-7.8613E6	2.6210E4	2.3541	-1.2113E-4

Table 8-2: Gas properties of common gases (Blair, 1999, p. 172).

$M_{CO_2} = 44.01$ g/mol, $M_{H_2O} = 18.015$ g/mol, $M_{N_2} = 28.013$ g/mol

R = 8314.4 J/kgK, T = 773 ºK, $c = \sqrt{\gamma RT}$

Exhaust composition @ AFR of 15; 0.125 CO_2 : 0.141 H_2O : 0.734 N_2, from:

$$2C_8H_{18} + 25\left[O_2 + \frac{79}{21}N_2\right] = 16CO_2 + 18H_2O + 94.05N_2$$

$$\overline{C_p} = \kappa_1 + 2\kappa_2 T + 3\kappa_3 T^2\,, \quad \overline{C_V} = \overline{C_p} - \bar{R}, \quad \text{and} \quad C_p = \frac{\overline{C_p}}{M}\,, \quad C_v = \frac{\overline{C_v}}{M}$$

Where $R = \frac{\bar{R}}{M}$ and $\gamma = \frac{C_p}{C_v}$

Calculation of specific heat and gas constant for CO_2:

$$R_{CO_2} = \frac{\bar{R}}{M} = \frac{8314.4}{44.01} = 188.92\frac{J}{kgK}$$

$$\overline{C_{p,CO_2}} = 4.1 * 10^4 + 2(7.28)(773) + 3(-8.08 * 10^{-4})(773)^2 = 50806.47\frac{J}{kgmolK}$$

$$C_{p,CO_2} = \frac{\overline{C_p}}{M} = \frac{50806.47}{44.01} = 1154.43\frac{J}{kgK}$$

$\overline{C_V} = \overline{C_p} - \bar{R}$, therefore; $\overline{C_{V,CO_2}} = 50806.47 - 8314.4 = 42492.07\frac{J}{kgmolK}$

$$C_{v,CO_2} = \frac{\overline{C_v}}{M} = \frac{42492.07}{44.01} = 965.51\frac{J}{kgK}$$

This gives $\gamma_{CO_2} = \frac{C_p}{C_v} = \frac{1154.43}{965.51} = 1.20$

Calculation of specific heat and gas constant for H_2O:

$$R_{H_2O} = \frac{\bar{R}}{M} = \frac{8314.4}{18.015} = 461.53 \frac{J}{kgK}$$

$$\overline{C_{p,H_2O}} = 2.08 * 10^4 + 2(7.96)(773) + 3(-7.27 * 10^{-4})(773)^2 = 31802.95 \frac{J}{kgmolK}$$

$$C_{p,H_2O} = \frac{\overline{C_p}}{M} = \frac{31802.95}{18.015} = 1765.36 \frac{J}{kgK}$$

$\overline{C_V} = \overline{C_p} - \bar{R}$, therefore; $\overline{C_{V,H_2O}} = 31802.95 - 8314.4 = 23488.55 \frac{J}{kgmolK}$

$$C_{v,H_2O} = \frac{\overline{C_v}}{M} = \frac{23488.55}{18.015} = 1303.83 \frac{J}{kgK}$$

This gives $\gamma_{H_2O} = \frac{C_p}{C_v} = \frac{1765.36}{1303.83} = 1.35$

Calculation of specific heat and gas constant for N_2:

$$R_{N_2} = \frac{\bar{R}}{M} = \frac{8314.4}{28.013} = 296.81 \frac{J}{kgK}$$

$$\overline{C_{p,N_2}} = 2.73 * 10^4 + 2(3.15)(773) + 3(-3.01 * 10^{-4})(773)^2 = 31630.33 \frac{J}{kgmolK}$$

$$C_{p,N_2} = \frac{\overline{C_p}}{M} = \frac{31630.33}{28.013} = 1129.13 \frac{J}{kgK}$$

$\overline{C_V} = \overline{C_p} - \bar{R}$, therefore; $\overline{C_{V,N_2}} = 31630.33 - 8314.4 = 23315.93 \frac{J}{kgmolK}$

$$C_{v,N_2} = \frac{\overline{C_v}}{M} = \frac{23315.93}{28.013} = 832.33 \frac{J}{kgK}$$

This gives $\gamma_{N_2} = \frac{C_p}{C_v} = \frac{1129.13}{832.33} = 1.36$

Calculation of specific heat and gas constant for exhaust gas:

Using the equations:

$$\mathbf{R_{air} = \Sigma\left(\varepsilon_{gas} R_{gas}\right)} \qquad \mathbf{C_{Pair} = \Sigma\left(\varepsilon_{gas} C_{Pgas}\right)}$$

$$\mathbf{C_{Vair} = \Sigma\left(\varepsilon_{gas} C_{Vgas}\right)} \qquad \mathbf{\gamma_{air} = \frac{C_{Pair}}{C_{Vair}}}$$

Figure 8-1: Calculations for properties of exhaust gases (Blair, 1999, p. 172).

$$R_{exh} = 0.125(188.92) + 0.141(461.53) + 0.734(296.81) = 306.55 \frac{J}{kgK}$$

$$C_{p,exh} = 0.125(1154.43) + 0.141(1765.36) + 0.734(1129.13) = 1222 \frac{J}{kgK}$$

$$C_{v,exh} = 0.125(965.51) + 0.141(1303.83) + 0.734(832.33) = 915.46 \frac{J}{kgK}$$

$$\gamma_{\text{exh}} = \frac{C_{p,exh}}{C_{v,exh}} = \frac{1222}{915.46} = 1.33$$

This leads to the acoustic velocity, c, to be:

$$c_{exh} = \sqrt{\gamma RT} = \sqrt{(1.33)(306.55)(773)} = 561.37\ m/s$$